



E-ISSN 2667-5846

# EXPERIMED

Volume **14** Issue **1** April 2024

[experimed.istanbul.edu.tr](http://experimed.istanbul.edu.tr)



# EXPERIMED

## INDEXING AND ABSTRACTING

Scopus

ULAKBIM TR Index

Chemical Abstracts Service (CAS)

EBSCO - Central & Eastern European Academic Source

SOBIAD

# EXPERIMED

## OWNER

Prof. Dr. Gunnur DENİZ

Department of Immunology, Istanbul University, Aziz Sancar Institute of Experimental Medicine, Istanbul, Türkiye

## RESPONSIBLE MANAGER

Prof. Dr. Bedia ÇAKMAKOĞLU

Department of Molecular Medicine, Istanbul University, Aziz Sancar Institute of Experimental Medicine, Istanbul, Türkiye

## CORRESPONDENCE ADDRESS

Istanbul University, Aziz Sancar Institute of Experimental Medicine,

Vakıf Gureba Avenue, 34093, Çapa, Fatih, İstanbul, Türkiye

Phone: +90 (212) 414 22 29

E-mail: [experimed@istanbul.edu.tr](mailto:experimed@istanbul.edu.tr)

## PUBLISHER

Istanbul Üniversitesi Yayınevi / Istanbul University Press

Istanbul University Central Campus,

34452 Beyazıt, Fatih / İstanbul, Türkiye

Phone: +90 (212) 440 00 00

---

Authors bear responsibility for the content of their published articles.

The publication language of the journal is English.

This is a scholarly, international, peer-reviewed and open-access journal published triannually in April, August and December.

---

**Publication Type:** Periodical

# EXPERIMED

## EDITORIAL MANAGEMENT BOARD

---

### Editor-in-Chief

Prof. Dr. Bedia CAKMAKOGLU

Department of Molecular Medicine, Istanbul University, Aziz Sancar Institute of Experimental Medicine, Istanbul, Türkiye – [bedia@istanbul.edu.tr](mailto:bedia@istanbul.edu.tr)

Prof. Dr. Hesenov Muşviq CƏLALOĞLU

Department of General Surgery, Chairman of the Azerbaijan Association of Endoscopic Laparoscopic Surgeons Public Union, Azerbaijan Medical University, Baku, Azerbaijan - [hesenov@amu.edu.az](mailto:hesenov@amu.edu.az)

### Co-Editors-in-Chief

Prof. Dr. Umut Can KUCUKSEZER

Department of Immunology, Istanbul University, Aziz Sancar Institute of Experimental Medicine, Istanbul, Türkiye – [uksezer@istanbul.edu.tr](mailto:uksezer@istanbul.edu.tr)

Assoc. Prof. Vuslat YILMAZ

Department of Neuroscience, Istanbul University, Aziz Sancar Institute of Experimental Medicine, Istanbul, Türkiye – [vuslat.yilmaz@istanbul.edu.tr](mailto:vuslat.yilmaz@istanbul.edu.tr)

### Managing Editor

Prof. Dr. Sema Sirma EKMEKCI

Department of Genetics, Istanbul University, Aziz Sancar Institute of Experimental Medicine, Istanbul, Türkiye – [sirmasem@istanbul.edu.tr](mailto:sirmasem@istanbul.edu.tr)

### Editorial Management Board Members

Dr. Canan AyseI ULUSOY

Department of Neuroscience, Istanbul University, Aziz Sancar Institute of Experimental Medicine, Istanbul, Türkiye – [canan.ulusoym@istanbul.edu.tr](mailto:canan.ulusoym@istanbul.edu.tr)

Dr. Baris ERTUGRUL

Department of Molecular Medicine, Istanbul University, Aziz Sancar Institute of Experimental Medicine, Istanbul, Türkiye – [baris.ertugrul@istanbul.edu.tr](mailto:baris.ertugrul@istanbul.edu.tr)

### Ethical Editor

Prof. Dr. Elif OZKOK

Department of Neuroscience, Istanbul University, Aziz Sancar Institute of Experimental Medicine, Istanbul, Türkiye – [eozykok@istanbul.edu.tr](mailto:eozykok@istanbul.edu.tr)

### Section Editors

Assoc. Prof. Sinem BIRELLER

Department of Biochemistry, Faculty of Pharmacy, Acıbadem Mehmet Ali Aydınlar University, Istanbul, Türkiye – [sinem.bireller@acibadem.edu.tr](mailto:sinem.bireller@acibadem.edu.tr)

Assoc. Prof. Ferda PACAL

Department of Lab Animal Science, Istanbul University, Aziz Sancar Institute of Experimental Medicine, Istanbul, Türkiye – [ferda.pacal@istanbul.edu.tr](mailto:ferda.pacal@istanbul.edu.tr)

Assoc. Prof. Ali Cihan TASKIN

Department of Lab Animal Science, Istanbul University, Aziz Sancar Institute of Experimental Medicine, Istanbul, Türkiye – [ataskin@istanbul.edu.tr](mailto:ataskin@istanbul.edu.tr)

### Language Editors

Elizabeth Mary EARL

Department of Foreign Languages, Istanbul University, Istanbul, Türkiye – [elizabeth.earl@istanbul.edu.tr](mailto:elizabeth.earl@istanbul.edu.tr)

### Statistics Editor

Sevda OZEL YILDIZ

Department of Biostatistic, Istanbul Medical Faculty, Istanbul University, Istanbul, Türkiye – [sevda@istanbul.edu.tr](mailto:sevda@istanbul.edu.tr)

# EXPERIMED

## EDITORIAL BOARD

---

**Aziz SANCAR** (Honorary Member)

Department of Biochemistry and Biophysics, University of North Carolina School of Medicine, Chapel Hill, North Carolina, USA – [aziz\\_sancar@med.unc.edu](mailto:aziz_sancar@med.unc.edu)

**Abid HUSSAINI**

Department of Pathology and Cell Biology, Columbia University, Taub Institute, New York, USA – [abid.hussaini@columbia.edu](mailto:abid.hussaini@columbia.edu)

**Ahmet GUL**

Department of Internal Medicine, Istanbul University School of Medicine, Istanbul, Turkiye – [agul@istanbul.edu.tr](mailto:agul@istanbul.edu.tr)

**Ali Onder YILDIRIM**

Department of Lung Biology and Diseases, Helmholtz Zentrum München, München, Germany – [oender.yildirim@helmholtz-muenchen.de](mailto:oender.yildirim@helmholtz-muenchen.de)

**Batu ERMAN**

Department of Molecular Biology, Genetics and Bioengineering, Sabanci University, Istanbul, Turkiye – [batu.erman@boun.edu.tr](mailto:batu.erman@boun.edu.tr)

**Çağla EROGLU**

Department of Cell Biology, Duke University, North Carolina, USA – [cagla.eroglu@duke.edu](mailto:cagla.eroglu@duke.edu)

**Ebba LOHMANN**

Department of Neurodegenerative Diseases, Tübingen University, Tübingen, Germany – [ebba.lohmann@uni-tuebingen.de](mailto:ebba.lohmann@uni-tuebingen.de)

**Elif APOHAN**

Department of Biology, İnönü University, Malatya, Turkiye – [elif.apohan@inonu.edu.tr](mailto:elif.apohan@inonu.edu.tr)

**Erdem TUZUN**

Department of Neuroscience, Istanbul University, Aziz Sancar Institute of Experimental Medicine, Istanbul, Turkiye – [erdem.tuzun@istanbul.edu.tr](mailto:erdem.tuzun@istanbul.edu.tr)

**Gökçe TORUNER**

Department of Hematology, MD Anderson Cancer Center, Houston, Texas, USA – [gatoruner@mdanderson.org](mailto:gatoruner@mdanderson.org)

**Gunnur DENİZ**

Department of Immunology, Istanbul University, Aziz Sancar Institute of Experimental Medicine, Istanbul, Turkiye – [gdeniz@istanbul.edu.tr](mailto:gdeniz@istanbul.edu.tr)

**Gürol TUNÇMAN**

Department of Genetics and Complex Diseases, Harvard University, Massachusetts, USA – [gtuncman@hsph.harvard.edu](mailto:gtuncman@hsph.harvard.edu)

**Hannes STOCKINGER**

Molecular Immunology Unit, Vienna School of Medicine, Pathophysiology Center, Vienna, Austria – [hannes.stockinger@medunivien.ac.at](mailto:hannes.stockinger@medunivien.ac.at)

**Rukset ATTAR**

Department of Obstetrics and Gynecology, Yeditepe University, Istanbul, Turkiye – [rattar@yeditepe.edu.tr](mailto:rattar@yeditepe.edu.tr)

**Ihsan GURSEL**

Department of Molecular Biology and Genetics, Bilkent University, Ankara, Turkiye – [ihsangursel@bilkent.edu.tr](mailto:ihsangursel@bilkent.edu.tr)

**Melih ACAR**

Texas University Pediatric Research Institute, Dallas, Texas, USA – [melihacar@gmail.com](mailto:melihacar@gmail.com)

**Numan ÖZGEN**

Department of Pathology and Immunology, Baylor University School of Medicine, Texas, USA – [numan.oezguen@bcm.edu](mailto:numan.oezguen@bcm.edu)

**Serhat PABUCCUOĞLU**

Department of Reproduction & Artificial Insemination, Istanbul University-Cerrahpaşa School of Veterinary, Istanbul, Turkiye – [serpab@iuc.edu.tr](mailto:serpab@iuc.edu.tr)

**Suhendan EKMEKÇIOĞLU**

MD Anderson Cancer Center, Texas University, Houston, Texas, USA – [sekmekcioglu@mdanderson.org](mailto:sekmekcioglu@mdanderson.org)

**Yusuf BARAN**

Department of Molecular Biology and Genetics, İzmir Institute of Technology, İzmir, Turkiye – [yusufbaran@iyte.edu.tr](mailto:yusufbaran@iyte.edu.tr)

# EXPERIMED

## CONTENTS

### REVIEW ARTICLE

- 1 **Potential Roles of MicroRNAs in Neurodegenerative Diseases**  
Medinenur Yozlu, Duygu Gezen Ak, Emrah Yucesan

### ORIGINAL ARTICLES

- 7 **A Clinical Sulfonamide Derivative Inhibits B-Raf Protein in Colorectal Cancer and Melanoma Cells. Is It a New Target for Cancer?**  
Emine Terzi, Beyza Ecem Oz Bedir
- 13 **Evaluating the Effect of Applying Cathodal tDCS to the Left Dorsolateral Prefrontal Cortex on Visual Working Memory**  
Yunus Emre Oksuz, Gokcer Eskikurt
- 21 **Efficacy of the GnRH Agonist Trigger in Oocyte and Embryo Quality Through Mitochondrial Unfolded Protein Response**  
Murat Basar
- 26 **Cytogenetic and FISH Examination of 3p Abnormalities in Lung Cancer Patients**  
Narmin Bakhshaliyeva, Ayse Cirakoglu, Hurrem Gul Ongen, Esin Bil Tuncay, Yelda Tarkan Arguden
- 40 **Effects of GDF-15 Level in Patients with Membranous Nephropathy**  
Aida Adikozalova, Sebahat Usta Akgul, Erol Demir, Hayriye Senturk Ciftci, Fatma Savran Oguz, Halil Yazici, Cigdem Kekik Cinar
- 46 **Effect of Ellagic Acid and Cryptotanshinone on Cell Viability/Cytotoxicity, Metastasis, and Oxidative Stress in Triple-Negative Breast Cancer Cells**  
Umit Yilmaz, Mehmet Fatih Seyhan
- 54 **Assessing the Impact of Hypercapnic Stimulation on Brain Connectivity Metrics During Functional Magnetic Resonance Imaging**  
Idiz Iset, Ali Bayram
- ### LETTER TO THE EDITOR
- 61 **Artificial Intelligence-Enhanced Application of CRISPR-Cas13a for Cancer Gene Therapy: A Breakthrough Concept**  
Tungki Pratama Umar

# Potential Roles of MicroRNAs in Neurodegenerative Diseases

Medinenur Yozlu<sup>1</sup> , Duygu Gezen Ak<sup>2</sup> , Emrah Yucesan<sup>1</sup> 

<sup>1</sup>Department of Neurogenetics, Institute of Neurological Sciences, Istanbul University-Cerrahpasa, Istanbul, Turkiye

<sup>2</sup>Department of Neuroscience, Institute of Neurological Sciences, Istanbul University-Cerrahpasa, Istanbul, Turkiye

ORCID ID: M.Y. 0000-0002-3580-7280; D.G.A. 0000-0001-7611-2111; E.Y. 0000-0003-4512-8764

**Cite this article as:** Yozlu M, Gezen Ak D, Yucesan E. Potential roles of MicroRNAs in neurodegenerative diseases. *Experimed* 2024; 14(1): 1-6.

## ABSTRACT

Neurodegenerative diseases are defined by advanced neuronal loss and can occur in hereditary or sporadic forms. As is generally known, the most common neurodegenerative diseases are Alzheimer's disease (AD) and Parkinson's disease (PD). Among these, AD is defined by the accumulation of beta-amyloid plaques, hyper phosphorylation of tau proteins, and chronic inflammation leading to neuronal loss. PD is related to the degeneration of dopaminergic neurons in the substantia nigra. Because of the wide heterogeneity of neurodegenerative diseases, various difficulties are encountered in diagnosing disease subtypes and developing effective treatment approaches. In recent years, microRNAs (miRNAs) have become efficient genetic biomarkers for several diseases. miRNAs regulate gene expressions post-transcriptionally and thus play a role in numerous neuronal and non-neuronal cell functions. Prior investigations have indicated the expression of miRNAs to become altered under pathological conditions, thereby suggesting that they may play a role in neurodegenerative diseases. This review focuses on the function of miRNAs in neurodegeneration and the possible contribution of altered levels of miRNAs and their target mRNAs in AD and PD patients compared to the controls shown in the previous studies. In short, altered expressions of miRNAs may play a role as potential diagnostic biomarkers with regard to neurodegenerative diseases.

**Keywords:** miRNAs, biomarker, neurodegenerative diseases, Alzheimer's disease, Parkinson's disease

## INTRODUCTION

### Neurodegenerative Diseases

Neurodegenerative diseases are associated with the progressive loss of neurons and are leading causes of death worldwide after cancer and cardiovascular diseases. Many different neurodegenerative diseases occur, but the most prevalent ones are Amyotrophic Lateral Sclerosis, Huntington's disease, Alzheimer's disease (AD), and Parkinson's disease (PD). Diseases occur in hereditary or sporadic forms depending on genetic and environmental factors (1). Although similar features are observed at the cellular level, the most important difference among these diseases is the affected cell and tissue types. For instance, while AD mainly occurs due to neuronal loss in the hippocampus and neocortex, the cells most affected in PD are dopaminergic neurons in the substantia nigra (1, 2).

Because of the wide heterogeneity of neurodegenerative diseases, both genetically and clinically, their prevalence also varies (3). About 6.7 million AD patients aged 65 and older were estimated to exist in the USA in 2023; however, approximately 930,000 Americans ( $\geq 65$  years) had been diagnosed with PD in 2020 (4, 5). In addition, this heterogeneity causes failures in diagnosing and distinguishing among disease subtypes and determining preferentially effective treatment methods. When diagnosing a disease, several different techniques can be applied separately or in combination. In the case of AD, monitoring methods such as positron emission tomography (PET) and magnetic resonance imaging (MRI) can be used, as well as cerebrospinal fluid (CSF) biomarkers such as amyloid beta ( $A\beta$ ) 42 and phospho-tau.  $A\beta$ 42 forms plaques and phospho-tau forms neurofibrillary tangles in the brain, contributing to the pathology of AD (6). Meanwhile,  $\alpha$ -synuclein in CSF and serum is a biomarker

**Corresponding Author:** Emrah Yucesan **E-mail:** emrah.yucesan@iuuc.edu.tr

**Submitted:** 24.11.2023 **Revision Requested:** 17.01.2024 **Last Revision Received:** 23.01.2024 **Accepted:** 05.02.2024 **Published Online:** 25.03.2024



Content of this journal is licensed under a Creative Commons Attribution-NonCommercial 4.0 International License.

for PD. In addition, PET, transcranial sonography (TCS), and dopamine transporter single-photon emission computed tomography (DAT SPECT) techniques can also be used in clinical diagnosis (7, 8).

The biochemical markers and imaging methods mentioned above have variable sensitivities and specificities (9). Moreover, due to the lack of curative treatments for almost all neurodegenerative diseases, the need for early diagnosis and effective therapeutic approaches before disease onset are absolutely present (10). Typically, AD and PD result from pathological instability influencing varied types of neurons at a diverse range of levels. This instability can be identified by alterations in the epigenome (9). MicroRNAs (miRNAs) control gene expression post-transcriptionally and have become a focus in this context (11).

### miRNAs and Therapeutic Implementations

miRNAs are small, endogenous non-coding RNA molecules about 21-25 nucleotides in length. The biogenesis of miRNAs starts in the nucleus finishes in the cytoplasm (12). Each miRNA contains an evolutionary conserved region 2-8 nucleotides long called the seed region. The 3' untranslated region (3'UTR) of the target messenger RNAs (mRNAs) contain complementary sequences to these seed regions, and thus miRNAs control gene expression by degrading mRNAs or inhibiting translation (1). A single miRNA may inhibit the translation of several mRNAs, and numerous miRNAs may control the same mRNA (13). In addition, miRNAs have critical roles in many biological processes, such as apoptosis, proliferation in response to immune stimuli, and differentiation (14–16). Thus, miRNAs' altered levels of expression have been associated with many diseases (1). Examining miRNA expression levels enables one to better understand the molecular pathology of diseases and can be used as potential biomarkers for the early diagnosis of disease. Roughly 70% of miRNAs are produced in the nervous system in humans and are involved in primary signaling pathways (17). Therefore, researchers in recent years have concentrated on examining impaired miRNA expression in brain development and neurodegeneration, with altered expression levels of specific miRNAs having been observed in distinct neurodegenerative diseases, including AD and PD (18).

In addition to the features mentioned above, various studies are present in the literature on miRNAs being used for therapeutic purposes. For instance, decreased expression of miR-125b has been associated with neurotoxic effects in AD, with up-regulated expression of miR-125b by 17 $\beta$ -estradiol being shown to protect neurons from neurotoxicity (19). In addition, miR-206 has been shown to promote the detrimental effect of Ass42 and to be up-regulated in the temporal cortex of the human brain in AD (20). Donepezil, a miR-206 inhibitor, can relieve the detrimental effects of Ass42 (21). As another example, miRNA's rejuvenation of miR-150 mimics reduced inflammatory cytokines in PD (22). MiR-7 mimics, which are used to recover miR-7 downregulation, have also been shown

in MPTP-induced Parkinsonian mice to reduce dopaminergic degeneration and to inhibit microglial activation (23). Another study showed the inhibition of miR-181 in PD to protect against neurodegeneration induced by alpha-synuclein overexpression (24).

As noted above, the positive results obtained from experimental processes conducted with the help of anti-miR have directed researchers towards implementing clinical applications using this approach. As examples, the anti-miR study (ClinicalTrials.gov Identifier: NCT04619420) that is currently in Phase 2 of a clinical trial for treating AD, cognitive dysfunction, and dementia and started on January 6, 2021 is present. That study has reported expectation to finish up on November 5, 2025 and includes 480 individuals. Another clinical study (ClinicalTrials.gov Identifier: NCT05462106) is in Phase 1 and 2 for the treatment of AD. It includes 140 individuals and was initiated on June 21, 2021, with completion planned for June 2026. In addition, a Phase 3 study (ClinicalTrials.gov Identifier: NCT02670083) was conducted between March 22, 2016, and May 31, 2019 with the participation of 813 individuals and aimed to treat AD. All the findings from these studies indicate that future clinical implications will occur regarding anti-miR applications and that more similar studies will be conducted.

### miRNAs in Alzheimer's Disease

AD is the most prevalent neurodegenerative disease and is characterized with a loss of neurons, memory loss, and cognitive impairments (25). Patients with AD are seen to express typical features such as personality changes, alterations in emotion, unsuitable social behaviors, and advanced memory impairments (26). Because aging is a significant risk for neurodegenerative diseases, the threat of AD progressing mainly elevates after the age of 65 (27). Ass peptide aggregation and neurofibrillary tangle accumulation due to tau phosphorylation in AD cause amyloidosis, neuronal loss, neuroinflammation, synaptic plasticity, and oxidative stress (28). The etiology of AD remains unclear because of the complexity of the cause and molecular mechanism of the disease; however, accumulation of extracellular Ass peptides and neurofibrillary tangles along with neuroinflammation form the essential biomarkers of AD (26). Because changes in miRNA expression contribute to AD pathogenesis, they could also be used as potential diagnostic biomarkers for the disease (29). In recent years, changes in the expression of many miRNAs have become associated with AD pathogenesis. For instance, miR-9 is a miRNA expressed in the nervous system and related to control of the morphological differentiation of post-mitotic neuronal cells; its level of expression is also seen to change in AD (30). Souza et al. conducted a study in 2020 to investigate the peripheral miR-9-5p expressions of 36 AD patients and 38 healthy controls using quantitative real-time polymerase chain reaction (qRT-PCR). They observed the expression of miR-9-5p in AD patients to have decreased 3-fold in comparison to the controls (31). Similarly, another study conducted by Yilmaz et al. in 2016 with 172 AD patients and 109 healthy controls

demonstrated the AD patients to have an approximately 5-fold decrease in miR-9-5p expression (32). As another example, the miR-29 family of miRNAs are known to post-transcriptionally regulate *BACE1* expression, with the expression of miR-29 being shown to be reduced in AD, resulting in increased *BACE1* expression and increased Ass accumulation (33). A study conducted by Hébert et al. in 2008 evaluated miR-29a and miR-29b-1 expression levels for 11 AD patients with elevated *BACE1* expression levels, 23 AD patients with normal *BACE1* expression levels, and 21 healthy controls using qRT-PCR. Their study showed the expression of miR-29a and -29b-1 to mainly decrease in AD patients, particularly those with elevated *BACE1* expression levels (33). Another miRNA family that suppresses *BACE1* expression is miR-15 (34). The miR-15 family has also been found to have a function in the apoptosis of neurons and tau phosphorylation. As an example of the importance of miR-15, a study conducted by Wu et al. in 2020 included 40 AD patients and 31 healthy controls. Their study examined the expression of 816 blood miRNAs in samples taken from 71 participants and observed essential variations in the expression levels of 71 miRNAs between the AD and control groups. Based on their study's results, they observed a decrease in the miR-15b expression in particular, compared to the controls (35). In addition to down-regulated miRNAs, other miRNAs are found to be upregulated in AD. Examples of the upregulated miRNAs can be given as miR-195, miR-106b-3p, and miR-34a (26). A study performed by Zang et al. in 2021 included 117 AD patients and 106 healthy controls; their study also evaluated the serum miR-128 level using qRT-PCR and found miR-128 expression to have significantly increased (36). Another study showed miR-128 to downregulate the expression of *PPAR-γ* and to intensify the Aβ-induced damage survival of neurons in AD (37). Thus, upregulated miR-128 can have a remarkable function in AD's progression. When taking the aforementioned into account, miRNAs obviously have essential roles in both the etiopathogenesis of AD and possess significant potential as genetic biomarkers. These details will be specified below through the similar features that are seen in PD.

### miRNAs in Parkinson's Disease

PD is the second most common neurodegenerative disease associated with the advanced loss of neurons in the brain, especially dopaminergic neurons in the substantia nigra. Degeneration of these neurons in PD patients may result in impaired motor function and clinical signs such as rigidity, postural instability, resting tremor, and bradykinesia, which are associated with a reduction in dopaminergic neurons (38). PD onset occurs generally after the age of 60 years and includes the interaction of genetic and elevated-risk environmental factors such as the consumption of dairy products, pesticides, traumatic brain injury, and a history of melanoma (39). PD involves the accumulation of α-synuclein in the Lewy bodies, which then impairs various pathways and activates neuroinflammation (40). Motor dysfunction begins to develop after approximately 70% of the dopaminergic neurons in the substantia nigra have degenerated. This early phase of PD takes 8-17 years

and involves complex mechanisms. Thus, the presence of preclinical biomarkers for PD is essential to the development of future neuroprotective approaches (41). Several specific miRNAs have been shown many times in the literature to have a function in the pathogenesis of PD. For example, Wu et al. in 2022 investigated *SNCA*-associated miRNA expressions in 75 PD patients and 73 healthy controls using qRT-PCR and found miR-153 and miR-223 expression levels to have decreased mainly in the PD patients compared to the controls (42). In 2020, Li et al. showed miR-150 to be another down-regulated miRNA in PD pathogenesis. They evaluated neuroinflammation-associated miR-150 expression in 80 PD patients and 60 healthy controls and ascertained miR-150 expression to have decreased in the PD patients when compared to the controls (22). In addition, the literature has shown up-regulated miRNA expression to occur in PD pathogenesis. For instance, miR-132 is an miRNA that has been negatively correlated with its downstream molecule nuclear receptor *NURR1* (also known as *NR4A2*), which is one of the main factors that sustain dopaminergic features. Yang et al. conducted a study in 2019 involving 667 people (269 sporadic PD patients, 222 healthy controls, and 176 individuals with several non-PD neurodegenerative diseases). They evaluated the expression levels of miR-132 and *NURR1* and indicated miR-132 expression levels to be elevated in PD patients when compared to the healthy and non-PD controls. *NURR1* was also crucially reduced in the PD patients compared to the healthy and non-PD controls, thus showing a negative correlation between reduced levels of *NURR1* expression and increased levels of miR-132 expression in PD (43). As mentioned above, the miR-29 family has decreased levels in AD pathogenesis. In addition, these miRNAs (miR-29a, -29b, and -29c) have been related to cognitive impairment in PD, with Han et al. assessing miR-29 expression levels in 98 PD patients and 40 healthy controls to examine this. They classified patients into three groups: PD patients with usual conditions (n = 39), PD patients with dementia (n = 22), and PD patients with mild cognitive impairment (n = 37) and found all miRNAs to be down-regulated in all three groups of patients compared to the healthy control group. In addition, they found the miR-29 expression levels in the PD patients with dementia to be lower than that for PD patients with normal conditions, thus relating the decreasing trend of these miRNAs to more severe PD (44). When considering the roles miRNAs play in physiological and pathological conditions alongside the alteration of their expression in diseases, miRNAs have the potential to serve as biomarkers for the early diagnosis and prognosis of disease and also as targets for therapeutic intervention.

### CONCLUSION

As explained with the examples above, miRNAs play important roles in many physiological conditions, with miRNA down-regulation having been able to be associated with many pathological states. Obviously, miRNAs also have a function in the molecular etiopathogenesis of neurodegenerative diseases. This role may involve up-regulation or down-regulation, as is the case in AD and PD, the two most common

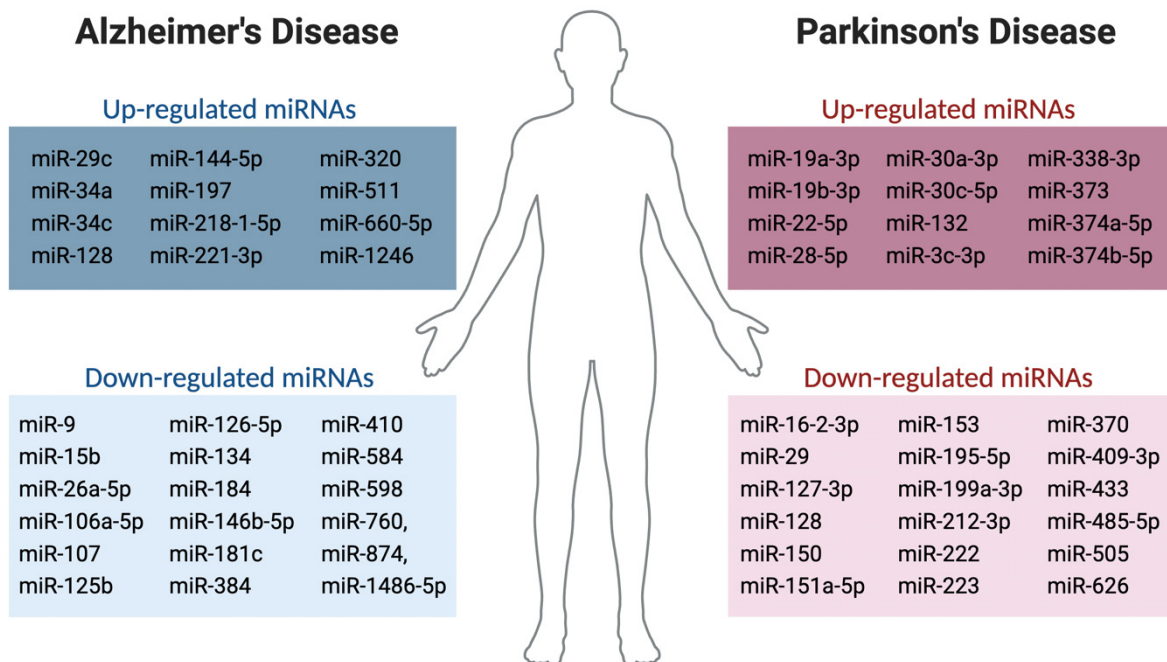


**Figure 1.** miRNAs alterations in Alzheimer's and Parkinson's diseases.

neurodegenerative diseases exemplified in this review. Figure 1 shows several upregulated and downregulated miRNAs in AD and PD (32, 33, 35, 45–48). The number of studies evaluating miRNAs will undoubtedly increase in the future, and several reasons are thought to exist for this. First of all, significance in demonstrating the roles miRNAs have regarding the clarification of the mechanisms and progression of neurodegenerative diseases. Another reason is the potential miRNAs have as genetic biomarkers. The most important aspect of this is that many studies have shown miRNAs to be able to be utilized in the early diagnosis and follow-up of the disease. Lastly, attempts have been made to develop various therapeutic approaches utilizing the regulatory functions of miRNAs, especially in recent years. Anti-miR oligonucleotides, antagomirs, locked nucleic acid anti-miRs, and miR masks that are used to suppress miRNAs, as well as miRNA expression vectors and miRNA mimics that are used to restore miRNA expression reveal other aspects of the importance these small non-coding molecules have (1).

This article has compiled up-to-date information on the subject of the functions miRNAs have in neurodegeneration by evaluating the case of AD and PD. As mentioned above, this study assumes that studies in this field will gain more importance and increase in number in the future.

D.G.A.; Drafting Manuscript- M.Y.; Critical Revision of Manuscript- E.Y., D.G.A.; Final Approval and Accountability- E.Y., M.Y., D.G.A.

**Conflict of Interest:** The authors declare that they have no competing interests.

**Financial Disclosure:** The authors declare that this study has received no financial support.

## REFERENCES

- Roy B, Lee E, Li T, Rampersaud M. Role of miRNAs in neurodegeneration: from disease cause to tools of biomarker discovery and therapeutics. *Genes (Basel)* 2022; 13(3): 425.
- Scheff SW, Price DA. Alzheimer's disease-related alterations in synaptic density: neocortex and hippocampus. *J Alzheimers Dis* 2006; 9(3 Suppl): 101-15.
- Ringman JM, Goate A, Masters CL, Cairns NJ, Danek A, Graft- Radford N, et al. Genetic heterogeneity in alzheimer disease and implications for treatment strategies. *Curr Neurol Neurosci Rep* 2014; 14(11): 499.
- 2022 Alzheimer's disease facts and figures. *Alzheimers Dement* 2022; 18(4): 700–89.
- Marras C, Beck JC, Bower JH, Roberts E, Ritz B, Ross GW, et al. Prevalence of Parkinson's disease across North America. *NPJ Parkinson's Disease* 2018; 4(1): 1–7.
- Ausó E, Gómez-Vicente V, Esquivá G. Biomarkers for Alzheimer's disease early diagnosis. *J Pers Med* 2020; 10(3): 1–27.
- Zubelzu M, Morera-Herreras T, Irastorza G, Gómez-Esteban JC, Murueta-Goyena A. Plasma and serum alpha-synuclein as a biomarker in Parkinson's disease: a meta-analysis. *Parkinsonism Relat Disord* 2022; 99: 107–15.

**Peer-review:** Externally peer-reviewed.

**Author Contributions:** Conception/Design of Study- E.Y., M.Y., D.G.A.; Data Acquisition- E.Y., M.Y.; Data Analysis/Interpretation- E.Y., M.Y.,

8. Suwijn SR, van Boheemen CJM, de Haan RJ, Tissingh G, Booij J, de Bie RMA. The diagnostic accuracy of dopamine transporter SPECT imaging to detect nigrostriatal cell loss in patients with Parkinson's disease or clinically uncertain parkinsonism: a systematic review. *EJNMMI Res* 2015; 5(1): 12.
9. Mayo S, Benito-León J, Peña-Bautista C, Baquero M, Cháfer-Pericás C. Recent evidence in epigenomics and proteomics biomarkers for early and minimally invasive diagnosis of Alzheimer's and Parkinson's diseases. *Curr Neuropharmacol* 2021; 19(8): 1273–303.
10. Manna I, de Benedittis S, Quattrone A, Maisano D, Iaccino E, Quattrone A. Exosomal miRNAs as potential diagnostic biomarkers in Alzheimer's disease. *Pharmaceuticals (Basel)* 2020; 13(9): 1–16.
11. Viswambharan V, Thanseem I, Vasu MM, Poovathinal SA, Anitha A. miRNAs as biomarkers of neurodegenerative disorders. *Biomark Med* 2017; 11(2): 151–67.
12. Idda ML, Munk R, Abdelmohsen K, Gorospe M. Noncoding RNAs in Alzheimer's disease. *Wiley Interdiscip Rev RNA* 2018; 9(2): 10.1002/wrna.1463.
13. Anglicheau D, Muthukumar T, Suthanthiran M. MicroRNAs: small RNAs with big effects. *Transplantation* 2010; 90(2): 105–12.
14. Bueno MJ, De Castro IP, Malumbres M. Control of cell proliferation pathways by microRNAs. *Cell Cycle* 2008; 7(20): 3143–8.
15. Su Z, Yang Z, Xu Y, Chen Y, Yu Q. MicroRNAs in apoptosis, autophagy and necroptosis. *Oncotarget* 2015; 6(11): 8474–90.
16. Leung AKL, Sharp PA. MicroRNA functions in stress responses. *Mol Cell* 2010; 40(2): 205–15.
17. Nowak JS, Michlewski G. miRNAs in development and pathogenesis of the nervous system. *Biochem Soc Trans* 2013; 41(4): 815–20.
18. Bushati N, Cohen SM. MicroRNAs in neurodegeneration. *Curr Opin Neurobiol* 2008; 18(3): 292–6.
19. Micheli F, Palermo R, Talora C, Ferretti E, Vacca A, Napolitano M. Regulation of proapoptotic proteins Bak1 and p53 by miR-125b in an experimental model of Alzheimer's disease: Protective role of 17 $\beta$ -estradiol. *Neurosci Lett* 2016; 629: 234–40.
20. Lee ST, Chu K, Jung KH, Kim JH, Huh JY, Yoon H, et al. miR-206 regulates brain-derived neurotrophic factor in Alzheimer disease model. *Ann Neurol* 2012; 72(2): 269–77.
21. Wang CN, Wang YJ, Wang H, Song L, Chen Y, Wang JL, et al. The anti-dementia effects of donepezil involve miR-206-3p in the hippocampus and cortex. *Biol Pharm Bull* 2017; 40(4): 465–72.
22. Li H, Yu L, Li M, Chen X, Tian Q, Jiang Y, et al. MicroRNA-150 serves as a diagnostic biomarker and is involved in the inflammatory pathogenesis of Parkinson's disease. *Mol Genet Genomic Med* 2020; 8(4): e1189.
23. Zhou Y, Lu M, Du RH, Qiao C, Jiang CY, Zhang KZ, et al. MicroRNA-7 targets nod-like receptor protein 3 inflammasome to modulate neuroinflammation in the pathogenesis of Parkinson's disease. *Mol Neurodegener* 2016; 11(1): 28.
24. Stein CS, McLendon JM, Witmer NH, Boudreau RL. Modulation of miR-181 influences dopaminergic neuronal degeneration in a mouse model of Parkinson's disease. *Mol Ther Nucleic Acids* 2022; 28: 1–15.
25. Vahia VN. Diagnostic and statistical manual of mental disorders 5: a quick glance. *Indian J Psychiatry* 2013; 55(3): 220.
26. Zhao Y, Zhang Y, Zhang L, Dong Y, Ji H, Shen L. The potential markers of circulating microRNAs and long non-coding RNAs in Alzheimer's disease. *Aging Dis* 2019; 10(6): 1293–301.
27. Hickman RA, Faustin A, Wisniewski T. Alzheimer Disease and its growing epidemic: risk factors, biomarkers, and the urgent need for therapeutics. *Neuro Clin* 2016; 34(4): 941–53.
28. Calabrò M, Rinaldi C, Santoro G, Crisafulli C. The biological pathways of Alzheimer disease: a review. *AIMS Neurosci* 2020; 8(1): 86–132.
29. Zhao Y, Jaber V, Alexandrov PN, Vergallo A, Lista S, Hampel H, et al. microRNA-based biomarkers in Alzheimer's disease (AD). *Front Neurosci* 2020; 14: 585432.
30. Yuva-Aydemir Y, Simkin A, Gascon E, Gao FB. MicroRNA-9: functional evolution of a conserved small regulatory RNA. *RNA Biol* 2011; 8(4): 557–64.
31. Souza VC, Morais GS, Henriques AD, Machado-Silva W, Perez DIV, Brito CJ, et al. Whole-blood levels of microRNA-9 are decreased in patients with late-onset Alzheimer Disease. *Am J Alzheimers Dis Other Dement* 2020; 35: 1533317520911573.
32. Yllmaz ŞG, Erdal ME, Özge AA, Sungur MA. Can peripheral microRNA expression data serve as epigenomic (upstream) biomarkers of Alzheimer's disease? *OMICs* 2016; 20(8): 456–61.
33. Hébert SS, Horr  K, Nicolai L, Papadopoulou AS, Mandemakers W, Silaharoglu AN, et al. Loss of microRNA cluster miR-29a/b-1 in sporadic Alzheimer's disease correlates with increased BACE1/ beta-secretase expression. *Proc Natl Acad Sci USA* 2008; 105(17): 6415–20.
34. Gong G, An F, Wang Y, Bian M, Yu LJ, Wei C. miR-15b represses BACE1 expression in sporadic Alzheimer's disease. *Oncotarget* 2017; 8(53): 91551–7.
35. Wu HZY, Thalamuthu A, Cheng L, Fowler C, Masters CL, Sachdev P, et al. Differential blood miRNA expression in brain amyloid imaging-defined Alzheimer's disease and controls. *Alzheimers Res Ther* 2020; 12(1): 59.
36. Zhang M, Han W, Xu Y, Li D, Xue Q. Serum miR-128 serves as a potential diagnostic biomarker for Alzheimer's disease. *Neuropsychiatr Dis Treat* 2021; 17: 269–75.
37. Geng L, Zhang T, Liu W, Chen Y. Inhibition of miR-128 abates A $\beta$ -mediated cytotoxicity by targeting PPAR- $\gamma$  via NF- $\kappa$ B inactivation in primary mouse cortical neurons and Neuro2a cells. *Yonsei Med J* 2018; 59(9): 1096–106.
38. Balestrino R, Schapira AHV. Parkinson disease. *Eur J Neurol* 2020; 27(1): 27–42.
39. Ascherio A, Schwarzschild MA. The epidemiology of Parkinson's disease: risk factors and prevention. *Lancet Neurol* 2016; 15(12): 1257–72.
40. Hallett PJ, Engelender S, Isacson O. Lipid and immune abnormalities causing age-dependent neurodegeneration and Parkinson's disease. *J Neuroinflammation* 2019; 16(1):153
41. Cacabelos R. Parkinson's disease: from pathogenesis to pharmacogenomics. *Int J Mol Sci* 2017; 18(3): 551.
42. Wu L, Xu Q, Zhou M, Chen Y, Jiang C, Jiang Y, et al. Plasma miR-153 and miR-223 levels as potential biomarkers in Parkinson's disease. *Front Neurosci* 2022; 16: 865139.
43. Yang Z, Li T, Li S, Wei M, Qi H, Shen B, et al. Altered expression levels of microRNA-132 and Nurr1 in peripheral blood of Parkinson's disease: potential disease biomarkers. *ACS Chem Neurosci* 2019; 10(5): 2243–9.
44. Han L, Tang Y, Bai X, Liang X, Fan Y, Shen Y, et al. Association of the serum microRNA-29 family with cognitive impairment in Parkinson's disease. *Aging* 2020; 12(13): 13518–28.

45. Guo R, Fan G, Zhang J, Wu C, Du Y, Ye H, et al. A 9-microRNA signature in serum serves as a noninvasive biomarker in early diagnosis of Alzheimer's disease. *J Alzheimer's Dis* 2017; 60(4): 1365–77.
46. Burgos K, Malenica I, Metpally R, Courtright A, Rakela B, Beach T, et al. Profiles of extracellular miRNA in cerebrospinal fluid and serum from patients with Alzheimer's and Parkinson's diseases correlate with disease status and features of pathology. *PLoS One* 2014; 9(5): e94839.
47. Khoo SK, Petillo D, Kang UJ, Resau JH, Berryhill B, Linder J, et al. Plasma-based circulating microRNA biomarkers for Parkinson's disease. *J Parkinsons Dis* 2012; 2(4): 321–31.
48. He S, Huang L, Shao C, Nie T, Xia L, Cui B, et al. Several miRNAs derived from serum extracellular vesicles are potential biomarkers for early diagnosis and progression of Parkinson's disease. *Transl Neurodegener* 2021; 10(1): 1–12.

# A Clinical Sulfonamide Derivative Inhibits B-Raf Protein in Colorectal Cancer and Melanoma Cells. Is It a New Target for Cancer?

Emine Terzi<sup>1</sup> , Beyza Ecem Oz Bedir<sup>1</sup> 

<sup>1</sup>Department of Medical Biology, Faculty of Medicine, Ankara Yildirim Beyazit University, Ankara, Turkiye

ORCID ID: E.T. 0000-0001-9106-3848; B.E.O.B. 0000-0002-0596-834X

**Cite this article as:** Terzi E, Oz Bedir BE. A clinical sulfonamide derivative inhibits B-Raf protein in colorectal cancer and melanoma cells. Is it a new target for cancer? *Experimed* 2024; 14(1): 7-12.

## ABSTRACT

**Objective:** Colorectal cancer (CRC) is a type of cancer spreading quickly around the world. Melanoma is an aggressive and lethal form of skin cancer. One of the striking biomarkers in cancer is carbonic anhydrase (CA)-IX, which catalyzes the hydration of carbon dioxide (CO<sub>2</sub>). CA inhibitors are being used clinically and studied extensively in clinical research. This study aimed to examine the CA inhibitor acetazolamide (AZA) in terms of the B-Raf protein in colorectal cancer and the melanoma cell line.

**Materials and Methods:** HT29 human colorectal cancer cells and A375 human melanoma cells were cultured. The appropriate dose of AZA on the cells was determined by the WST-1 test. The enzyme-linked immunosorbent assay (ELISA) was used to determine the effect of AZA on the B-Raf protein in HT29 and A375 cells.

**Results:** HT29 and A375 cell lines treated with AZA showed a dramatic decrease in CA-IX levels ( $p < 0.05$ ). In addition, AZA significantly reduced B-Raf protein levels in the HT29 and A375 cell lines ( $p < 0.05$ , for both).

**Conclusion:** This study revealed AZA, a CA inhibitor, to be effective in CRC and melanoma. In future studies, combining the effects of AZA and B-Raf inhibitors may present an alternative approach in cancer treatment.

**Keywords:** Acetazolamide, B-Raf, carbonic anhydrase-IX, colorectal cancer, melanoma

## INTRODUCTION

Colorectal cancer (CRC) is a type of cancer responsible for 9.2% of cancer-related deaths. In terms of prevalence, it ranks second in women and third in men, with 5- and 10-year survival rates being 65% and 58%, respectively (1). CRC may be localized or metastasized in the lymph nodes. Most patients with CRC have been reported to have metastases in the liver. Endoscopic, surgical, and oncological treatment strategies exist for CRC (2). Due to being the most hazardous and aggressive form of skin cancer and comprising only about 5% of all cutaneous malignancies, melanoma is the primary cause of skin cancer-related mortality (3). Because of the high risk of spreading, research is being performed

to find risk factors and determine the best course of action for treatment.

Carbonic anhydrases (CAs) are metalloenzymes that contain Zn<sup>2+</sup>. They reversibly convert CO<sub>2</sub> into HCO<sub>3</sub><sup>-</sup>/H<sup>+</sup> and are processed to maintain pH homeostasis in an organism (4). Acetazolamide (AZA), a sulfonamide derivative, is clinically implemented in the treatment of glaucoma, epilepsy, and heart failure (5). CA-IX is a cancer-related isoform and is overexpressed in carcinomas of the uterus, cervix, kidney, esophagus, lung, breast, colon, and brain (4, 6). Studies on cell models have shown CA-IX to have a pH-regulating function under hypoxic conditions and to help maintain the slightly alkaline intracellular pH that is necessary for

**Corresponding Author:** Beyza Ecem Oz Bedir **E-mail:** beyzaecem.oz@hotmail.com

**Submitted:** 18.10.2023 **Revision Requested:** 12.11.2023 **Last Revision Received:** 23.01.2024 **Accepted:** 17.02.2024 **Published Online:** 25.03.2024



Content of this journal is licensed under a Creative Commons Attribution-NonCommercial 4.0 International License.

the survival of cancer cells (7). CA-IX has also been shown to be able to interact with many signaling pathways in cancer cells (8, 9).

Mitogen-activated protein kinase (MAPK) pathways are essential in the transition from extracellular signals to intracellular responses and regulate many cellular functions (10). MAPK signaling pathways consist of Ras, Raf, MEK, and extracellular-signal-regulated kinase (ERK) proteins. The cells inhibit apoptosis as a response to a variety of stress factors, such as radiation, hypoxia, hydrogen peroxide, and chemotherapeutic agents, to increase the survival of the cells (11, 12). The Ras-Raf-MEK-ERK cascade is a vital regulatory pathway for cell growth, proliferation, differentiation, and apoptosis. Signaling with this pathway typically occurs for various plasma membrane growth-factor receptors that activate Ras family GTPases. Activated Ras proteins can recruit, complex with, and activate members of the Raf kinase family in the plasma membrane. Raf proteins stimulate the MEK/ERK cascade and ensure the transcription of related genes. B-Raf is a protein kinase that phosphorylates serine/threonine, which is involved in this pathway and is an oncogenic marker for solid tumors such as melanoma, papillary thyroid carcinoma, colorectal carcinoma, and gliomas (13). B-Raf mutations are found in about 10% of CRC patients and are linked with a poor prognosis; they are also resistant to chemotherapeutic treatment. However, recently developed B-Raf inhibitors have been directed towards melanoma and shown significant clinical activity in CRC (14). The main limitations in the use of B-Raf inhibitors involve resistance development and the toxicity linked to B-Raf inhibition (15).

B-Raf oncogenic driver mutations are found in approximately 50% of cutaneous melanomas in which the Ras-Raf pathway has been altered. The most prevalent (90%) aberration in the B-Raf gene is the V600E/K mutation which is commonly seen in cutaneous melanoma (16, 17). Vemurafenib (VMF) (B-Raf inhibitor) and trametinib (MEK inhibitor) are among the compounds currently being used in the clinical treatment of melanoma. However, arthralgia, burnout, diarrhea, fever, photosensitivity, skin, ocular, and cardiovascular toxicity are the most frequent adverse effects of the treatment. In addition to the side effects, the main disadvantage of this form of therapy is that the cancer cells can develop resistance to the therapy (18).

CA-IX, which is overexpressed in many tumor types, is also a pH-regulating enzyme, thus making it a potential target for carcinogenesis. CA-IX inhibition returns extracellular pH to normal values, resulting in a delay in tumor growth. This study therefore predicts that targeting CA-IX would be valuable as an alternative mechanism of carcinogenesis. The main goal in this research is to assess the impact of AZA, a CA inhibitor, on the B-Raf protein in HT29 CRC and A375 melanoma cell lines. Detecting a relationship between CA-IX inhibition and the B-Raf protein can become a new approach in targeting the MAPK pathway. This is a preliminary study investigating the

potential a sulfonamide derivative has for inhibiting B-Raf in cancer treatment.

## MATERIALS AND METHODS

### Cell Experiments

Human colorectal cancer cells (HT29) and human melanoma cells (A375) were gifted by Dr. Tuba Ozdemir Sancı (Ankara Yıldırım Beyazıt University, Medical Faculty, Histology and Embryology Department). The cells were cultivated in Dulbecco's Modified Eagle Medium (DMEM), a high glucose medium (Biowest, L0102), with 10% heat-inactivated fetal bovine serum (FBS; Capricorn, FBS-HI-11A), 1% penicillin-streptomycin, 1% amphotericin, and 1% gentamycin at 37°C in a 5% CO<sub>2</sub> humidified chamber incubator. AZA and VMF were purchased from Sigma-Aldrich and SelleckChem, respectively. The cells were passaged with 80-90% confluency, and a trypsin-EDTA (Gibco, 25200-056) solution was used for detaching the cells.

### Inhibitor Preparation

The inhibitors used in the current study are AZA (Sigma, BCBZ9159) and VMF (Cayman Chemical, 1-800-364-9897). Due to the A375 and HT29 cell lines having the BRAFV600E mutation, the study evaluated VMF as a positive control. All inhibitors were prepared as stock solutions by dissolving them in dimethyl sulfoxide (DMSO) at a final concentration of 300 µM. Then HT29 and A375 cells were seeded into 6-well plates (0.3 × 10<sup>6</sup> cells/well) and tested for various concentrations of AZA, and VMF (0, 2.5, 5, 10, 25, 50, 100, 200 µM) for 24<sup>th</sup> and 48<sup>th</sup> hours.

### Cytotoxicity Assay (WST-1)

The WST-1 test was carried out to find out the appropriate dose of AZA and VMF on HT29 cells. The principle of this assay is that cellular mitochondrial dehydrogenases convert the tetrazolium salt WST-1 into formazan crystals. For the WST-1 test, the HT29 and A375 cells were seeded into 96-well plates and incubated. After incubation, AZA and VMF were prepared at concentrations of 0, 2.5, 5, 10, 25, 50, 100 and 200 µM and applied to the cells. The measurements were analyzed at the 24<sup>th</sup> and 48<sup>th</sup> hours. To eliminate the effects from DMSO, the concentrations were added to the negative control wells at a rate where AZA and VMF were dissolved along with the medium. 10 µL of the WST-1 solution (Cayman Chemical, 10008883) were added to each well and incubated at 37°C for 2-4 hours. Following incubation, the appropriate inhibitor concentration for the cells was determined by measuring at 450 nm. The following equation was used when calculating the viability values of the cells:

$$\text{Viability\%} = (\text{Average OD}_{\text{inhibitor}} \times 100) \div \text{Average OD}_{\text{control}}$$

While the following equation was used when calculating the inhibition value:

$$\text{Inhibition\%} = 100 - \left( \frac{\text{Average OD inhibitor} \times 100}{\text{Average OD control}} \right)$$

The inhibitor concentration values were converted into a graph by utilization of Graphpad Prism 9.1.0 software, after which the inhibitor dose (IC<sub>50</sub>) value that inhibited 50% of the cells was calculated. All experiments were performed in triplicates.

## ELISA

To prepare the cell lysate, phosphate-buffered saline (PBS) was first used to wash the cells. Next, a lysis buffer containing 50 mM Tris, 150 μM NaCl, 1% NP-40 (Intron Biotechnology, IBS-BN015) and proteinase inhibitor factor (Intron Biotechnology, PIC001) were used to lyse the cells, after this step, the cells were centrifuged (+4°C, 17,000 g, 15 min). The supernatant was then aliquoted.

The Enzyme-Linked Immunosorbent Assay (ELISA) was used to determine the changes in the CA-IX and B-Raf levels of AZA and VMF in the HT29 and A375 cell lines. The BT Lab Human Carbonic Anhydrase IX ELISA Kit (E2273Ha, BT Lab, China) and Human B-Raf ELISA kit (E3906Hu, BT Lab, China) were used in the study. Standard solutions were first prepared for the ELISA protocol. The standard solution contains 120 μL of standard (40 ng/mL) and 120 μL of standard diluent to create 20 ng/mL (CA-IX) and 2400 ng/L (B-Raf) standard stock solutions. The standard stock solution was diluted 1:2 to obtain 10 ng/mL, 5 ng/mL, 2.5 ng/mL and 1.25 ng/mL standard solutions for CA-IX and 1200 ng/L, 600 ng/L, 300 ng/L, and 150 ng/L for B-Raf. 50 μL of all standards were added to the wells. Next, 40 μL of biotinylated anti-CA-IX and 10 μL of anti-B-Raf antibody were added to the wells. Subsequently, 50 μL of streptavidin-HRP was added to all wells and incubated at 37°C for 60 minutes. After incubation, the wells were washed 5 times with a wash buffer, then 50 μL of substrate solution A and 50 μL of substrate solution B were added to each well. This was incubated at 37°C for 10 min in the dark. Following the incubation, analysis was conducted at 450 nm using the Thermo Scientific Varioskan™ Spectrophotometer.

## Statistical analyses

The statistical analysis was carried out using GraphPad Prism 9.1.0. The one-way analysis of variance (ANOVA) test was conducted for the B-Raf ELISA test and Student's t-test for the CA-IX ELISA test. The statistical significance level was determined as p<0.05.

## RESULTS

The HT29 and A375 cells were treated with AZA and VMF at doses of 0, 2.5, 5, 10, 25, 50, 100, and 200 μM at the 24<sup>th</sup> and 48<sup>th</sup> hours to help determine the appropriate cytotoxic dose for the cells. According to WST-1 results, viability rates for the HT29 cells treated with AZA for 24 hours were 100%, 100%, 94%, 87%, 50%, 35%, 30%, and 17% at respective concentrations of 0, 2.5, 5, 10, 25, 50, 100, and 200 μM. The IC<sub>50</sub> value for AZA is

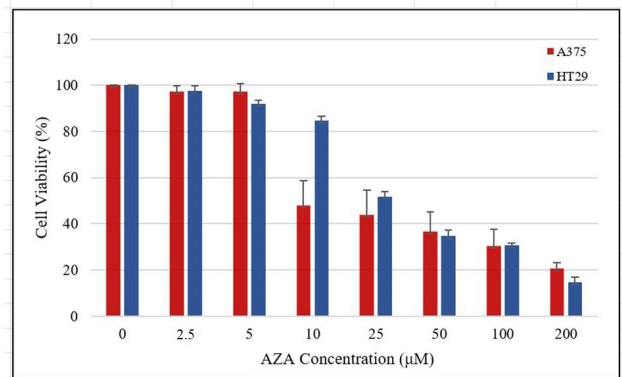


**Figure 1.** The % cell viability of the AZA-treated A375 and HT29 cells. The HT29 and A375 cells were treated with AZA at doses

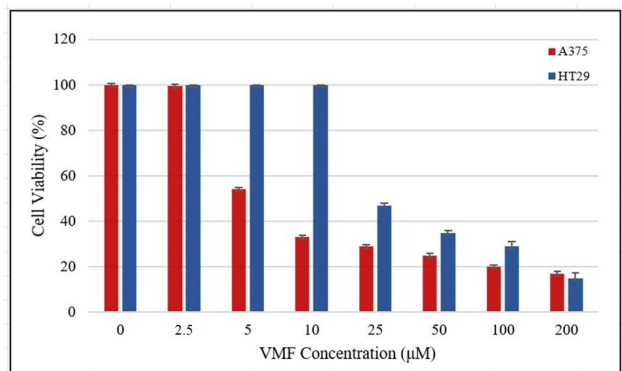


**Figure 2.** The % cell viability of the VMF-treated A375 and HT29 cells. The HT29 and A375 cells were treated with VMF at doses of 0, 2.5, 5, 10, 25, 50, 100, and 200 μM at the 24<sup>th</sup> and 48<sup>th</sup> hours.

found to be 34.71 μM. Viability rates for HT29 cells treated with VMF for 24 hours at concentrations of 0, 2.5, 5, 10, 25, 50, 100, and 200 μM were 100%, 100%, 100%, 100%, 48%, 35%, 27%, and 18%, respectively. The IC<sub>50</sub> value for VMF was found to be 35.84 μM (Figures 1, 2).

For the A375 melanoma cells, viability rates for cells treated with AZA for 24 hours were 100%, 100%, 54%, 33%, 29%, 25%, 20%, and 17% at respective concentrations of 0, 2.5, 5, 10, 25, 50, 100, and 200 μM. The IC<sub>50</sub> value for AZA was found to be 9.75 μM. Viability rates for the A375 cells treated with VMF for 24 hours at concentrations of 0, 2.5, 5, 10, 25, 50, 100, and 200 μM were 100%, 68%, 32%, 27%, 23%, 22%, 17%, and 14%, respectively. The IC<sub>50</sub> value for VMF was found to be 4.93 μM (Figures 1, 2).

In order to examine the integrity of the cells, an inverted microscope was used following 24 hours of AZA and VMF application. The numbers of HT29 and A375 cells were observed to have decreased significantly at the end of this period (Figures 3, 4).

The effects of AZA on CA-IX were determined using ELISA.

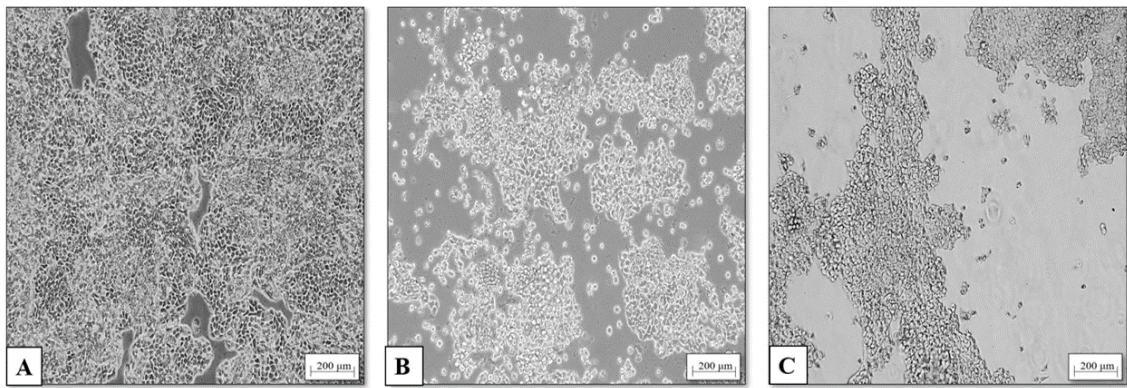


**Figure 3.** Inverted microscope images of the CRCs after 24<sup>th</sup> hour of inhibitor treatment. A) HT29 cells without an inhibitor B) AZA-treated HT29 cells C) VMF-treated HT29 cells (Bar = 200 µm) (AZA concentration = 34.71 µM, VMF concentration = 35.84 µM).

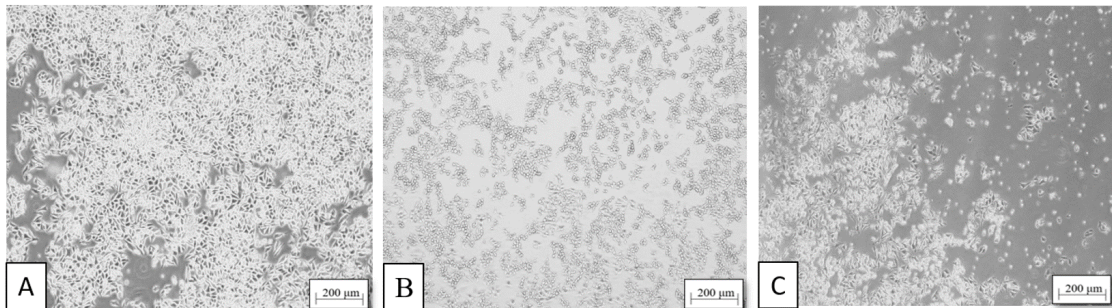


**Figure 4.** Inverted microscope images of the melanoma cells after 24<sup>th</sup> hour of inhibitor treatment: A) A375 cells without inhibitor; B) AZA-treated A375 cells; C) VMF-treated A375 cells (Bar = 200 µm) (AZA concentration = 34.71 µM, VMF concentration = 35.84 µM).

The change in CA-IX levels was determined by measuring the absorbance in cells with the presence and absence of AZA treatment. As a result, the concentration of CA-IX was found to be 5.93 ng/mL in the HT29 cells without AZA and 4.1 ng/mL in

the HT29 cells with AZA. Treating the HT29 cells with AZA was found to dramatically decrease CA-IX levels ( $p < 0.05$ ). For the A375 cell line, the concentration of CA-IX was found to be 6.36 ng/mL in cells without AZA and 3.46 ng/mL in cells with AZA.

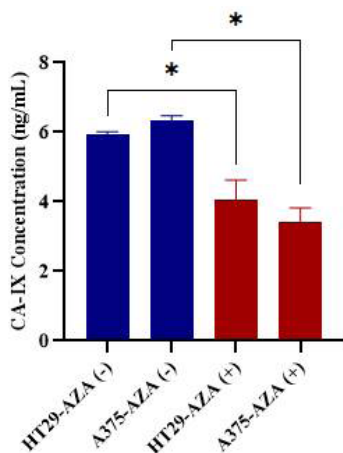


**Figure 5.** CA-IX protein levels in the control and AZA-treated HT29 and A375 cells. \*  $p < 0.05$

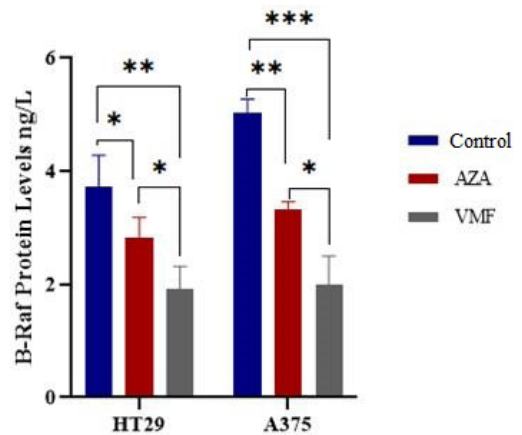


**Figure 6.** B-Raf protein levels in the control, AZA-treated, and VMF-treated HT29 and A375 cells. \*  $p < 0.05$ , \*\*  $p < 0.01$ , \*\*\*  $p < 0.001$

The CA-IX levels were shown to have considerably decreased in the A375 cells treated with AZA ( $p < 0.05$ ; Figure 5).

The effects of AZA on B-Raf protein levels in the HT29 and A375 cells were assessed using ELISA, with VMF being used as a positive control. As a result, B-Raf protein levels were found to be 3.7 ng/L in the negative control cells, 2.81 ng/L in the AZA-treated HT29 cells, and 1.94 ng/L in the VMF-treated positive control cells. When comparing the AZA-treated cells to the control cells, B-Raf protein levels were considerably lower in the AZA-treated cells ( $p < 0.05$ ). However, B-Raf protein levels were higher in the AZA-treated HT29 cells compared to the VMF-treated HT29 cells. VMF demonstrated a more effective inhibition effect than AZA ( $p < 0.05$ ). For the A375 cells, B-Raf protein levels were found to be 5.03 ng/L in the negative control cells, 3.36 ng/L in the AZA-treated cells, and 2 ng/L in the VMF-treated positive control cells. AZA was found to dramatically affect a decrease in the B-Raf protein levels compared to the control cells ( $p < 0.05$ ). However, B-Raf protein levels are higher in the AZA-treated A375 cells than in the VMF-treated A375 cells. VMF demonstrates a more effective inhibition than AZA ( $p < 0.05$ ; Figure 6).

## DISCUSSION

With approximately 900,000 deaths annually, CRC is amongst the deadliest cancers. Age, dietary habits, and smoking can be listed as the risk factors that affect the development of CRC. Surgery, chemotherapy, radiotherapy, and immunotherapy are currently being used in clinical treatments (19). Cancer signaling pathways trigger cell proliferation, angiogenesis, escape from apoptosis, and metastasis in CRC. One of the signaling pathways involved in these processes is the Ras-Raf-ERK pathway. Alterations in this pathway have been reported as targets for CRC therapy (20, 21). As a result, inhibiting this pathway is important as a molecular therapeutic approach in the treatment of CRC. B-Raf is located in MAPK's Ras-Raf-MEK-ERK signaling pathway and activates the transcription factors through phosphorylation of MEK and ERK. This activation regulates cell proliferation, survival, and growth (22).

Although melanoma is less common than other forms of skin cancer, it nevertheless causes over 73% of deaths from skin cancer (23, 24). Therapeutic approaches have improved understanding of melanoma pathogenesis in recent years, with activation of the MAPK pathway in melanoma being known to promote rapid tumor proliferation. The activator B-Raf mutation V600E and related mutations at this codon are critical to the MAPK signaling pathway in melanoma cell lines (25).

CA-IX is a tumor-associated CA isoenzyme, and CA-IX expression is induced through HIF-1. As a result, CA-IX might serve as a hypoxia marker and prognostic indicator. CA-IX is overexpressed in malignancies of the uterus, kidney, esophagus, and breast and in melanoma (4). CA-IX preserves cancer cells from hypoxia and intracellular acidity as the tumor grows. It promotes angiogenesis, extracellular matrix degradation, epithelial-mesenchymal transformation, invasiveness, tumor-

stroma cross-communication, and signaling by increasing extracellular acidosis. In addition, CA-IX can interact with several signaling pathways and mechanisms in cancerous cells (9). The phosphorylated IC residues of CA-IX have been shown to be associated with carcinogenesis. This has been suggested to perhaps stimulate intracellular signaling pathways (8). CA-IX is a promising target for anti-cancer therapy. AZA is the first diuretic agent of sulfonamides and is used for the inhibition of CA isoenzymes (26). Studies have shown AZA to reduce colony formation and regress tumor growth in various cancer types (27). The current study has planned to show the effect of AZA, a CA inhibitor, on B-Raf, an oncogenic protein, based on the association CA-IX has with cancer signaling pathways in the HT29 colorectal cancer and A375 melanoma cell lines. The study used the B-Raf inhibitor VMF as a positive control and observed AZA to reduce B-Raf protein levels significantly but not as effectively as VMF. No previous research is present in the literature, showing the effect of AZA on the B-Raf protein. However, studies are found to have shown the effect that sulfonamide-derived inhibitors have on the B-Raf protein. Tsai et al. showed difluorophenyl-sulfonamides to have high selectivity and potential for oncogenic B-Raf protein inhibition (28). VMF is a B-Raf inhibitor with a sulfonamide group targeting the BRAFV600E mutation. In addition, dabrafenib is another selective B-Raf inhibitor compound containing a sulfonamide group (29). Ali et al. suggested that imidazole derivative compounds containing terminal sulfonamide groups to be able to be potential inhibitors of BRAFV600E (30). This current preliminary study has determined AZA, a classical well-known sulfonamide derivative, to have an inhibitory effect on the B-Raf protein, in parallel with other studies.

Also in parallel with other studies, the current study has shown AZA, a sulfonamide-derived CA inhibitor, to have an inhibitory effect on B-Raf protein in CRC and melanoma. This study makes an important contribution to the literature in terms of targeting the B-Raf protein with different molecules and helping to develop new sulfonamide-derived inhibitors for cancer treatment. The investigation of AZA on the B-Raf gene in CRC and melanoma might serve as a guide for future research in this area.

---

**Ethics Committee Approval:** This study utilized commercially available cell lines HT29 and A375. Ethical approval was deemed unnecessary as the research did not involve human or animal subjects, nor did it entail primary cell cultures derived from human or animal subjects.

**Peer-review:** Externally peer-reviewed.

**Author Contributions:** Conception/Design of Study- E.T.; Data Acquisition- E.T.; Data Analysis/Interpretation- E.T., B.E.O.B.; Drafting Manuscript- E.T., B.E.O.B.; Critical Revision of Manuscript- B.E.O.B.; Final Approval and Accountability- B.E.O.B.

**Conflict of Interest:** The authors declare that they have no competing interests.

**Financial Disclosure:** The authors declare that this study has received no financial support.

## REFERENCES

- Li J, Ma X, Chakravarti D, Shalpour S, DePinho RA. Genetic and biological hallmarks of colorectal cancer. *Genes Dev* 2021; 35(11-12):787-820.
- Haraldsdottir S, Einarsdottir HM, Smaradottir A, Gunnlaugsson A, Halfdanarson TR. Krabbamein í ristli og endaparmi [Colorectal cancer - review]. *Laeknabladid* 2014; 100(2): 75-82.
- Villani A, Scalvenzi M, Micali G, Lacarrubba F, Fornaro L, Martora F, et.al. Management of advanced invasive melanoma: New strategies. *Adv Ther* 2023; 40(8): 3381-94.
- Takacova M, Holotnakova T, Barathova M, Pastorekova S, Kopacek J, Pastorek J. Src induces expression of carbonic anhydrase IX via hypoxia-inducible factor 1. *Oncol Rep* 2010; 23(3): 869-74.
- Kumar S, Rulhania S, Jaswal S, Monga V. Recent advances in the medicinal chemistry of carbonic anhydrase inhibitors. *Eur J Med Chem* 2021; 209: 112923.
- Pastorek J, Pastorekova S. Hypoxia-induced carbonic anhydrase IX as a target for cancer therapy: from biology to clinical use. *Semin Cancer Biol* 2015; 31: 52-64.
- Pastorekova S, Gillies RJ. The role of carbonic anhydrase IX in cancer development: links to hypoxia, acidosis, and beyond. *Cancer Metastasis Rev* 2019; 38(1-2): 65-77.
- Pastorekova S, Kopacek J, Pastorek J. Carbonic anhydrase inhibitors and the management of cancer. *Curr Top Med Chem* 2007; 7(9): 865-78.
- Ward C, Meehan J, Gray M, Kunkler IH, Langdon SP, Argyle DJ. Carbonic anhydrase IX (CAIX), cancer, and radiation responsiveness. *Metabolites* 2018; 8(1): 13.
- Lake D, Corrêa SA, Müller J. Negative feedback regulation of the ERK1/2 MAPK pathway. *Cell Mol Life Sci* 2016; 73(23): 4397-413.
- Roberts PJ, Der CJ. Targeting the Raf-MEK-ERK mitogen-activated protein kinase cascade for the treatment of cancer. *Oncogene* 2007; 26(22): 3291-310.
- Low HB, Zhang Y. Regulatory roles of MAPK phosphatases in cancer. *Immune Netw* 2016; 16(2): 85-98.
- Pakneshan S, Salajegheh A, Smith RA, Lam AK. Clinicopathological relevance of BRAF mutations in human cancer. *Pathology* 2013; 45(4): 346-56.
- Passardi A, Scarpi E, Ulivi P. Molecular and translational research on colorectal cancer. *Int J Mol Sci* 2020; 21(11): 4105.
- Mishra H, Mishra PK, Ekielski A, Jaggi M, Iqbal Z, Talegaonkar S. Melanoma treatment: from conventional to nanotechnology. *J Cancer Res Clin Oncol* 2018; 144(12): 2283-302.
- Jenkins RW, Fisher DE. Treatment of advanced melanoma in 2020 and beyond. *J Invest Dermatol* 2021; 141(1): 23-31.
- Davis LE, Shalin SC, Tackett AJ. Current state of melanoma diagnosis and treatment. *Cancer Biol Ther* 2019; 20(11): 1366-79.
- Lopes J, Rodrigues CMP, Gaspar MM, Reis CP. Melanoma management: from epidemiology to treatment and latest advances. *Cancers (Basel)* 2022; 14(19): 4652.
- Dekker E, Tanis PJ, Vleugels JLA, Kasi PM, Wallace MB. Colorectal cancer. *Lancet* 2019; 394(10207): 1467-80.
- Tabana YM, Dahham SS, Shah AM, Majid A. Major signaling pathways of colorectal carcinogenesis. *Recent Adv Colon Cancer* 2016; 1: 1-2.
- Previs RA, Coleman RL, Harris AL, Sood AK. Molecular pathways: translational and therapeutic implications of the Notch signaling pathway in cancer. *Clin Cancer Res* 2015; 21(5): 955-61.
- Li L, Zhao GD, Shi Z, Qi LL, Zhou LY, Fu ZX. The Ras/Raf/MEK/ERK signaling pathway and its role in the occurrence and development of HCC. *Oncol Lett* 2016; 12(5): 3045-50.
- Carr S, Smith C, Wernberg J. Epidemiology and risk factors of melanoma. *Surg Clin North Am* 2020; 100(1): 1-12.
- Nicholas S, Mathios D, Jackson C, Lim M. Metastatic melanoma to the brain: surgery and radiation is still the standard of care. *Curr Treat Options Oncol* 2013; 14(2): 264-79.
- Garbe C, Eigentler TK. Vemurafenib. *Recent Results Cancer Res* 2018; 211: 77-89.
- Supuran CT. Carbonic anhydrase inhibitors and their potential in a range of therapeutic areas. *Expert Opin Ther Pat* 2018; 28(10): 709-12.
- Mokhtari RB, Kumar S, Islam SS, Yazdanpanah M, Adeli K, Cutz E, et. al. Combination of carbonic anhydrase inhibitor, acetazolamide, and sulforaphane, reduces the viability and growth of bronchial carcinoid cell lines. *BMC Cancer* 2013; 13:378.
- Tsai J, Lee JT, Wang W, Zhang J, Cho H, Mamo S, et.al. Discovery of a selective inhibitor of oncogenic B-Raf kinase with potent antimelanoma activity. *Proc Natl Acad Sci U S A* 2008; 105(8): 3041-6.
- Bellón T, Lerma V, González-Valle O, González Herrada C, de Abajo FJ. Vemurafenib-induced toxic epidermal necrolysis: possible cross-reactivity with other sulfonamide compounds. *Br J Dermatol* 2016; 174(3): 621-4.
- Ali EMH, Abdel-Maksoud MS, Ammar UM, Mersal KI, Ho Yoo K, Jooryeong P, et.al. Design, synthesis, and biological evaluation of novel imidazole derivatives possessing terminal sulphonamides as potential BRAFV600E inhibitors. *Bioorg Chem* 2021; 106: 104508.

# Evaluating the Effect of Applying Cathodal tDCS to the Left Dorsolateral Prefrontal Cortex on Visual Working Memory

Yunus Emre Oksuz<sup>1</sup> , Gokcer Eskikurt<sup>2</sup> 

<sup>1</sup>Department of Neuroscience, Istinye University, Istanbul, Turkiye

<sup>2</sup>Department of Psychology, Faculty of Humanities and Social Sciences, Istinye University, Istanbul, Turkiye

ORCID ID: Y.E.O. 0000-0002-2952-3759; G.E. 0000-0003-4898-8639

**Cite this article as:** Oksuz YE, Eskikurt G. Evaluating the effect of applying cathodal tDCS to the left dorsolateral prefrontal cortex on visual working memory. *Experimed* 2024; 14(1): 13-20.

## ABSTRACT

**Objective:** Contemporary research has studied non-invasive brain stimulation modalities regarding their impact on various cognitive functions, particularly in the areas of learning and memory. Studies are being pursued to delve into the manipulation of these cognitive facets through this methodology. The aim of the current study was to examine the effects of application of cathodal transcranial direct current stimulation (tDCS) to the left dorsolateral prefrontal cortex (DLPFC), on visual working memory.

**Materials and Methods:** The study consisted of two separate groups, an active and a sham group, in which a total of 42 university students participated. Two mA cathodal direct current was applied to the left dorsolateral prefrontal cortex. To measure visual working memory, the study applied a visual 1-back task consisting of Chinese letters before and after tDCS and compared the obtained data.

**Results:** The study observed significant differences between the active and sham groups, with the active group having an increased number of omissions, a decreased number of correct responses, and prolonged response times.

**Conclusion:** The findings of the study revealed the suppressive effect of cathodal tDCS on visual working memory. Studies in the literature revealed various results regarding the contributions of left and right DLPFC on working memory. The findings of this study showed that right DLPFC also has an effect on visual working memory.

**Keywords:** Working memory, tDCS, *n*-back task

## INTRODUCTION

Memory-related studies began in the 18<sup>th</sup> century and have continued to the present day. The scholarly work titled "The Magical Number Seven, Plus or Minus Two," authored by Miller, could be assumed to have exerted a profound influence on the conceptualization of short-term memory. Miller's study emphasized individuals to be able to typically hold an average of seven numbers in their short-term memory and underscored this capacity to be able to vary with individual differences (1).

Within the realm of contemporary psychological discourse, the multicomponent model as propounded by Baddeley and Hitch in 1974 has garnered widespread acceptance. This theoretical framework encompasses three fundamental constituents: the phonological loop, the visuospatial sketchpad, and the central executive (2).

This study focused on the temporary retention of visual information in the visuospatial sketchbook (3).

To date, experimental research has provided evidence that both the right and left dorsolateral prefrontal cortex (DLPFC) are involved in numerous cognitive functions,

**Corresponding Author:** Yunus Emre Oksuz **E-mail:** yunusemreksuz@msn.com

**Submitted:** 21.11.2023 **Revision Requested:** 18.01.2024 **Last Revision Received:** 27.01.2024 **Accepted:** 14.02.2024



Content of this journal is licensed under a Creative Commons Attribution-NonCommercial 4.0 International License.

including but not limited to learning, memory, and the study and processing of cognitive structures (4). This finding has played a significant role in accepting the notion that the DLPFC forms the core of working memory (5).

Transcranial direct current stimulation (tDCS) aims to stimulate brain tissue by placing anode and cathode electrodes on the scalp. When applying tDCS, anodal stimulation induces depolarization of the membrane potential in the targeted cerebral area, thus bringing it closer to the threshold (6). In contrast, cathodal stimulation induces hyperpolarization in the stimulated area (7).

Contemporary research provides examples where tDCS has been applied to manipulate cognitive performance. Nitsche et al. observed inhibition in the motor cortex following application of cathodal tDCS for 5-7 minutes. The same effect was reported to have been repeated in a new stimulation applied after an hour post-stimulation (8).

Another study on the left DLPFC gave participants forward and backward counting tasks after applying cathodal tDCS. That study presented participants with a 5-min 2-forward task followed by a 5-min 3-back task. The study revealed a significant difference between the active and sham groups, with the active group showing improved performance on the forward counting task, unlike the sham group. However, no significant difference was found in the execution of the backward counting task (9).

Another study on healthy adults divided 12 participants into two separate groups, one group receiving a 2 mA anodal tDCS and the other a sham stimulation. During and after the tDCS stimulation, participants were presented with 3-back tasks and Sternberg tasks. As a result of the study, the reaction time of the active group was shown to be decreased compared to the sham group (10).

A meta-analysis of brain imaging research on *n*-back tasks suggested the right DLPFC to be a region associated with both information manipulation (updating) and retention (11). The right DLPFC has been recognized to play a specific role in attentional control, which is closely related to selective attention and maintenance of task-related information (12). Meanwhile,

this region has also been shown to be important for inhibition control, such as the suppression of inappropriate responses (12, 13). Cathodal tDCS over the right DLPFC has been shown to be able to improve recognition memory performance by suppressing interference in the task, with cathodal tDCS on the right DLPFC also reported to significantly increase nonverbal recognition memory performance (14). Therefore, both anodal and cathodal tDCS of the right DLPFC may have the potential to improve working memory. A study examining the effect of tDCS applied to the right DLPFC on different components of working memory showed cathodal tDCS to facilitate the maintenance of working memory and anodal tDCS to have a suppressive effect (15). The literature contains studies showing the right DLPFC to be associated with non-verbal processes in working memory and the left DLPFC to be associated with verbal working memory (16-19). Recent studies have shown both types of stimulation applied to the right DLPFC to have a positive effect on visual working capacity (12-14). The aim of this current study was to examine the effects of application of cathodal tDCS to the left DLPFC on visual working memory, regarding the visual 1-back task.

## MATERIALS AND METHODS

The study involved the participation of 42 healthy university students between the ages of 18-30 who are right-handed and unfamiliar with Chinese characters. Two separate groups took part in the study: an active group and a sham group, with the participants being randomly assigned to the groups.

After the participants signed the informed consent form, they were informed about the tasks and procedures to be performed for about 5 minutes. The participants were then given a 1-minute trial test regarding a visual 1-back task. After the trial, participants performed a visual 1-back task lasting approximately 5 minutes. After completing the visual 1-back task, the participants were immediately applied 20 minutes of cathodal tDCS. After the tDCS, the other form of the visual 1-back task was administered. The whole experiment lasted approximately 1 hour, including the insertion and removal of the electrodes. All participants in this study gave signed informed consent before being included in the study. This

石 好 奇 店 面 女 信  
士 国 人 来 阳 行 男

Figure 1. Chinese letters used in the pretest.

性 空 跑 寿 命 生 去  
活 多 死 上 香 了 心

**Figure 2.** Chinese letters used in the posttest.

study was found ethically and scientifically appropriate by Istinye University, Clinical Research Ethics Committee, through decision no. 4/2023.K-14, thus obtained ethical approval.

### Visual 1-Back Task

The study gave participants a task consisting of 28 different Chinese characters to assess their visual working memory performance. The task is called the *n*-back task, in which the participants were asked to press the number 1 or number 2 key on the keyboard according to the characters displayed on the screen. The *n* value expresses the number of times the stimulus on the screen will be the same as the previous stimulus, with *n* = 1 in this study. Accordingly, the participants were asked to memorize the Chinese character shown on the screen. They were asked to press the number 1 key if the next stimulus was the same as what had been shown on the previous screen, or to press the number 2 key if it was different.

Although the participants became familiar with the characters during the pre-tDCS test (Figure 1), a different stimulus set was used in the post-tDCS (Figure 2). Stimuli consisting of Chinese characters were presented for 300 ms in the middle of a 24 cm x 42 cm screen using the program E-Prime 3.0 (Figure 3).

Responses during the test were given using a QWERTY Turkish keyboard, with the number 1 and number 2 keys on the right side of the keyboard being designated as the target and standard keys, respectively. During the administration, a total of 50 stimuli were presented to each participant, with 35% of these stimuli being identified as targets. Of the characters, 17 were categorized as "target" characters while 33 were categorized as "standard" characters. The stimuli were presented on the screen for 300 msc at 1500 msec intervals. When participants failed to press a key in time, the response was defined as an "omission" error. A response involving an incorrectly pressed key is defined as a "commission" error (Figure 4).

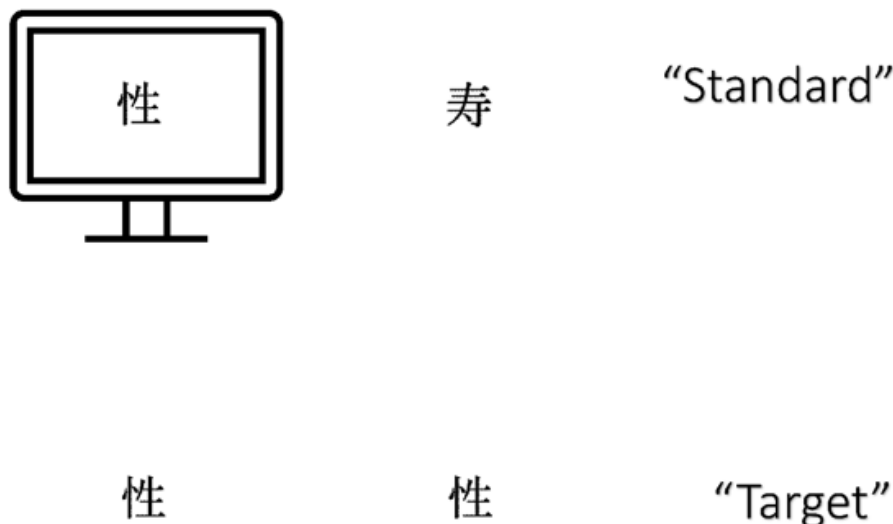


**Figure 3.** Task chart.

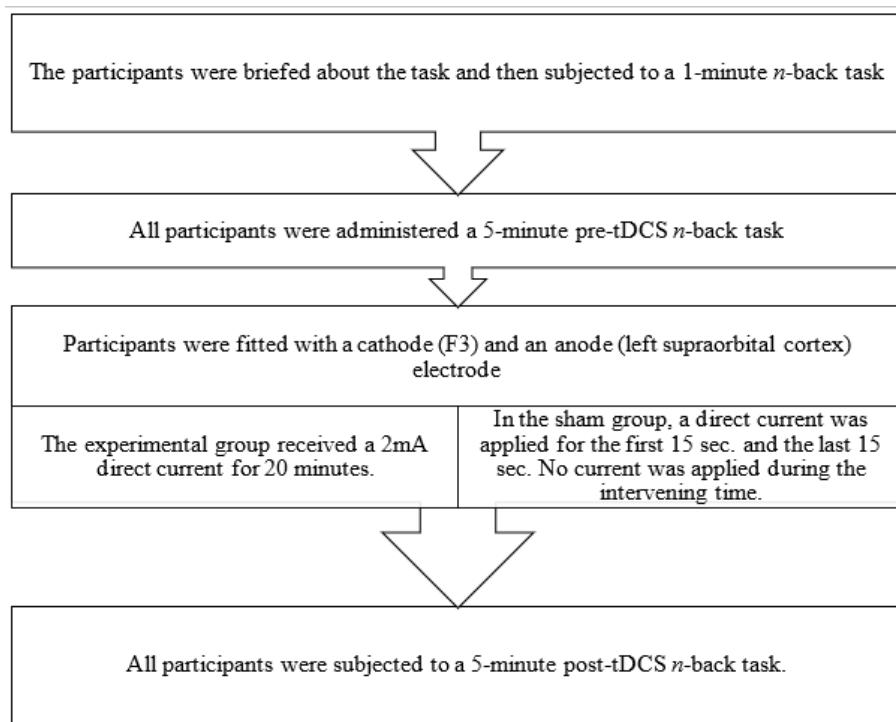


**Figure 4.** Experimental chart.

The study had the cathode electrode placed in the F3 region in accordance with the 10-20 EEG system and corresponding to the left DLPFC, with the anodal electrode placed on the left supraorbital cortex. The study uses electrodes measuring 5x7 cm<sup>2</sup> (Figure 5).

### Application of tDCS

The active group received 2 mA of direct current for 20 minutes. The sham group received a current that was increased to 2 mA within the first 15 seconds, continued for 15 seconds

upon reaching 2 mA, and then decreased to zero again within 15 seconds to create the sensation of having received the test current, with no current being applied for the rest of the time.

### Statistical Analyses

The data obtained from the visual 1-back task were analyzed using IBM-SPSS 26 software. As the values obtained did not fit the Gaussian distribution, nonparametric statistical methods were used for further analysis. In addition, between-group comparisons were evaluated using Mann-Whitney U test and within-group comparisons were evaluated using Wilcoxon test. Significance limit was accepted as  $p < 0.05$ .

### RESULTS

A mini-mental test was administered to the 42 participants before the study. When analyzing the within-group values, the active group showed an average score of 28.9, while the sham group had an average score of 28.7 ( $p = 0.309$ ; Table 1).



**Figure 5.** Placement of the cathode (blue) and anode (red) electrodes.

Table 1. Comparison of mini-mental test values between groups	
	Mini-Mental Test
Z	-1.016
p-value	0.309
Mann-Whitney U test	

**Table 2.** Comparison between groups for the pre-tDCS visual 1-back task results

	Standard Stimulus		Target Stimulus		Commission		
	Number of Omissions (mean ± SD)	Number (mean ± SD)	Response Time (msec) (mean ± SD)	Number (mean ± SD)	Response Time (msec) (mean ± SD)	Number (mean ± SD)	Response Time (msec) (mean ± SD)
<b>Pre-tDCS active group</b>	8.47 ± 7.06	26.57 ± 5.96	193 ± 59.60	14.14 ± 2.72	190.57 ± 58.30	3.80 ± 3.01	170.38 ± 79.81
<b>Pre-tDCS sham group</b>	10.90 ± 8.76	22.09 ± 6.68	196.09 ± 63.94	14.04 ± 3.02	200.28 ± 62.70	5.14 ± 3.86	194.57 ± 86.76
<b>Z</b>	-0.733	-1.779	-0.277	-0.038	-0.667	-0.963	-2.233
<b>p-value</b>	0.464	0.075	0.782	0.969	0.505	0.336	0.217

Mann-Whitney U Test, SD: Standard deviation, TDCS: transcranial direct current stimulation

### Comparison of Visual 1-Back Task Values Pre- and Post-tDCS

#### Visual 1-back Task Values Pre-tDCS

Before the tDCS application, no statistically significant difference was observed between the two groups in terms of the number of omissions (p=0.464), number of commissions (p= 0.336), number of standard stimuli (p=0.075), standard stimulus-response time (p=0.782), number of target stimuli (p=0.969), target stimulus-response time (p=0.505), and commission response times (p=0.217; Table 2).

#### Comparing the Active Group’s Visual 1-Back Task Values

The within-group analyses revealed statistically significant differences to occur within the active group regarding the number of omissions (p=0.043), standard stimulus-response

time (p<0.0001), number of target stimuli (p<0.0001), target stimulus-response time (p<0.0001), number of commissions (p=0.003), and commission response time (p<0.0001), but not regarding the number of standard stimuli (p=0.775; Table 3).

#### Comparing the Sham Group’s Visual 1-Back Task Values

The data obtained from the sham group pre- and post-tDCS were examined and revealed statistical differences regarding standard stimulus-reaction time (p=0.007), number of target stimuli (p=0.004), target stimulus-reaction time (p<0.0001), and commission response time (p=0.046). However, no significant difference was found regarding the number of omissions (p=0.107), the number of standard stimuli (p=0.075), or the number of commissions (p=0.160; Table 4).

**Table 3.** Within-group comparison of the active group’s pre- and post-tDCS visual n-back task results

	Number of Omissions (mean ± SD)	Standard Stimulus		Target Stimulus		Commission	
		Number (mean ± SD)	Response Time (msec) (mean ± SD)	Number (mean ± SD)	Response Time (msec) (mean ± SD)	Number (mean ± SD)	Response Time (msec) (mean ± SD)
<b>Pre-tDCS group</b>	8.47 ± 9.83	26.57 ± 5.96	193 ± 59.60	14.14 ± 2.72	190.57 ± 58.30	3.80 ± 3.01	170.38 ± 79.81
<b>Post-tDCS group</b>	11.19 ± 7.35	19 ± 7.04	247 ± 41.76	9.09 ± 2.40	238.90 ± 43.10	6.62 ± 3.57	245 ± 49.13
<b>Z</b>	-2.021 <sup>b</sup>	-0.285 <sup>c</sup>	-3.841 <sup>b</sup>	-4.023 <sup>c</sup>	-3.737 <sup>b</sup>	-2.984 <sup>b</sup>	-3.563 <sup>b</sup>
<b>p-value</b>	<b>0.043</b>	0.775	<b>p&lt;0.0001</b>	<b>p&lt;0.0001</b>	<b>p&lt;0.0001</b>	<b>0.003</b>	<b>p&lt;0.0001</b>

Wilcoxon Signed Ranks Test, SD: Standard deviation; tDCS: Transcranial direct current stimulation; b: Based on negative ranks; c: Based on positive ranks.

**Table 4.** Within group gomparrison of the sham group's pre- and post-tDCS visual *n*-back task results

	Standart Stimulus		Target Stimulus		Commission		
	Number of Omissions (mean ± SD)	Number (mean ± SD)	Response Time (msec) (mean ± SD)	Number (mean ± SD)	Response Time (msec) (mean ± SD)	Number (mean ± SD)	Response Time (msec) (mean ± SD)
<b>Pre-tDCS group</b>	10.90 ± 8.76	22.90 ± 6.68	196.09 ± 63.94	14.94 ± 3.02	200.28 ± 62.70	5.14 ± 3.86	194.57 ± 86.76
<b>Post-tDCS group</b>	9.52 ± 9.83	24.52 ± 8.27	171.66 ± 62.58	15.19 ± 2.54	168.57 ± 68.37	3.76 ± 2.79	154.71 ± 68.54
<b>Z</b>	-1.612 <sup>b</sup>	-1.778 <sup>c</sup>	-2.677 <sup>b</sup>	-2.914 <sup>c</sup>	-3.529 <sup>b</sup>	1.406 <sup>b</sup>	-1.999 <sup>b</sup>
<b>p-value</b>	0.107	0.075	<b>0.007</b>	<b>0.004</b>	<b>&lt;0.0001</b>	0.160	<b>0.046</b>

Wilcoxon Signed Ranks Test; SD: Standard deviation; tDCS: Transcranial direct current stimulation; b: Based on negative ranks; c: Based on positive ranks.

**Between Group Comparison of Difference in Data Regarding the Pre- and Post-tDCS Visual N-Back Results**

When comparing the differences between the two groups' pre- and post-tDCS results, substantial variances were identified between the groups regarding number of omissions (p=0.013), standard stimulus-response time (p<0.0001), target stimulus count (p<0.0001), number of commissions (p<0.0001), and commission response time (p<0.0001). Meanwhile, no discernible statistical disparity was found regarding the standard stimulus quantification (p=0.181; Table 5).

When comparing the two groups' differences between the pre- and post-tDCS visual 1-back task results, statistical differences were found regarding the number of omissions (p=0.013), standard stimulus-response time (p<0.0001), number of target stimuli (p<0.0001), target stimulus-reaction time (p<0.0001), number of commissions (p<0.0001), and commission response time (p<0.0001) between the groups. However, no statistical difference was found regarding the number of standard stimuli

(p=0.181; Table 5).

**DISCUSSION**

This study randomly assigned 42 healthy adult volunteers to the active and sham groups and performed the visual 1-back task to measure visual working memory performance pre- and post-tDCS application. In conclusion, when comparing the statistical values within and between groups, the study found the performance of the active group to be lower than that of the sham group.

Barbey et al. reported that left DLPFC damage caused impairment in verbal, auditory, and spatial tasks related to working memory (20). This study applied stimulation to the left DLPFC by considering studies in the literature that have emphasized the role the left DLPFC has in working memory (9, 21). Similar to the findings reported in the literature, the results from the current study observed impairment in working memory tasks in response to the suppression applied to the left DLPFC.

**Table 5.** Between group comparison of the two groups' pre- and post-tDCS visual *n*-back task data differences

	Standart Stimulus		Target Stimulus		Commission		
	Difference In The Number of Omissions	Difference In The Number of Standard Stimuli	Standard Stimulus-Response Time Difference (msec)	Difference in the number of target stimuli	Difference in Response Times (msec)	Difference in Number of Commission	Difference in Response Times (msec)
<b>Mean Data Difference</b>	0.66	0.61	14.95	8.30	-1.95	0.66	24.19
<b>Z</b>	-2.485	-1.337	-4.780	-5.550	-5.108	-3.518	-3.837
<b>p-value</b>	<b>0.013</b>	0.181	<b>&lt;0.0001</b>	<b>&lt;0.0001</b>	<b>&lt;0.0001</b>	<b>&lt;0.0001</b>	<b>&lt;0.0001</b>

Mann-Whitney U test; SD: Standard deviation; tDCS: Transcranial direct current stimulation.

When examining the between-groups values for the pre-test, no statistically significant difference was found in the number of targets, omissions, commissions, and standard stimuli, as well as in their response times. This shows no significant difference to exist between the participants in both groups and that standardization had been strengthened (Table 2).

When comparing the pre- and post-test values in the active group, an increase was observed to occur in the number of omissions and commissions, a decrease in the number of correct target stimuli, and an increase in all reaction times (Table 3). In the sham group, an increase was found to occur in the number of correct target stimuli and a shortening in the target stimulus duration and commission reaction times (Table 5).

An increase in the number of omissions and commissions was observed in the active group's post-tDCS task. Also, the active group's post-tDCS commission response times were prolonged. In contrast, no significant differences were seen in the sham group's target numbers or omission numbers. In addition, a slight decrease was found in the number of commissions and commission response times for the sham group (Table 4). Reviewing other studies in the literature, results similar to those in the current study were observed when applying cathodal tDCS to the left DLPFC (8). Javadi and Walsh's (22) study on 32 participants observed similar negative effects when applying cathodal tDCS on verbal working memory as were observed in the current study regarding visual working memory.

A meta-analysis of 61 studies by Dedoncker et al. has reported anodal tDCS stimulation to improve performance regarding *n*-back tasks (i.e., 1-back, 2-back, and 3-back tasks) with response times being significantly reduced (23). However, no significant differences were found in the sham groups in the studies Dedoncker et al. have reviewed (23). In contrast, the current study suggests that improvements had been observed in the sham group possibly due to the shorter interval before starting the tasks pre- and post-tDCS compared to other studies. This supports the idea that performance can be increased by increasing the number of trials in cognitive assessments.

Moreover, when considering that both groups had gained experience after the first test, the fact that no improvement had occurred in the number of commissions and response times in the active group, with an increase in that group even occurring regarding the number of commissions and a significant prolongation in response times, shows the effect that applying cathodal tDCS to the left DLPFC has on visual working memory.

The lack of improvement in the active tDCS group relative to the sham tDCS group regarding the standard stimuli post-tDCS task (Table 3) confirms the suggestion of improved performance depending on the number of trials in the cognitive assessments (21, 23). In addition to these studies, examples are also found in the literature to have tried to modulate working memory with regard to visual and verbal dimensions (20-24). These examples

mostly used *n*-back tasks created with complex or geometric shapes. Contrary to these examples, the current study created a visual 1-back task consisting of 28 different Chinese characters. Fregni et al. study, which applied cathodal tDCS to the left DLPFC, performed a similar 1-back task with Latin letters; their application did not create a significant difference with regard to working memory (25). However, the current study observed a very significant effect from the cathodal tDCS; the difference between the current study's results compared to those from Fregni et al.'s study are thought to be due to the current study's use of a visual 1-back task, which is difficult to verbalize, instead of a verbalizable *n*-back task, as Latin letters can be quickly verbalized (25).

This study has attempted to reveal the concrete effects the tDCS has on visual working memory and found a remarkable difference between the sham and active groups. This supports the studies examined in Dedoncker et al.'s (23) meta-analysis.

Unlike Fregni et al., the current study presented Chinese characters as stimuli, because the participants would have difficulty in verbalizing these, thus eliminating the stimuli being translated into verbal memory (25). This is thought to have contributed to a clearer demonstration of the effect tDCS has on visual working memory. The difference observed regarding the results of Fregni et al.'s (25) reveals the need for further studies using tDCS to better understand the differences. The inability to translate the presented visual stimuli into verbal memory and the clear effects of tDCS on visual working memory are considered the distinguishing features of the current study.

This study's findings are consistent with those in the literature, suggesting that the left DLPFC is critical for preserving verbal and spatial information in working memory. This study has been conducted with cathodal tDCS and *n*-back tasks and is thought to be able to contribute to the literature on the concrete results tDCS has shown on working memory, and therefore also on cognitive performance tasks. In this way, the current study is thought to be able to help future studies on tDCS.

---

**Ethics Committee Approval:** This study is approved by Istinye University, Clinical Research Ethics Committee (No: 4/2023.K-14).

**Informed Consent:** The participants signed the informed consent form, they were informed about the tasks and procedures to be performed for about 5 minutes

**Peer-review:** Externally peer-reviewed.

**Author Contributions:** Conception/Design of Study- Y.E.O., G.E.; Data Acquisition- Y.E.O., G.E.; Data Analysis/Interpretation- Y.E.O., G.E.; Drafting Manuscript- Y.E.O., G.E.; Critical Revision of Manuscript- Y.E.O., G.E.; Final Approval and Accountability- Y.E.O., G.E.

**Conflict of Interest:** The authors declare that they have no competing interests.

**Financial Disclosure:** The authors declare that this study has received no financial support.

## REFERENCES

1. Miller GA. The magical number seven, plus or minus two: some limits on our capacity for processing information. *Psychol Rev* 1956; 63(2): 81–97.
2. Baddeley AD. Working memory. *Philosophical transactions of the Royal Society B: Biological Sciences* 1983; 302(1110): 311–24.
3. Goldstein BE. *Cognitive psychology: connecting mind, research, and everyday experience*. Singapore: Cengage Learning Asia Pte Ltd; 2020.
4. Kolb B, Whishaw IQ. *Fundamentals of human neuropsychology*. New York: Macmillan Learning; 2021.
5. Rottschy C, Langner R, Dogan I, Reetz K, Laird AR, Schulz JB, et al. Modelling neural correlates of working memory: A coordinate-based meta-analysis. *NeuroImage* 2012; 60(1): 830–46.
6. Luque-Casado A, Rodríguez-Freiria R, Fogelson N, Iglesias-Soler E, Fernández-del-Olmo M. An integrative clustering approach to tDCS individual response variability in cognitive performance: beyond a null effect on working memory. *Neuroscience* 2020; 443: 120–30.
7. Liebetanz D. Pharmacological approach to the mechanisms of transcranial DC-stimulation-induced after-effects of human motor cortex excitability. *Brain* 2002; 125(10): 2238–47.
8. Nitsche MA, Nitsche MS, Klein CC, Tergau F, Rothwell JC, Paulus W. Level of action of cathodal DC polarisation induced inhibition of the human motor cortex. *Clin Neurophysiol* 2003; 114(4): 600–4.
9. Andrews SC, Hoy KE, Enticott PG, Daskalakis ZJ, Fitzgerald PB. Improving working memory: the effect of combining cognitive activity and anodal transcranial direct current stimulation to the left dorsolateral prefrontal cortex. *Brain Stimul* 2011; 4(2): 84–9.
10. Teo F, Hoy KE, Daskalakis ZJ, Fitzgerald PB. Investigating the role of current strength in tDCS modulation of working memory performance in healthy controls. *Front Psychiatry* 2011; 2: 45.
11. McKenna R, Rushe T, Woodcock KA. Informing the structure of executive function in children: a meta-analysis of functional neuroimaging data. *Front Hum Neurosci* 2017; 11: 154
12. Li S, Cai Y, Liu J, Li D, Feng Z, Chen C, Xue G. Dissociated roles of the parietal and frontal cortices in the scope and control of attention during visual working memory. *NeuroImage* 2017, 149: 210-9
13. Aron AR, Robbins TW, Poldrack RA. Inhibition and the right inferior frontal cortex: one decade on. *Trends Cogn Sci* 2014; 18(4): 177-85.
14. Smirni D, Turriziani P, Mangano GR, Cipolotti L, Oliveri M. Modulating memory performance in healthy subjects with transcranial direct current stimulation over the right dorsolateral prefrontal cortex. *PLoS One* 2015; 10(12): e0144838.
15. Wang J, Tian J, Hao R, Tian L, Liu Q. Transcranial direct current stimulation over the right DLPFC selectively modulates subprocesses in working memory. *PeerJ* 2018; 6: e4906.
16. McLaughlin NCR, Wiebe D, Fulwiler C, Gansler DA. Differential contributions of lateral prefrontal cortex regions to visual memory processes. *Brain Imag Behav* 2009; 3(2): 202-11.
17. Petrides M. Specialized system for the processing of mnemonic information within the primate frontal cortex. *Philos Trans R Soc Lond B Biol Sci* 1996; 351(1346):1455-62.
18. Stern CE, Owen AM, Tracey I, Look RB, Rosen BR, Petrides M. Activity in ventrolateral and middorsolateral prefrontal cortex during nonspatial visual working memory processing: evidence from functional magnetic resonance imaging. *NeuroImage* 2000, 11(5), 392–9.
19. Curtis CE, Rao VY, D'Esposito M. Maintenance of spatial and motor codes during oculomotor delayed response tasks. *J Neurosci* 2004, 24: 3944–52.
20. Barbey AK, Koenigs M, Grafman J. Dorsolateral prefrontal contributions to human working memory. *Cortex* 2013; 49(5): 1195-205
21. Roediger III HL, Karpicke JD. Test-enhanced learning: Taking memory tests improves long-term retention. *Psychol Sci* 2006; 17(3): 249-55.
22. Javadi AH, Walsh V. Transcranial direct current stimulation (tDCS) of the left dorsolateral prefrontal cortex modulates declarative memory. *Brain Stimul* 2012; 5(3): 231–41.
23. Dedoncker J, Brunoni AR, Baeken C, Vanderhasselt MA. A systematic review and meta-analysis of the effects of transcranial direct current stimulation (tDCS) over the dorsolateral prefrontal cortex in healthy and neuropsychiatric samples: influence of stimulation parameters. *Brain Stimul* 2016; 9(4): 501–17.
24. Waldhauser GT, Johansson M, Bäckström M, Mecklinger A. Trait anxiety, working memory capacity, and the effectiveness of memory suppression. *Scand J Psychol* 2011; 52(1): 21-7.
25. Fregni F, Boggio PS, Nitsche M, Bermanpohl F, Antal A, Feredoes E, et al. Anodal transcranial direct current stimulation of prefrontal cortex enhances working memory. *Exp Brain Res* 2005; 166(1): 23–30.

# Efficacy of the GnRH Agonist Trigger in Oocyte and Embryo Quality Through Mitochondrial Unfolded Protein Response

Murat Basar<sup>1,2</sup> 

<sup>1</sup>Department of Obstetrics, Gynecology, and Reproductive Sciences, Yale School of Medicine, New Haven, CT, USA.

<sup>2</sup>Yale Fertility Center, 200 West Campus Drive, Orange, CT, USA

ORCID ID: M.B. 0000-0001-7766-409X

**Cite this article as:** Basar M. Efficacy of the GnRH agonist trigger in oocyte and embryo quality through mitochondrial unfolded protein response. *Experimed* 2024; 14(1): 21-25.

## ABSTRACT

**Objective:** Gonadotropin-releasing hormone agonist (GnRHa) trigger induces both Luteinizing hormone (LH) and follicle stimulating hormone (FSH) surges, impacting oocyte maturation, and mitochondrial dysfunction, is responsible for chromosomal anomalies during meiotic divisions. This study aimed to investigate the effect of GnRHa instead of human chorionic gonadotropin (hCG) triggers on unfolded protein responses against embryonic stress in oocytes and embryos.

**Materials and Methods:** Female mice were divided into control, hCG-triggered, and GnRHa-triggered groups. Superovulation was performed. Oocytes were retrieved 13h after hCG or GnRHa injection, and two pronuclei (2PN) oocytes were retrieved 24h after the appearance of a vaginal plug. ATF5, GRP78, and HSP60 protein levels were analyzed by Western blot. One-way ANOVA and Students' t-test were used for statistical analysis.

**Results:** When comparing the GnRHa group to the hCG group, their respective oocyte maturation rates (79.8% vs. 75.9%), oocyte areas (10198  $\mu\text{m}^2$  and 9474  $\mu\text{m}^2$ ), 2PN rates (78% vs. 72%), and blastocyst formation rates (82% vs. 77%) were significantly higher ( $p < 0.05$ ). The HSP60 protein level was significantly lower in the GnRHa group compared to the hCG group (22% vs. 55%,  $p < 0.05$ ). Additionally, the ATF5 protein level was significantly lower in the hCG group compared to the GnRHa group ( $p < 0.0001$ ).

**Conclusion:** GnRHa trigger improves oocyte nuclear and cytoplasmic maturation, as well as blastocyst formation rates. The underlying mechanism for this effect is the downregulation of HSP60 and upregulation of ATF5 levels.

**Keywords:** mtUPR, GnRHa, mitochondrial stress, hCG

## INTRODUCTION

The accurate timing of ovulation must be successfully detected and then controlled if assisted reproductive technologies are to be effective. In controlled ovarian stimulation treatments used to treat infertility, injecting 5,000–10,000 IUs of human chorionic gonadotropin (hCG) used to be considered the gold standard for inducing granulosa cell luteinization, oocyte maturation, and follicle rupture (1). Gonadotropin-releasing hormone agonist (GnRHa) has also been proven to effectively trigger egg maturation mid-cycle by promoting the rise of endogenous gonadotropins. Still, this came to be a valuable alternative to

hCG only at the development of the short protocol, where spontaneous ovulation is prevented by the GnRHa, leaving room for the agonist to be successfully used for triggering.

Despite all its advantages, triggering with an agonist results in a defective luteal phase, which among other things reduces implantation and raises the risk of spontaneous pregnancy loss in fresh embryo transfers, thus leading to the freeze-all era (2, 3).

Even though many studies have assessed whether the usage of GnRHa and hCG affects stress response, it remains unclear. During embryo development, increased

**Corresponding Author:** Murat Basar **E-mail:** murat.basar@yale.edu

**Submitted:** 07.12.2023 **Revision Requested:** 09.01.2024 **Last Revision Received:** 19.02.2024 **Accepted:** 20.02.2024 **Published Online:** 25.03.2024



Content of this journal is licensed under a Creative Commons Attribution-NonCommercial 4.0 International License.

endoplasmic reticulum (ER) stress activates the unfolded protein response (UPR), leading to reduced blastocyst formation rates (4-6).

Among the molecules that regulate the mitochondrial unfolded protein response (mtUPR), heat shock protein 60 (HSP60) and mitochondrial HSP70 (mtHSP70) facilitate the protein folding function in the mitochondrial matrix (7), activating transcription factor 5 (ATF5) maintains mitochondrial activity during mitochondrial stress and promotes organelle recovery, and glucose-regulated protein 78 (GRP78) dissociation triggers the UPR endoplasmic reticulum (UPRer) that restores protein homeostasis.

The underlying hypothesis of this study is that, because of the high demand for mitochondrial homeostasis in preimplantation development (from oocyte to blastocyst), GnRH $\alpha$  triggers support for oocyte and blastocyst formation by suppressing mitochondrial stress.

## MATERIALS AND METHODS

Mice were maintained according to Yale University's requirements for animal research, and all procedures were approved by the Institutional Animal Care and Use Committee (protocol no. 2022-11300). Mouse embryos were collected using standard protocols under the guidelines approved by the Yale Institutional Animal Care and Use Committee. In short, 5-week-old C57BL/6 female mice (Charles River Labs) were super-ovulated by intraperitoneal (IP) injection of 5 Units of pregnant mare serum gonadotropin (PMSG; Folligon, Sigma-Aldrich). An additional injection of 5 Units of hCG (Chorulon, Sigma-Aldrich) was given 48 hours after the PMSG injection. To obtain two-cell embryos, females were placed individually with 12-week-old C57BL/6 males immediately after the hCG injection. The following morning, the effectiveness of mating was confirmed by the presence of a vaginal plug (day 1; D1). Two-cell embryos were collected from the oviducts at 44–48 hours after hCG

injection. Two-cell embryos were obtained by puncturing the ampulla portion of the oviduct with a needle in the HEPES-buffered media under the stereomicroscope.

## Animals

All mice care, breeding, and experimental protocols were conducted according to the Yale University School of Medicine Animal Research Requirements. The protocols used were approved by the Institutional Animal Care and Use Committee (2022-11300). 3-month-old female Balb/c mice (25-30 g) were used in 3 groups: control group, triggered with hCG, and triggered with GnRH $\alpha$  (n = 30 per group).

## Oocyte and Embryo Collection

To collect the metaphase II (MII) stage mature oocytes, 10 IUs of hCG (Sigma, St. Louis, MO) or GnRH $\alpha$  were injected 48 h after the PMSG (Sigma, St. Louis, MO) injection. Control group mice were injected with 0.09% NaCl. Unfertilized MII oocytes were collected from oviducts 14-16 h after the hCG injection (8). After oocytes were retrieved, their diameter was measured from two different positions (Research Instrument, Cronus 3, Video Capture, and Embryo Analysis Software) to calculate the mean oocyte area (n = 15 per group).

To collect the fertilized (2PN) oocytes (n = 15 per group), the female Balb/c mice were mated with males after receiving the hCG or GnRH $\alpha$  injection. The following morning, after the effectiveness of mating was confirmed by the presence of a vaginal plug, female mice were sacrificed by cervical dislocation. The 2PN oocytes were obtained by puncturing the ampulla portion of the oviduct with a needle in the HEPES-buffered media under the stereomicroscope and cultured until day 5 (D5) of embryonic development. Fertilization and blastocyst formation rates were calculated accordingly.

All embryos were cultured in groups of 12 in 50- $\mu$ L medium drops at 37°C in 6% CO $_2$ , 5% O $_2$ , and 89% N $_2$  for 96 h without

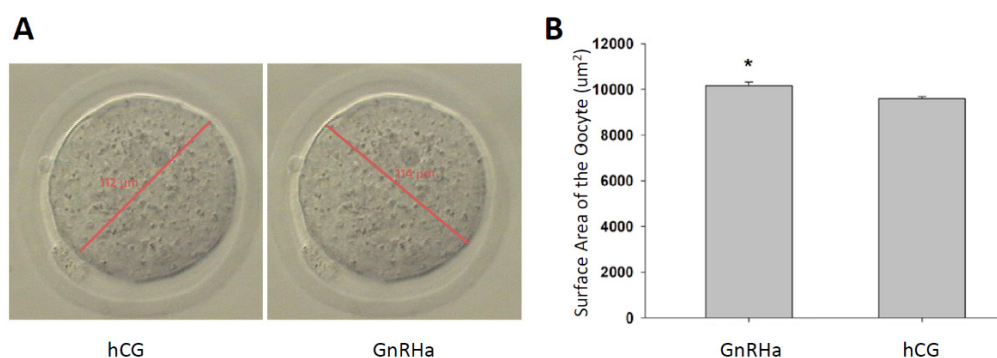


**Figure 1.** Morphological evaluation. Triggering with GnRH $\alpha$  improves blastocyst formation rate as well as oocyte cytoplasmic and nuclear maturation.

changeovers. An inverted microscope was used to examine the embryos at  $\times 200$  magnification at the end of D5.

### Western Blot

Embryos from each group were collected and incubated on ice for 30 minutes in a 5  $\mu\text{L}$  phosphate-buffered saline (PBS), and 5  $\mu\text{L}$  lysis buffer. The samples were mixed with 10 mL of Laemmli buffer, boiled for 5 minutes before being cooled on ice, and centrifuged at 2,000 rpm for 5 minutes at 4°C. GRP78 protein levels were determined using rabbit monoclonal anti-GRP78 (Cell Signaling Technology, Cat. No. 3117), anti-ATF5 (Sigma Aldrich, Cat. No. SAB4500895), and anti-HSP60 antibodies (Cell Signaling Technology, Cat. No. 12165) in the previously described standard Western Blot protocol (4).

Equal loading of proteins (10  $\mu\text{g}$ ) in each lane was confirmed by staining the membrane with Ponceau 2S (Sigma, St. Louis, MO). Ponceau red signals for anti-GRP78, anti-HSP60, and anti-ATF5 were quantified using a digital imaging and analysis system (AlphaEase,  $\alpha$  Innotech Corp., San Leandro, CA), as well as a laser densitometer (Molecular Dynamics, Inc., Sunnyvale, CA) for the auto radiographic bands. Anti-GRP78, anti-HSP60, and anti-ATF5 expressions were normalized by dividing the arbitrary densitometry units for anti-GRP78, anti-HSP60, and anti-ATF5 by the amount of Ponceau red staining for each band.

### Statistical Analyses

All experiments were repeated at least three times. Statistical analysis of the data was performed with Student's t-test and one-way analysis of variance (ANOVA), with a  $p < 0.05$  being considered statistically significant.

## RESULTS

### Oocyte Diameter as an Indicator of Cytoplasmic Maturity

Oocytes have two types of maturity. The first one is nuclear maturity, which can be noticed by assessing the polar body in the oocyte (metaphase II). The second is cytoplasmic maturity. The only indicator for this parameter is the oocyte area.

The mean oocyte area is significantly higher in the GnRHa-triggered group than in the hCG-triggered one ( $p < 0.05$ , 10198  $\mu\text{m}^2$  and 9474  $\mu\text{m}^2$ , respectively; Figures 1A-1B). Additionally, nuclear maturation has been assessed, revealing the maturation rate in the GnRHa-triggered group to be significantly higher than in the hCG-triggered group ( $p < 0.05$ , 79.8% vs. 75.9%, respectively).

The fertilization and blastocyst formation rates have also been checked due to the oocyte cytoplasmic and nuclear maturation being significantly higher in the GnRHa-triggered group. Both fertilization rates ( $p < 0.05$ , 78% vs. 72%, respectively) and blastocyst formation rate ( $p < 0.01$ , 82% vs. 77%, respectively) are significantly higher in the GnRHa-triggered group compared to the hCG-triggered group.

### mtUPR is altered in GnRH groups

To examine the mtUPR activity in the mice, the oocytes were treated with ethidium bromide (EB, 0.4  $\mu\text{g}/\text{mL}$ ) for three hours to stimulate the mtUPR, as described previously (9), after which the HSP60 protein levels were evaluated. The HSP60 levels in the EB-treated group were significantly increased compared

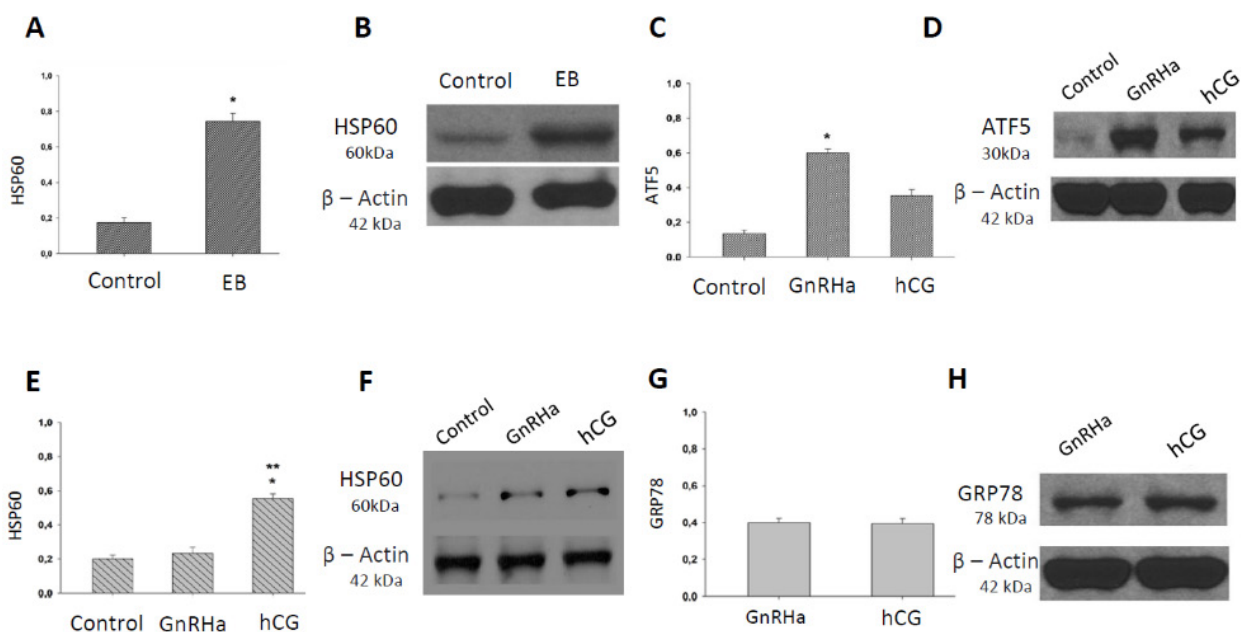


**Figure 2.** GnRHa-trigger improves oocyte and embryo quality by activating mtUPR.

to the control group (78% vs. 17%, respectively; Figures 2A-2B). Furthermore, the oocytes from the hCG-treated mice have significantly higher levels of HSP60 compared to the control and GnRHa-treated groups (22% for GnRHa, 55% for hCG, and 20% for control;  $p < 0.05$ ; Figures 2E-2F).

Additionally, the ATF5 level was assessed as a regulator of mtUPR. The oocytes from the mice triggered with hCG have a 41% ATF5 level, compared to 62% in the mice triggered with GnRHa ( $p < 0.0001$ ; Figures 2C-2D).

To ensure that all these effects are due to mtUPR but not UPRer, the study checked the GRP78 level, which is the marker for UPRer. The results show no significant difference in GRP78 levels between the GnRHa-treated and hCG-treated mice (24% and 25%, respectively;  $p > 0.05$ ; Figures 2G-2H).

## DISCUSSION

Embryo competency is determined by oocyte quality, which is influenced by various parameters including treatment mode (9). Triggering oocyte maturation is the last critical step of ovulation induction. GnRHa has been widely used in ovarian stimulation to prevent endogenous fast augmentation of the luteinizing hormone (LH) surge, which is essential for the development of the corpus luteum. As previously stated, triggering with a GnRH agonist causes a shorter duration of the LH surge than triggering with hCG, resulting in less LH support for the growing corpus luteum and possibly causing early luteolysis (10-12). Luteolysis has been proposed to result in much lower levels of estradiol and progesterone following GnRH agonist triggering than hCG triggering (10).

This study's findings provide valuable insights into the efficacy of GnRHa triggering for enhancing oocyte and embryo quality through mtUPR. Our results align with and sometimes extend the findings reported in the existing literature (11, 12).

The observed increase in oocyte maturation rates and oocyte diameter within the GnRHa group correlates well with the findings of Sukur et al., who reported enhanced cytoplasmic maturity in oocytes following GnRHa triggering (13). However, the current study has extended these findings by quantitatively assessing oocyte diameter, thus providing a more nuanced understanding of cytoplasmic maturity. The improvement in fertilization and blastocyst formation rates in the GnRHa-treated group resonates with the work of Yang et al. (14). However, the current study further elucidates the underlying molecular mechanisms, specifically focusing on the role of mtUPR, a perspective not extensively covered in their research.

The present study's differential expression of HSP60 and ATF5 provides a deeper understanding of mitochondrial stress in oocyte and embryo development. This finding adds to the framework established by Moehle et al. (2019), who first suggested the role of mtUPR in oocyte quality but did not differentiate between the specific impacts of HSP60 and ATF5 (15).

The present research supports the theoretical model proposed by Dumollard et al., which emphasizes the critical role of mitochondrial health in oocyte and embryo viability (16). The current study has provided empirical evidence that strengthens this theoretical model by demonstrating the specific changes in mitochondrial stress markers.

This study's findings being consistent and extending those in the existing literature suggests a potential shift in clinical practice towards the preferential use of GnRHa triggering in assisted reproductive technologies. The results advocate for a more nuanced approach that considers the rates of fertilization and blastocyst formation, as well as the molecular markers that are indicative of oocyte and embryo health.

The study has shown that using GnRHa during superovulation positively affects oocyte development and embryonic growth. These advancements are mediated through the modulation of mitochondrial stress responses, underscoring the vital role of mitochondrial homeostasis in reproductive efficacy. This research could significantly contribute to the optimization of fertilization (IVF) protocols, potentially leading to higher fertility treatment success rates.

---

**Ethics Committee Approval:** Mice were maintained according to Yale University requirements for animal research, and all procedures were approved by the Institutional Animal Care and Use Committee (protocol no. 2022-11300).

**Peer-review:** Externally peer-reviewed.

**Conflict of Interest:** The author declare that they have no competing interests.

**Financial Disclosure:** The author declare that this study has received no financial support.

## REFERENCES

- Hu KL, Wang S, Ye X, Zhang D, Hunt S. GnRH agonist and hCG (dual trigger) versus hCG trigger for follicular maturation: a systematic review and meta-analysis of randomized trials. *Reprod Biol Endocrinol* 2021; 19(1): 78.
- Gao F, Wang Y, Fu M, Zhang Q, Ren Y, Shen H, Han H. Effect of a "Dual Trigger" using a GnRH agonist and hCG on the cumulative live-birth rate for normal responders in GnRH-antagonist cycles. *Front Med (Lausanne)* 2021; 8: 683210.
- Griesinger G, Diedrich K, Devroey P, Kolibianakis EM. GnRH agonist for triggering final oocyte maturation in the GnRH antagonist ovarian hyperstimulation protocol: a systematic review and meta-analysis. *Hum Reprod Update* 2006; 12(2): 159-68.
- Basar M, Bozkurt I, Guzeloglu-Kayisli O, Sozen B, Tekmen I, Schatz F, et al. Unfolded protein response prevents blastocyst formation during preimplantation embryo development in vitro. *Fertil Steril* 2014; 102(6): 1777-84.
- Khatun H, Ihara Y, Takakura K, Egashira J, Wada Y, Konno T, et al. Role of endoplasmic reticulum stress on developmental competency and cryo-tolerance in bovine embryos. *Theriogenology* 2020; 142: 131-7.

6. Michalak M, Gye MC. Endoplasmic reticulum stress in periimplantation embryos. *Clin Exp Reprod Med* 2015; 42(1) :1-7.
7. Kumar R, Chaudhary AK, Woytash J, Inigo JR, Gokhale AA, Bshara W, et al. A mitochondrial unfolded protein response inhibitor suppresses prostate cancer growth in mice via HSP60. *J Clin Invest* 2022; 132(13): e149906.
8. Seli E, Lalioti MD, Flaherty SM, Sakkas D, Terzi N, Steitz JA. An embryonic poly(A)-binding protein (ePAB) is expressed in mouse oocytes and early preimplantation embryos. *Proc Natl Acad Sci U S A* 2005; 102(2): 367-72.
9. Baart EB, Macklon NS, Fauser BJ. Ovarian stimulation and embryo quality. *Reprod Biomed Online* 2009; 18 Suppl 2: 45-50.
10. Andersen CY, Humaidan P, Ejdrup HB, Bungum L, Grondahl ML, Westergaard LG. Hormonal characteristics of follicular fluid from women receiving either GnRH agonist or hCG for ovulation induction. *Hum Reprod* 2006; 21(8): 2126-30.
11. Humaidan P, Alsbjerg B. GnRHa trigger for final oocyte maturation: Is HCG trigger history? *Reprod Biomed Online* 2014; 29(3): 274-80.
12. Humaidan P, Kol S, Papanikolaou EG, Copenhagen Gn RHATWG. GnRH agonist for triggering of final oocyte maturation: time for a change of practice? *Hum Reprod Update* 2011; 17(4): 510-24.
13. Sukur YE, Ozmen B, Ozdemir ED, Seval MM, Kalafat E, Sonmezer M, et al. Final oocyte maturation with two different GnRH agonists in antagonist co-treated cycles at risk of ovarian hyperstimulation syndrome. *Reprod Biomed Online* 2017; 34(1): 5-10.
14. Yang BC, Uemura T, Minaguchi H. Effects of a gonadotropin releasing hormone agonist on oocyte maturation, fertilization, and embryonal development of mice. *J Assist Reprod Genet* 1995; 12(10): 728-32.
15. Moehle EA, Shen K, Dillin A. Mitochondrial proteostasis in the context of cellular and organismal health and aging. *J Biol Chem* 2019; 294(14): 5396-407.
16. Dumollard R, Duchen M, Carroll J. The role of mitochondrial function in the oocyte and embryo. *Curr Top Dev Biol* 2007; 77: 21-49.

# Cytogenetic and FISH Examination of 3p Abnormalities in Lung Cancer Patients\*

Narmin Bakhshaliyeva<sup>1</sup> , Ayse Cirakoglu<sup>2</sup> , Hurrem Gul Ongen<sup>3</sup> , Esin Bil Tuncay<sup>4</sup> , Yelda Tarkan Arguden<sup>2</sup> 

<sup>1</sup>Department of Genetics, Institute of Graduate Studies in Health Sciences, Istanbul University, Istanbul, Turkiye

<sup>2</sup>Department of Medical Biology, Cerrahpasa Faculty of Medicine, Istanbul University-Cerrahpasa, Istanbul, Turkiye

<sup>3</sup>Department of Pulmonary Diseases, Cerrahpasa Faculty of Medicine, Istanbul University-Cerrahpasa, Istanbul, Turkiye

<sup>4</sup>Yedikule Chest Diseases and Thoracic Surgery Training and Research Hospital, Istanbul, Turkiye

ORCID ID: N.B. 0000-0001-8173-4142; A.C. 0000-0003-0330-2277; H.G.O. 0000-0001-7139-9002; E.B.T. 0009-0005-0230-1936; Y.T.A. 0000-0002-5405-3365

**Cite this article as:** Bakhshaliyeva N, Cirakoglu A, Ongen HG, Bil Tuncay H, Tarkan Arguden Y. Cytogenetic and FISH examination of 3p abnormalities in lung cancer patients. *Experimed* 2024; 14(1): 26-39.

## ABSTRACT

**Objective:** Deletions or loss of heterozygosity in chromosome 3p are very common in small-cell lung cancer (SCLC) and lung adenocarcinoma (ADC) cases. These are typically found in tumor cells but rarely observed in lymphocytes. This study aimed to evaluate the frequency of 3p deletions and/or abnormalities in the blood of lung cancer patients using conventional cytogenetics and fluorescence *in situ* hybridization (FISH), by targeting the fragile histidine triad diadenosine triphosphatase (FHIT) gene located at the commonly deleted region of 3p14.2, in lung cancers.

**Materials and Methods:** The study examined 24 SCLC patients, 30 ADC patients, and 20 healthy controls. It used standard procedures to perform a 72-h lymphocyte culture, G-banding, and FISH.

**Results:** All patient group cases showed multiple numerical and structural abnormalities, with numerical abnormalities being more prominent and involving all chromosomes. The following two 3p abnormalities were detected in one patient: del(3)(p22) and t(3;5)(p25;q31). FISH showed positive results regarding FHIT deletion in 9 (30%) ADC, and 7 (29%) SCLC patients.

**Conclusion:** Regardless of the rarity of 3p abnormalities in lymphocytes, a high frequency of chromosomal aberrations may indicate genomic instability. Nevertheless, due to being a time-consuming and expertise-requiring technique, conventional cytogenetics is not recommended for lung cancer monitoring. However, the FISH results suggested that using FISH to examine FHIT gene status in lymphocytes could be a promising biomarker for lung cancer.

**Keywords:** Small cell lung carcinoma, FISH technique, adenocarcinoma, cytogenetics, chromosome 3, FHIT

## INTRODUCTION

Lung cancers are one of the main types of cancer-caused deaths, worldwide (1). Many studies have shown the effects of genetic factors on lung cancer. Small cell lung cancer (SCLC) covers 20-25% of all lung cancers; it has a different clinicopathological course involving paraneoplastic syndromes and a tendency

to metastasize, requires an aggressive clinical process, and is insensitive to chemotherapy and radiation (1, 2). Lung adenocarcinomas (ADC) comprise nearly 40% of all lung cancers (3). 3p abnormalities are the most common chromosomal abnormalities in SCLCs and ADC, and cytogenetic studies have shown 3p deletion to be a characteristic finding for small cell and ADC lung cancers (4-9). Even when no chromosome 3p anomalies are

\*This study was produced from the master's thesis and was presented at 13th Balkan Congress of Human Genetics and 13th National Congress of Medical Genetics with International Participation.

**Corresponding Author:** Narmin Bakhshaliyeva **E-mail:** b.narmin@hotmail.com

**Submitted:** 23.12.2023 **Revision Requested:** 18.01.2024 **Last Revision Received:** 31.01.2024 **Accepted:** 13.02.2024 **Published Online:** 25.03.2024



Content of this journal is licensed under a Creative Commons Attribution-NonCommercial 4.0 International License.

found, a loss of heterozygosity in 3p is shown (5, 8, 10). With cytogenetic and molecular genetic techniques, 3p deletion or 3p loss of heterozygosity has been observed in 100% of SCLC cases and 80% of ADC cases (4, 8-13). These abnormalities are typically detected in a patient's tumor cells, but rare cases exist where this has been observed in lymphocyte cultures from peripheral blood samples (11, 14, 15). Although these studies have shown chromosomal abnormalities specific to SCLC to be able to be seen in blood samples, the number of cases is insufficient to understand whether these findings can be used to obtain information about the course of the disease. Because peripheral blood is easy to collect and manipulate and suitable for recurring examinations, knowing whether cancer-specific chromosomal abnormalities in peripheral blood are common enough to be used as indicators are desirable for the prediction of cancer development, prognosis, and metastasis.

Similar to most epithelial tumors, lung cancer consists of the accumulation of multiple genetic and/or epigenetic changes that can result from deletions, mutations, or changes in gene methylation. Chromosomal deletions are associated with regions of tumor suppressor genes (16). Recent studies have identified various tumor suppressor genes (TSGs) that play or may be able to play a role in carcinogenesis in regions of chromosome 3 that are also deleted in SCLC and ADC cases (4, 5, 7, 9, 17). For example, many TSGs such as fragile histidine triad diadenosine triphosphatase (FHIT) at 3p14; ROBO/DUTTI at 3p12; and Ras association domain family member 1 alpha (RASSF1a), the histocompatibility allele H-37, FUS RNA-binding

protein (FUS1), and semaphorin 3B (SEMA3B) at 3p21 are lost as a result of these deletions (5, 7, 9, 16, 18). Other TSGs found in chromosomal regions commonly deleted in lung cancers include the adenomatous polyposis coli (APC) regulator of WNT signaling pathway (5q21), retinoblastoma (RB) (13q), p53 (17p), and p16 (9p21) (11). The FHIT gene is involved in the accumulation of di-adenosine tetraphosphate, thus causing DNA synthesis and proliferation. It is located at 3p14.2 and overlaps with a common fragile site known as Fra3B, which is prone to damage and leads to chromosome aberrations. Loss or reduced expression of FHIT is found in preneoplastic lesions and cancers, including lung cancer. This results in replication stress, DNA breaks, aneuploidy, copy-number changes small insertions and deletions, and point mutations (19).

This study aimed to use conventional cytogenetics and fluorescence *in situ* hybridization (FISH) techniques to evaluate the frequency of 3p deletions and abnormalities in the peripheral blood samples of lung cancer patients.

Based on the information in the literature, the study has deemed the inclusion of lung ADC to be appropriate, considering its similarity to SCLC in terms of such features as carrying 3p anomalies and its aggressive course. The study used a FISH probe for the FHIT gene located on 3p14.2, which is within the commonly deleted region of 3p in lung cancers, in order to be able to detect deletions smaller than the scope of what cytogenetics can detect. The FHIT gene has been chosen from among the numerous genes residing in the relevant

**Table 1. Clinical characteristics of the cases**

	ADC (n = 30)	SCLC (n = 24)	Control (n = 20)
Gender			
Female	10	4	12
Male	20	20	8
Age (year), min-max (median)	46-87 (61.5)	47-90 (57)	31-51 (44)
Grade			
1	4	-	
2	8	3	
3	3	13	
4	8	8	
Metastase	13	8	
Bone	4	1	
Brain	3	4	
Liver	2	-	
Esophagus	2	-	-
Head-neck	-	1	
Brain+Bone	1	-	
Liver+Bone	1	1	
Liver+Muscle	-	1	
Smoking	14	5	-

ADC-adenocarcinoma; SCLC-small-cell lung cancer

region because it is a known tumor suppressor gene and has already been associated with lung cancer (5, 7, 18, 20-22). The study used conventional cytogenetic techniques to examine chromosomal abnormalities in peripheral blood cultures and used the FISH method to investigate the loss of the FHIT gene in the 3p14 region.

## MATERIALS AND METHODS

### Subjects

The study has enrolled a total of 54 untreated lung cancer cases (24 SCLC and 30 ADC) and 20 healthy (non-smoker ≥ 30 years of age) control subjects. The study has been conducted in accordance with the Helsinki Declaration and was approved by the Cerrahpasa Faculty of Medicine Medical Ethics Committee (Reference No. 83045809-604.01.02-A49), with all patients and individuals in the control group having signed informed consent forms. Of the 30 ADC cases, 10 were female, and 20 were male. Of the 24 SCLC cases, four were female, and 20

were male. Of the 30 ADC patients, 16 were smokers, and 14 were non-smokers. Of the 24 SCLC patients, 19 were smokers, and 5 were non-smokers. The median age was 61 for the ADC cases and 57 for the SCLC cases, while the median age was 63 for ADC and 60 for SCLC. Metastases were detected in 13 of the 30 ADC patients and in 8 of the 24 SCLC patients. Table 1 lists the clinical characteristics of the cases. The study used conventional cytogenetics to examine 3p and other chromosomal abnormalities in the peripheral blood samples of all patients and control subjects and used FISH techniques to examine their FHIT gene status.

### Conventional Cytogenetics

A standard 72 h lymphocyte culture procedure was applied to the heparinized blood samples of the patients and control subjects. Giemsa-Trypsin-Leishman (GTL) banding was used for chromosome banding, and metaphases were evaluated in accordance with the International System for Human Cytogenomic Nomenclature (ISCN) 2016. Consistent with the

**Table 2. Distribution of structural anomalies between SCLC and ADC disease**

Abnormality	Case Number		Metastatic case
	SCLC	ADC	
del(18)(p11)	2	4	A16-Esophagus Met K9-Brain Met
del(6)(q15q21)	1	3	A2-Bone Met
del(22)(q12)	1	1	A2-Bone Met
del(X)(p11)	-	1	-
del(3)(p22)	1	-	-
t(3;5)(p25;q31)	1	-	-
add(3)(q29)	-	1	-
del(7)(p13)	-	1	A16-Esophagus Met
i(7)(p10)	-	1	A30-Brain Met
i(7)(q10)	-	1	A30-Brain Met
inv(9)(p12q13)	1	-	-
dic(9;11)(q34;p15)	-	1	A2-Bone Met
inv(10)(q23q24)	-	1	A12-Bone Met
add(10)(q26)	-	1	A2-Bone Met
del(14)(q24)	-	1	A12-Bone Met
chtg(16)(q21)	-	1	-
der(18)del(18)(p11)del(18)(q12q22)	1	-	-
del(20)(q13)	1	-	K17-Brain Met

ADC-adenocarcinoma; SCLC-small-cell lung cancer; Met: Metastasis

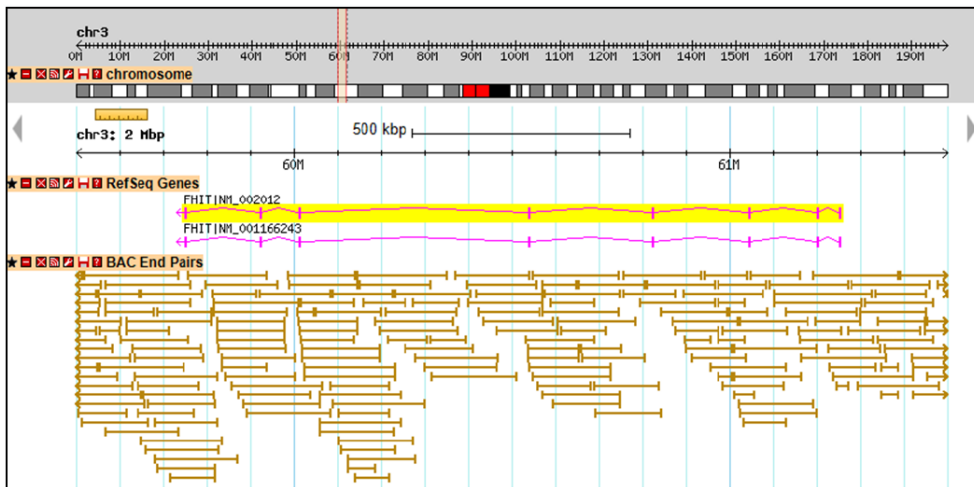


**Figure 1.** The 3p14.2 (FHIT) DNA FISH probe.

ISCN rules, the chromosomal gains and structural abnormalities observed in two metaphases and chromosome losses observed in three metaphases were considered clonal. Whenever possible, 100 metaphases were evaluated for each case, of which 20 were captured and analyzed on an image analyzer (Ankagen/IMGESS/Karyotyping Gv2.5) and 30 were analyzed under the microscope. If no chromosomal abnormality was present in these metaphases, another 50 metaphases would then be scored for chromosome 3 abnormalities. If 3p or any other chromosomal

abnormality was observed in any stage, all metaphases of the case were captured and analyzed on the image analyzer.

### FISH

FISH analyses were performed using a custom-designed, quality-controlled FHIT probe (provided by Medimiks Medical Biotechnology Systems & Services Ltd.) The centromere probe for chromosome 3 was used for the control signal (Figure 1).

**Table 3. Statistical results of patients with FHIT anomaly diagnosed with ADC and SCLC according to clinical status variables**

	SCLC (24)	ADC (30)	p-value
<b>Age (year), median (min-max)</b>	59.83 (47-90)	63.07 (46-87)	0.166
<b>FHIT, n (%)</b>			
Deletion positive	7 (29.2)	9 (30)	0.947
Deletion negative	17 (70.8)	21 (70)	
<b>Metastasis, n (%)</b>			
Yes	8 (33.3)	13 (43.3)	0.454
No	16 (66.7)	17 (56.7)	
<b>Grade, n (%)</b>			
Grade I	0 (0)	4 (13.3)	<b>0.015</b>
Grade II	3 (12.5)	8 (26.7)	
Grade III	13 (54.2)	5 (16.7)	
Grade IV	8 (33.3)	13 (43.3)	
<b>Smoking, n (%)</b>			
Yes	19 (79.2)	16 (53.3)	<b>0.048</b>
No	5 (20.8)	14 (46.7)	
<b>Gender, n (%)</b>			
Female	4 (16.7)	10 (33.3)	0.165
Male	20 (83.3)	20 (66.7)	

\*ADC-adenocarcinoma; SCLC-small-cell lung cancer

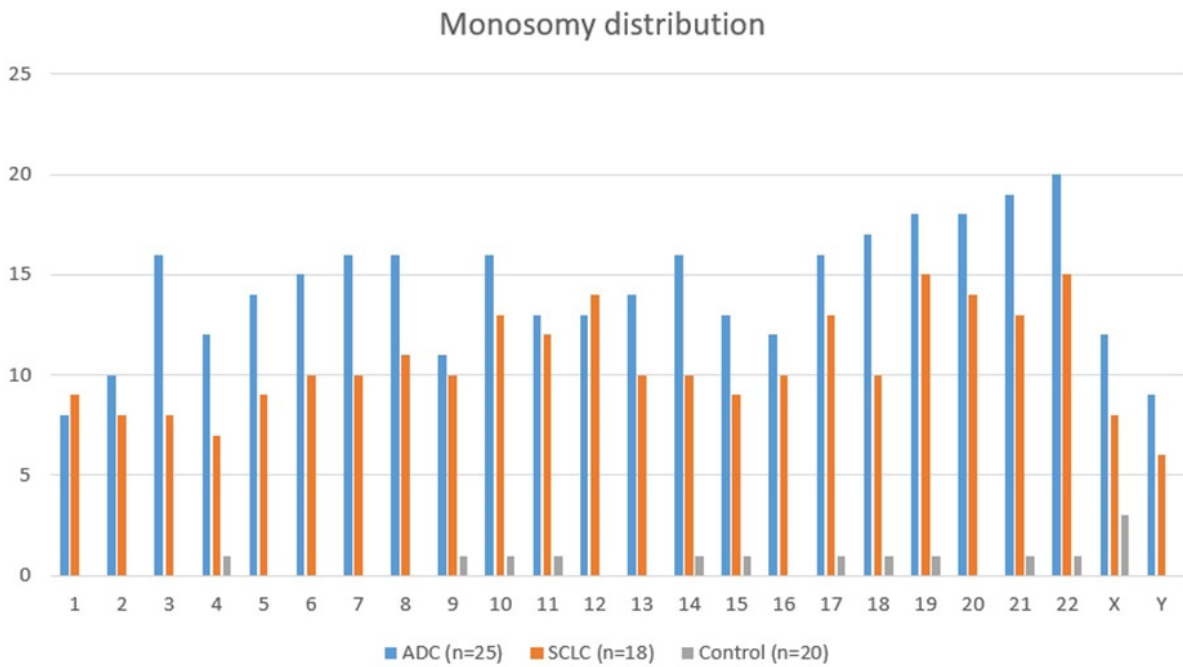


**Figure 2.** The distribution of monosomies over all the chromosomes between the SCLC and ADC cases.

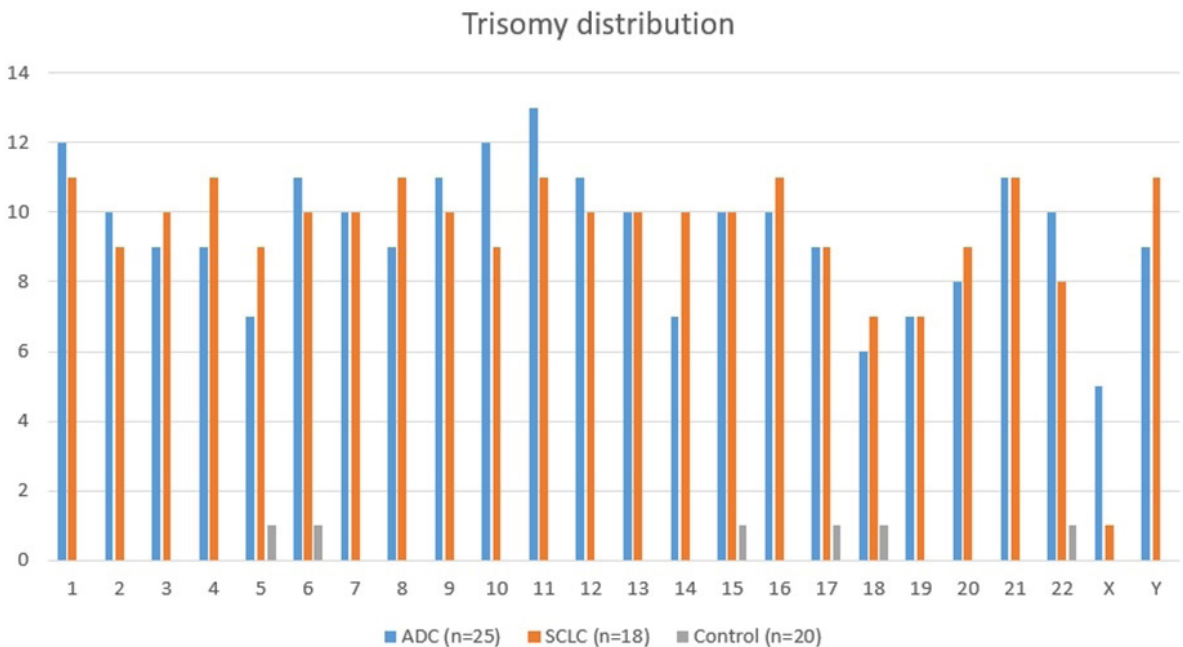


**Figure 3.** The distribution of trisomies over all the chromosomes between the SCLC and ADC cases.

Slides were prepared from cell suspensions and left to dry at room temperature. Following dehydration in subsequent alcohol series (70%, 85%, 100%) and air dried, the probes were applied on slides and denatured at 74°C for 2 min. Hybridization was carried out at 37°C for 18 h in a dark humidified cabin. After post-hybridization washes, the slides were counterstained with

DAPI (4'-6'-diamidine-2-phenylindole) and examined under the fluorescence microscope (Olympus BX51, Tokyo, Japan). An average of 200 (range = 100-320) interphase nuclei were analyzed independently by two investigators. The cut-off value was calculated using the  $\beta$  inverse function in Microsoft Excel with a 95% confidence level on the control group's signals as 5%.

## Statistical Analyses

The SPSS 20 package program was used for the statistical analysis, with  $p < 0.05$  being accepted as the statistical significance limit.

Mean, standard deviation, median, minimum, and maximum values are given in the descriptive statistics for continuous data, with percentage values presented in discrete data.

Chi-square is used to compare groups according to metastasis, stage, smoking status, gender, and FHIT deletion. The Mann-Whitney U test is used to compare the ages and FHIT deletions in the two patient groups.

## RESULTS

### Conventional Cytogenetics

The study examined 100 metaphases for the 18 SCLC, 25 ADC, and 20 control subjects and obtained good-quality metaphases. Karyotype formulas of the ADC and SCLC patients are provided in Supplementary Tables 1 and 2, respectively.

All the patients had clonal chromosomal abnormalities with composite karyotypes in both the SCLC and ADC groups. The clonal structural abnormalities observed in the series involved  $del(18)(p11)$  in six patients (2 SCLC, 4 ADC),  $del(6)(q15q21)$  in four patients (1 SCLC, 3 ADC), and  $del(22)(q12)$  in two patients (1 SCLC, 1 ADC). In addition to the recurrent abnormalities observed among patients, Table 2 also presents the clonal structural abnormalities that are unique to individual cases. No structural abnormalities were found in the control subjects.

A comparison of metastatic status and karyotype formulas from the ADC and SCLC cases are shown in Supplementary Tables 1 and 2, respectively.

Clonal numerical anomalies were detected in all patients from both patient groups. Monosomies of all chromosomes were observed in both patient groups and were the most prominent abnormalities in this study. Monosomy 22 (81% in 15 SCLC and 20 ADC) and monosomy 19 (77% in 15 SCLC and 18 ADC) were the most frequent abnormalities. Monosomy 3 was noted in 56% (8 SCLC and 16 ADC) of the cases. The control group had three cases of monosomy X, which was the only monosomy observed in more than one control group case. All monosomies except monosomy X were significantly higher in the study groups than in the control group ( $p < 0.05$ ), whereas no significant difference was found between the study groups ( $p > 0.05$ ). Clonal trisomies of all chromosomes were also observed in both patient groups. Trisomy 11 was the most recurring and was detected in 56% (11 SCLC and 13 ADC) of the cases. Trisomy of chromosome 3 was seen in 44% (10 SCLC and 9 ADC) of the cases. All trisomies occurred significantly more frequently than in the control group ( $p < 0.05$ ), but no significant difference was observed between the study groups ( $p > 0.05$ ). Figures 2 and 3 present the distributions of

monosomies and trisomies for all chromosomes among the SCLC, ADC, and control cases. Figure 4 shows one example of a complex karyotype image of an ADC case.

### FISH

Interphase FISH was applied to the peripheral lymphocyte preparations of 30 untreated ADC, 24 untreated SCLC, and 20 healthy control subjects using a custom-designed, quality-controlled FHIT (3p14.2) gene probe, with at least 200 cells being evaluated for each case. FHIT deletion was positive in 9 (30%) ADC and 7 (29%) SCLC patients. No significant difference was found between the ADC and SCLC groups ( $p > 0.05$ ). No significant difference was also found between the ADC and SCLC groups in terms of such anomalies as monoallelic and biallelic deletions, monosomy, or rearrangements ( $p > 0.05$ ). Monoallelic deletions were significantly higher in ADC and SCLC patients than in the control group ( $p < 0.001$  for both groups). Biallelic deletions were significantly higher in the ADC cases than in the control group ( $p < 0.05$ ). Monosomic cells were significantly higher in the ADC and SCLC patients than in the control group ( $p < 0.01$  and  $p < 0.001$ , respectively). Rearrangements were significantly higher in the ADC and SCLC patients than in the control group ( $p < 0.05$  and  $p < 0.01$ , respectively). No trisomic cells were observed in any group.

When comparing the patients according to their FHIT deletions and clinical variables such as stage, metastasis, smoking, gender, and age, no significant differences were found (Table 3). Figure 5 shows one example of a FHIT FISH image from an SCLC case.

### DISCUSSION

In cases with no constitutional chromosomal abnormalities, many cancer-related chromosomal abnormalities are first seen in peripheral lymphocytes as constitutional abnormalities before being observed in tumor cells, such as in  $del(13q)$  in retinoblastoma, 3p abnormalities in renal cell carcinoma,  $del(5q)$  in colorectal carcinomas, or  $del(11p)$  in Wilms' tumor. In addition, some cancer cases have cancer-related chromosome anomalies in a small number of peripheral lymphocytes (11, 14, 23), with 3p deletions being prominent cytogenetic findings in SCLC and non-small cell lung (NSCLC) tumor tissues. These abnormalities have been reported rarely in the peripheral lymphocytes of SCLC patients (8, 11, 14, 15).

Because peripheral lymphocytes are easy to collect and process and are suitable for recurrent analyses, they would be valuable sources for predicting cancer development, prognosis, and future metastasis should cancer-related chromosomal abnormalities be scannable in this type of tissue. Efforts have also been made to evaluate this possibility in different cancers (23) apart from lung cancers (8, 11, 14, 15). However, more cases must be studied in order to be able to deduce the approach as being a feasible method.

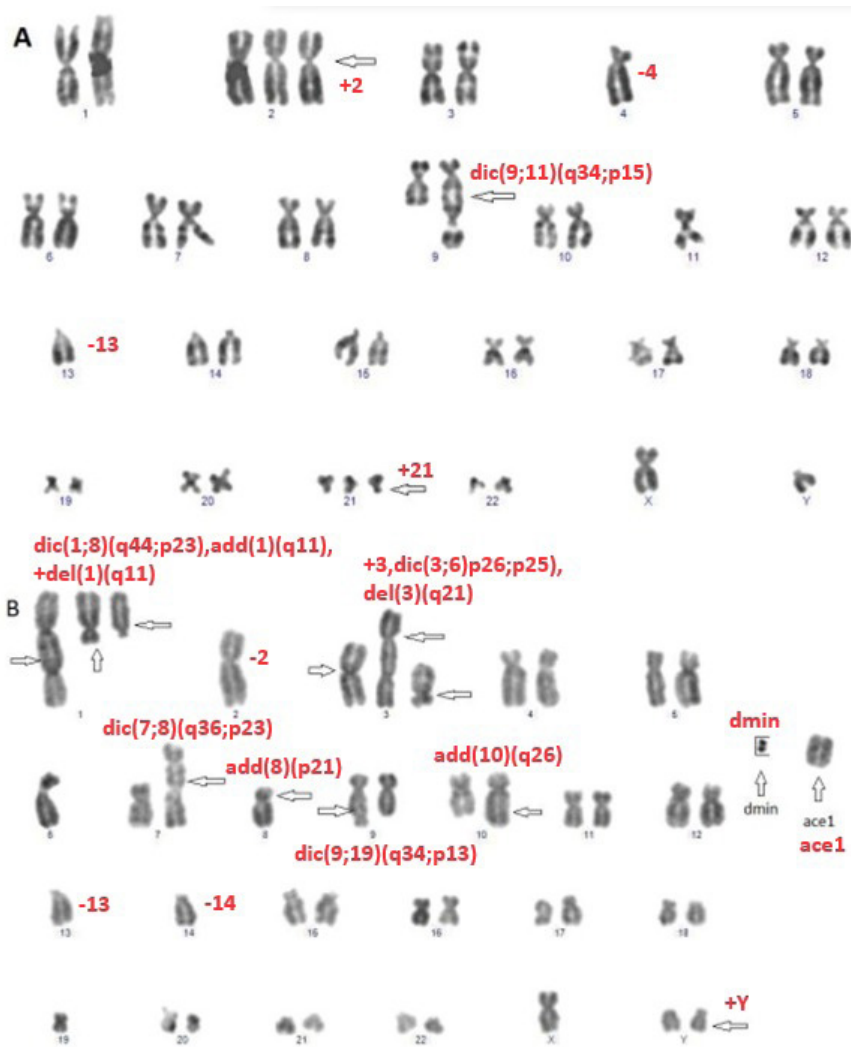


**Figure 4.** Two karyotype image examples of an ADC case (Case No. A2) containing numerical and structural abnormalities.  
 A. 46, XY, +2, -4, dic(9; 11) (q34; p15), -13, +21;  
 B. 43, XY, +Y, dic(1; 8) (q44; p23), add(1) (q11), +del(1) (q11), 2, +3, dic(3;6) (p26; p25), del(3) (q21), dic(7;8) (q36;p23), add(8)(p21), dic(9;19)(q34;p13), add(10)(q26), -13,-14, ace1, dmin

To enlarge the data on the subject, the current study has analyzed the peripheral lymphocytes of 24 untreated SCLC and 30 untreated lung ADC cases, alongside 20 healthy control subjects and observed complex karyotypes in both groups of cancer patients. Numerical abnormalities were observed to be more prominent than structural ones. Being present in 81% (15 SCLC and 20 ADC) of the cases, this study observed monosomy 22 as the most frequently occurring abnormality, followed by monosomy 19 at a rate of 77% (15 SCLC and 18 ADC). Monosomy 3 was noted in 56% (8 SCLC and 16 ADC) of the cases. All monosomies except for X, which was observed in three cases in the control group, were significantly higher than in the control group ( $p < 0.05$ ). However, no significant difference was observed between the two study groups ( $p > 0.05$ ).

This study found recurrent structural anomalies to occur in del(18)( p11) (14%; 4 ADC and 2 SCLC), del(6)(q15q21) (9%; 3 ADC and 1 SCLC), and del(22)(q12) (5%; 1 ADC and 1 SCLC). Structural chromosome 3 abnormalities were detected in only 2 (5%; 1 ADC and 1 SCLC) patients and occurred in del(3)(p22), t(3;5)(p25;q31) for the SCLC patient and add(3)(q29) for the ADC patient.

Abnormal karyotyped cells occurred at a rate of 1-10% in the control group, 13-91% in the SCLC group, and 18-75% in the ADC group ( $p < 0.05$ ). This discrepancy between the ratios of patient and control groups could indicate the genomic instability and heterogeneity of tumor cells. In fact, this abnormal-to-normal cell ratio in itself can be considered a better indicator of malignancy compared to looking for specific chromosomal abnormalities in peripheral blood. This index will

also cover the cells with nonclonal abnormalities that have previously been ignored as background noise and not included in the karyotype formulas but only recently were considered as significant indicators of genome instability (24).

A previous study reported cytogenetic results regarding peripheral lymphocytes in two SCLC cases (8). One of the cases involved a 57-year-old woman (Case 1) who had bone metastasis at the time of diagnosis and later developed a brain metastasis. The other patient was a 71-year-old man (Case 2), and the smoking history was positive for both patients. Blood samples were collected before the cytotoxic therapy. Case 1 had an extremely complex karyotype consisting of diploid and tetraploid clones heavy with structural and numerical chromosomal abnormalities. She had various chromosome 3 abnormalities, both clonal and nonclonal. This case was the main reason for planning to perform the current study. Case 2 had a less complicated karyotype without clonal chromosome 3 abnormalities, while nonclonal  $inv(3)(p14q29)$  was observed in two cells (one diploid, one tetraploid) in Case 1. Although the current study did not observe the same chromosome 3 abnormalities in its cases, a common breakpoint was observed: 3q29 was seen to be involved in two different inversions of 3 in the previous study and in one ADC case (patient A10) in the current study. The inversions with the 3q29 breakpoint that were observed in the previous study were  $inv(3)(p14q29)$  and  $inv(3)(q21q29)$ , with  $inv(3)(p14q29)$  being observed in the one cell of Case 2, as well as the one diploid and one tetraploid cell of Case 1. Meanwhile,  $add(3)(q29)$  was the abnormality associated with the breakpoint 3q29 in the current study's ADC case for patient A10. No other common structural chromosomal abnormalities were observed between the two cases in the previous study or in the cases of the current

study. As for numerical abnormalities, no trisomies had been found in the previous study, while some monosomies had been found in Case 1. Among these were monosomies 2, 8, 12, 16, and 17 in the diploid clone and monosomies X, 1, 7, 13, 17, 21, and 22 in the tetraploid clone. Monosomy 22 is one of the most frequent abnormalities of the current series, along with monosomy 19, with these being seen in 35 and 33 cases (81% and 77%), respectively. The previous study examined 63 cells in total for Case 1. Only six of these cells showed a normal karyotype, while 33 cells had at least one clonal abnormality and were included in the composite karyotype. Also, 24 cells carried nonclonal abnormalities. Overall, 90.4% of the cells were abnormal. However, the previous study investigated 100 cells for Case 2, with only 11 abnormal karyotyped cells (either clonal or nonclonal) being found. Therefore, this case would be indistinguishable from normal subjects when using peripheral blood cytogenetics if one of the nonclonal abnormalities is not  $inv(3)(p14q29)$ , which is known as an abnormality associated with lung cancer.

Dave et al. reported cytogenetic results regarding the primary tumors and peripheral lymphocytes of 10 lung cancer cases (9 NSCLS and 1 SCLC) (14). They reported concordance between chromosomes altered in the lymphocytes and tumor cells of the same case, although sometimes the abnormality was able to differ. Moreover, they stated this to imply that "the susceptibility of particular chromosomes to break more frequently than others" is what is transmitted from the progenitor cells. However, they observed mainly numerical abnormalities in their work, with practically all chromosomes appearing altered. They concluded the genomic instability at the chromosomal level in the peripheral blood lymphocytes to correspond with tumors and "peripheral blood lymphocyte chromosomal

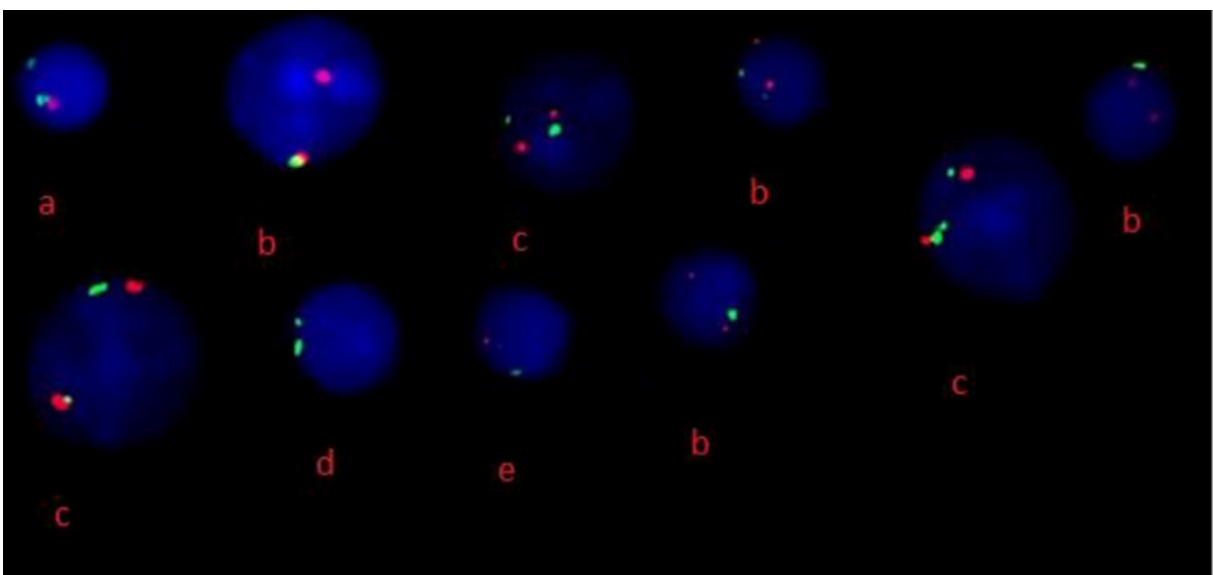


**Figure 5.** FISH image of an SCLC case (Case No. K9) containing (a): monoallelic (2G1R) deletion, (b) rearrangements (2R1G), (c) normal cell (2R2G), (d) biallelic (2G) deletion, and (e) monosomy (1R1Y). (Note: Green = centromere region of the 3rd chromosome, red = FHIT gene region of the 3rd chromosome)

analysis has a promising future in the genetic analysis of lung cancers" (14). Along with this comparative report between the tumor and peripheral blood of the same cases, Dave et al. also published the results of a broader cohort that examined only the peripheral lymphocytes of 96 untreated lung cancers and 74 normal control subjects in the same year. They declared in their report that more than 15% of their cases had structural or numerical chromosomal abnormalities for chromosomes 1, 3, 5, 7, 9, 12, 14, and 21 (11). These chromosomes had also been reported as being frequently involved in over 20% of the cases in their first-mentioned study (14). As for chromosome 3, their comparative study observed that, while chromosome 3 had been structurally rearranged in all 10 tumors, it had been rearranged in the peripheral lymphocytes in six cases (14).

De Fusco et al. reported chromosome aberrations of peripheral blood in seven SCLC cases. They found no chromosome 3 abnormalities but observed four aneuploid cells in one case: -Y in two cells, +5 and +12 in one, and +8 and +12 in another cell. Because +5, +8, and +12 were involved in the complex karyotype of the tumor tissue of the same patient and because the patient who had entered remission after treatment had relapsed and developed brain metastasis afterward, they commented that the aneuploid peripheral cells might have been circulating the tumor cells responsible for the metastasis (15).

When considering the cases in the literature alongside the current study, peripheral blood cytogenetics can be helpful as an indicator of chromosome instability with the observation of higher percentages of karyotypically abnormal -especially aneuploid- metaphases, as well as specific chromosomal abnormalities for the malignancy in question. However, quite a number of metaphases (100 if possible) need to be examined, and this is time- and effort-consuming in addition to also requiring expertise. Time and effort issues can be overcome to some extent through automatization when scanning the slides and capturing and analyzing the metaphases. However, finalizing the analyses will still require quite a lot of time and effort of an expert cytogeneticist. Therefore, conventional cytogenetics does not seem very practical for this purpose.

In addition to the cytogenetic analyses, this study performed FISH analyses to identify any possible submicroscopic deletions in the 3p14-21 critical region by targeting the FHIT gene in this region. FHIT is a tumor suppressor gene and a DNA caretaker. Loss of heterozygosity (LOH) in FHIT has been reported in previous studies and is considered an early alteration in lung cancer (5, 7, 25-27), with loss of FHIT expression causing genomic instability.

The current study detected FHIT deletion in about 30% of the patients (9 ADC and 7 SCLC), which was significantly higher than in the control group ( $p < 0.05$ ). Although the LOH of FHIT is reported in more than 50% of precancerous lesions and tumors, when considering that the material this study examined was peripheral blood, the rate in this study can be

considered high. FHIT deficiency causes replication stress and DNA breaks. Replication stress can lead to micronucleus formation, aneuploidy, copy number alterations, and deletions at common fragile sites.

Owing to co-localization with FRA3B, the abnormal expression of FHIT boosts replication stress in this region, leading to FHIT deletions (28). FHIT loss causes genomic instability, leads to a mutator phenotype with a very high mutational rate, and accelerates tumorigenesis, progression, and metastasis. Because of these effects, FHIT mutations are considered as a driver mutation in cancer and could serve as a prognostic biomarker for many cancers (19, 26). Regarding the current study's rate using FISH, obtaining these deletions and mutations in circulating cells in the blood can possibly be considered significant. However, the FHIT status in the tumor tissue remained unclear in this study's patients due to being unable to access the tumor materials for a comparison. This can be considered as a limitation of the study. Further studies are needed for comparing FHIT status in blood and tumor samples and for assessing its potential as a biomarker.

In conclusion, the FISH technique could be useful for detecting FHIT loss in blood samples apart from tumor tissues. FISH is also capable of indicating aneuploidy as a marker of genomic instability. Present and future reports will enable the selection of recurring aneuploidies to scan with centromeric FISH probes along with relevant locus-specific probes to create a FISH panel for lung cancer.

---

**Ethics Committee Approval:** The study has been conducted in accordance with the Helsinki Declaration and was approved by the Cerrahpaşa Faculty of Medicine Medical Ethics Committee (Reference No. 83045809-604.01.02-A49).

**Informed Consent:** All patients and individuals in the control group having signed informed consent forms.

**Peer-review:** Externally peer-reviewed.

**Author Contributions:** Conception/Design of Study- Y.T.A., A.C., N.B., H.G.O.; Data Acquisition- H.G.O., E.B.T., N.B.; Data Analysis/ Interpretation- Y.T.A., A.C., N.B.; Drafting Manuscript- Y.T.A., N.B.; Critical Revision of Manuscript- Y.T.A., A.C., N.B.; Final Approval and Accountability- Y.T.A., A.C., N.B., H.G.O., E.B.

**Conflict of Interest:** The authors declare that they have no competing interests.

**Financial Disclosure:** This project was supported by the Istanbul University Scientific Research and Project Commission (Project No. 23831).

## REFERENCES

- Schwendel A, Langreck H, Reichel M, Schröck E, Ried T, Diel M, et al. Primary small-cell lung carcinomas and their metastases are characterized by a recurrent pattern of genetic alterations. *Int J Cancer* 1997; 74(1): 86-93.

2. Graziano SL, Cowan BY, Carney DN, Bryke CR, Mitter NS, Johnson BE, et al. Small cell lung cancer cell line derived from a primary tumor with a characteristic deletion of 3p. *Cancer Res* 1987; 47(8): 2148-55.
3. Chang JG, Chen CC, Wu YY, Che TF, Huang YS, Yeh KT, et al. Uncovering synthetic lethal interactions for therapeutic targets and predictive markers in lung adenocarcinoma. *Oncotarget* 2016; 7(45): 73664-80.
4. Ashman JN, Brigham J, Cowen ME, Bahia H, Greenman J, Lind M, et al. Chromosomal alterations in small cell lung cancer revealed by multicolour fluorescence in situ hybridization. *Int J Cancer* 2002; 102(3): 230-6.
5. Iijima H, Tomizawa Y, Dobashi K, Saito R, Nakajima T, Mori M. Allelic losses on chromosome 3p are accumulated in relation to morphological changes of lung adenocarcinoma. *Br J Cancer* 2004; 91(6): 1143-8.
6. Petersen I, Langreck H, Wolf G, Schwendel A, Psille R, Vogt P, et al. Small-cell lung cancer is characterized by a high incidence of deletions on chromosomes 3p, 4q, 5q, 10q, 13q and 17p. *Br J Cancer* 1997; 75(1): 79-86.
7. Sozzi G, Veronese ML, Negrini M, Baffa R, Cotticelli MG, Inoue H, et al. The FHIT gene 3p14.2 is abnormal in lung cancer. *Cell* 1996; 85(1): 17-26.
8. Tarkan-Argüden Y, Hacıhanefioglu S, Ongen G, Erk M, Cenani A. 3p abnormalities in peripheral lymphocytes in small cell lung cancer. *Tumori* 2009; 95(4): 535-7.
9. Zabarovsky ER, Lerman MI, Minna JD. Tumor suppressor genes on chromosome 3p involved in the pathogenesis of lung and other cancers. *Oncogene* 2002; 21(45): 6915-35.
10. Balsara BR, Testa JR. Chromosomal imbalances in human lung cancer. *Oncogene* 2002; 21(45): 6877-83.
11. Dave BJ, Hopwood VL, King TM, Jiang H, Spitz MR, Pathak S. Genetic susceptibility to lung cancer as determined by lymphocytic chromosome analysis. *Cancer Epidemiol Biomarkers Prev* 1995; 4(7): 743-9.
12. Mori N, Yokota J, Oshimura M, Cavenee WK, Mizoguchi H, Noguchi M, et al. Concordant deletions of chromosome 3p and loss of heterozygosity for chromosomes 13 and 17 in small cell lung carcinoma. *Cancer Res* 1989; 49(18): 5130-5.
13. Todd S, Franklin WA, Varella-Garcia M, Kennedy T, Hilliker CE, Jr., Hahner L, et al. Homozygous deletions of human chromosome 3p in lung tumors. *Cancer Res* 1997; 57(7): 1344-52.
14. Dave B, Hopwood V, Spitz M, Pathak S. Shared cytogenetic abnormalities in lung-tumors and corresponding peripheral-blood lymphocytes. *Int J Oncol* 1995; 7(6): 1297-305.
15. De Fusco PA, Frytak S, Dahl RJ, Weiland LH, Unni KK, Dewald GW. Cytogenetic studies in 11 patients with small cell carcinoma of the lung. *Mayo Clin Proc* 1989; 64(2): 168-76.
16. Khan S, Coulson JM, Woll PJ. Genetic abnormalities in plasma DNA of patients with lung cancer and other respiratory diseases. *Int J Cancer* 2004; 110(6): 891-5.
17. Hurr K, Kemp B, Silver SA, el-Naggar AK. Microsatellite alteration at chromosome 3p loci in neuroendocrine and non-neuroendocrine lung tumors. Histogenetic and clinical relevance. *Am J Pathol* 1996; 149(2): 613-20.
18. Sozzi G, Pastorino U, Moiraghi L, Tagliabue E, Pezzella F, Ghirelli C, et al. Loss of FHIT function in lung cancer and preinvasive bronchial lesions. *Cancer Res* 1998; 58(22): 5032-7.
19. Niu Z, Jiang D, Shen J, Liu W, Tan X, Cao G. Potential role of the fragile histidine triad in cancer evo-dev. *Cancers (Basel)* 2023; 15(4).
20. Ilic M, Ilic I. Epidemiology of pancreatic cancer. *World J Gastroenterol* 2016; 22(44): 9694-705.
21. Karras JR, Paisie CA, Huebner K. Replicative stress and the FHIT gene: roles in tumor suppression, genome stability and prevention of carcinogenesis. *Cancers (Basel)* 2014; 6(2): 1208-19.
22. Kawanishi M, Kohno T, Otsuka T, Adachi J, Sone S, Noguchi M, et al. Allelotype and replication error phenotype of small cell lung carcinoma. *Carcinogenesis* 1997; 18(11): 2057-62.
23. Pathak S. Cytogenetics of epithelial malignant lesions. *Cancer* 1992; 70(6 Suppl): 1660-70.
24. Heng HH, Liu G, Bremer S, Ye KJ, Stevens J, Ye CJ. Clonal and non-clonal chromosome aberrations and genome variation and aberration. *Genome* 2006; 49(3): 195-204.
25. Burke L, Khan MA, Freedman AN, Gemma A, Rusin M, Guinee DG, et al. Allelic deletion analysis of the FHIT gene predicts poor survival in non-small cell lung cancer. *Cancer Res* 1998; 58(12): 2533-6.
26. Karras JR, Schrock MS, Batar B, Huebner K. Fragile genes that are frequently altered in cancer: players not passengers. *Cytogenet Genome Res* 2016; 150(3-4): 208-16.
27. Zhou Q, Chen J, Qin Y, Sun Z, Liu L, Sun Z, et al. [A study on the allelic deletion and mutation of FHIT gene in human non-small cell lung cancer]. *Zhongguo Fei Ai Za Zhi* 2001; 4(1): 10-4.
28. Saldivar JC, Park D. Mechanisms shaping the mutational landscape of the FRA3B/FHIT-deficient cancer genome. *Genes Chromosomes Cancer* 2019; 58(5): 317-23.

Supplementary Table 1: Comparison of karyotype formulas with metastatic status of ADC cases		
ADC Case No	Karyotype Formula	Metastasis Status
A1	38~45,XY,-Y[6],-8[5],-9[3],-10[3],-11[5],- 12[5],-13[3],-14[3],-17[3],-18[4],-19[5],- 20[7],-21[6],-22[3][cp20]/18~28,X,+Y[2],+1[3],+9[2],+11[2],+13[2],-18[3][cp3]/46,XY[71]	Liver Met
A2	38~48,XY,+Y[2],-1[3],-2[4],+2[2],-3[3],-4[3],-5[3],del(6)(q15q21)[3],- 8[5],dic(9;11)(q34;p15)[2],+10[2],add(10)(q26)[2],+11[3],-13[4],+13[2],-15[3],- 17[6],-19[4],+19[2],-21[4],+21[3],- 22[4]+22[2],del(22)(q12)[2],ace1[6],dmin[5][cp27]/17~31,X,+Y[3],+2[2],+9[2],+13[2][cp3]/46, XY[55]	Bone Met
A3	38~45,XY,-8[8],-11[4],-14[4],-16[4],-17[4],-18[4],del(18)(p11)[2],-19[6],-20[8],-21[8],-22[6][cp30]/46,XY,del(6)(q15q21)[2]/46,XY[55]	-
A4	32~45,XX,-X[9],chtg(16)(q21)[4][cp12]/47,XX,+21[2]/46,XY[74]	-
A5	40~46,XX,-X[9],+Y[2],-2[3],-3[3],-6[3],-7[3],-10[3],-15[3][cp15]/16~34,X,+1[3],+2[5],+3[4],+4[4],+5[6],+6[3],+7[4],+8[4],+9[4],+10[4],+11[6],+12[3],+13[3],-15[3],+15[3],+16[5],-17[3],+17[3],+19[2],+20[2],+21[4],-22[4],+22[2][cp10]/46,XX[68]	-
A6	35~45,XY,-Y[6],-4[4],-6[4],-7[5],-18[4],-21[3][cp14]/ 46,XY[78]	-
A7	36~45,XY,-5[3],-7[4],-10[6],-15[4],-16[5],-17[3],-22[7][cp17]/27~33,X,+1[3],+6[2],+7[2],+10[2],+15[2],+16[2],+17[2],+18[3]+19[2],+20[2],+21[2][cp3]/47,XY,+21[2]/46,XY[68]	-
A8	39~45,XY,-Y[4],-2[3],-6[3],-14[4],-16[4],-19[4],-20[5][cp15]/25~33,X,+2[3],+11[3],+12[2],+14[2],+15[3][cp3]/46,XY[56]	Liver Met
A9	37~45,XX,-X[9],-2[3],-3[3],-5[3],-6[3],-7[3],-8[4],-14[3],-18[3],-19[5],-21[5],-22[6][cp25]/26~28,X,+6[2],+9[2],+10[2],+11[3],+12[4],+13[3],+15[3],+22[2][cp4]/46, XX[51]	Brain Met
A10	36~46,XX,-X[17],del(X)(p11)[2],-3[3],add(3)(q29)[4],-5[4],-6[4],-7[3],-8[5],- 10[6],-13[3],-14[3],15[3],-18[3],-19[5],- 20[3],-21[3],- 22[3][cp37]/47,XX,+X[3]/47~48,XX,+8[3],+ 10[2][cp3]/28~32,X,+1[2],+3[2],+7[2],+12[2],+17[2][cp2]/46,XX[52]	-
A11	38~47,XX,-X[21],-4[3],-5[4],- 6[6],del(6)(q15q21)[4],-7[3],-8[7],-9[6],-10[12],-11[6],-12[4],-13[6],-14[5],-15[5],- 16[7],-17[4],-19[4],-20[7],-21[7],-22[6][cp50]/18~33,X,+X[3],+1[3],+2[3],+3[2],+4[3],+5[2],+6[3],+7[3],+8[2],+9[4],+10[3],+11[3],+12[4],+13[3],+14[3],+16[5],+17[3],+18[4],+19[2],+20[5],+21[4],+22[4][cp 7]/46,XX[36]	-
A12	39~46,XY,inv(10)(q23q24)[5],del(14)(q24)[4],-18[4],-19[5],-20[4],-21[4],- 22[4][cp22]/27~32,X,+Y[2],+1[3],+4[2],+6[2],+7[2],+9[2],+12[2],+15[2],+16[2],+22[2][cp3]/46,XY[70]	Bone Met
A13	NMFE	-
A14	NMFE	Liver Met+ Bone Met

<b>A15</b>	35~45,XY,-X[6],-Y[6],-1[4],-2[13],-3[16],-4[9],-5[3],-6[16],-7[10],-8[15],-9[14],-10[9],-11[10],-12[13],-13[18],-14[14],-15[11],-16[11],-17[20],-18[4],-19[11],-20[9],-21[13],-21[4],-22[9][cp56]/26~33,X,- X[5],+Y[6],+1[9],+2[5],+3[11],+4[8],+5[10],+6[3],+7[7],-8[4],+8[3],+9[5],-10[3],+10[6],-11[3],+11[9],+12[11],-13[5],+13[9],+14[7],-15[6],+15[4],-16[3],+16[8],-17[4],+17[5],+18[11],+19[5],+20[4],-21[6],+21[9],-22[3],+22[9][cp18]/46,XY[20]	-
<b>A16</b>	35~46,XX,-X[28],-2[9],-3[17],-4[6],-5[7],-6[8],-7[6],del(7)(p13)[3],-8[8],-9[4],-10[7],-11[4],-12[7],-13[4],-14[7],-15[11],-16[8],-17[9],-17[3],-18[9],del(18)(p11)[5],-19[20],-20[12],-21[9],-22[10][cp57]/21~33,X,-X[4],+X[2],+1[6],+2[4],-3[3]+3[4],+4[3],+5[6],+6[6],+7[4],+8[3],+9[5],+10[5],+11[4],+12[4],+13[5],-14[4],+14[4],+15[7],+16[2],+17[3],-20[3],+20[4],+21[5],+22[6][cp12]/46,XX[26]	Esophagus Met
<b>A17</b>	35~50,XX,-X[6],+X[5],-2[6],-3[4],-4[8],-6[8],-7[5],-7[3],-8[8],-9[3],-10[4],+10[2]-11[4],-13[5],-14[3],-15[4],-20[12],-21[9],-21[4],-22[12][cp43]/46,XX[44]	-
<b>A18</b>	35~45,XY,-3[5],-4[3],-5[3],-7[3],-9[5],-10[10],-12[4],-14[6],-17[8],-18[4],-20[6],-21[9],-22[5][cp27]/46,XY[50]	Esophagus Met
<b>A19</b>	36~46,XY,-Y[4],-1[4],-3[4],-8[8],-11[4],-12[6],-16[6],-17[4],-18[4],del(18)(p11)[2],-19[6],-20[6],-21[6],-22[6][cp32]/46,XY[46]	-
<b>A20</b>	NMFE	-
<b>A21</b>	NMFE	Brain Met+Bone Met
<b>A22</b>	NMFE	Bone Met
<b>A23</b>	40~46,XY,-5[3],-8[13],-9[6],-13[7],-14[4],-15[4],-17[6],-18[4],-19[15],-20[6],-21[6],-22[8][cp43]/22~33,X,+Y[16],+1[9],-2[6],+2[5],+3[8],-4[3],+4[6],+5[6],+6[12],-7[4],+7[9],+8[2],+9[7],+10[6],-11[6],+11[5],-12[3],+12[6],-13[3],+13[8],-14[4],+14[3],-15[7],+15[6],+16[6],-17[5],+17[6],+18[5],-19[3],+19[3],+20[5],-21[3],+21[5],-22[6],+22[3][cp17]/46,XY[32]	Brain Met
<b>A24</b>	35~46,XY,-Y[3],-1[7],-3[7],-4[10],-5[11],-7[4],-9[8],-10[9],-11[4],-12[15],-13[8],-14[6],-16[6],-17[7],del(18)(p11)[5],-	-
<b>A25</b>	19[16],-20[8],-21[3],-22[11][cp50]/22~34,X,- X[7],+Y[11],+1[5],+2[6],+3[4],+5[4],-6[4],+6[6],+7[5],+8[3],-9[6],+9[5],+10[6],+11[7],+12[6],13[4],+13[6],+14[9],+15[10],+16[7],-17[3],+17[7],+18[6],del(18)(p11)[2],+20[3],-21[3],+21[4],+22[6][cp14]/46,XY[29]	-
<b>A26</b>	40~46,XY,-X[3],-3[5],-6[4],-7[4],-10[4],-12[3],-13[6],-18[4],-19[5],-20[3][cp21]/46,XY[64]	-
<b>A27</b>	35~45,XY,-Y[3],-1[6],-3[6],-4[4],-5[7],-6[4],-7[4],-8[8],-9[7],-10[12],-11[5],-12[3],-13[7],-15[4],-16[11],-16[4],-17[10],-18[9],-19[4],-19[4],-20[12],-21[12],-22[8][cp42]/27~30,X,+Y[2],+1[2],+2[4],+4[2],+6[4],+7[2],+8[2],+9[2],+11[2],+12[2],+16[2],+17[2],+18[2],+19[2],+20[2][cp4]/46,XY[44]	-
<b>A28</b>	36~46,XY,-1[4],-3[4],-5[5],-6[4],-7[5],-8[7],-9[5],-10[7],-13[4],-14[5],-15[6],-17[4],-18[4],-19[5],+21[4][cp25]/46,XY[57]	-
<b>A29</b>	36~45,XY,-X[5],-Y[10],-2[5],-3[9],-4[9],-5[9],-6[6],-7[5],-8[15],-9[9],-10[11],-11[9],-12[7],-13[9],-14[9],-15[7],-16[9],-17[18],-18[10],-19[16],-20[19],-21[10],-22[18],-22[7][cp50]/46,XY[32]	-
<b>A29</b>	35~45,XY,-1[4],-3[4],-8[4],-10[4],-11[4],-12[8],-14[3],-15[3],-16[9],-17[8],-18[6],-19[4],-20[12],-21[13],-22[8][cp29]/28-34,X,+Y[3],+2[3],+3[4],+4[4],+8[4],+10[2],+11[3],+13[4],+15[2][cp4]/46,XY[31]	Bone Met

<b>30</b>	35~48,XY,+X[2],-Y[4],-1[6],-3[7],+3[6],-4[7],-5[5],-6[8],+6[2],der(7)t(7;7)(p10;q10)der(7)(q10;q10)[5],i(7)(q10)[7],-8[10],-10[4],-11[4],+11[2],-12[9],-13[10],-14[3],-15[7],-16[8],-17[3],-18[6],-19[6],-20[9],-21[13],-22[12],+22[3][cp34]/19~27,X,-X[5],+1[2],-2[4],+4[2],+5[2],-8[3],-13[3],+14[3],+16[3],-18[3],+21[3],+22[2][cp6]/46,XY[23]	Brain Met
*ADC-adenocarcinoma; Met-Metastasis; NMFE- No Metaphase Found to Evaluate		

<b>Supplementary Table 2: Comparison of karyotype formulas with metastatic status of SCLC cases</b>		
<b>SCLC Case No</b>	<b>Karyotype Formula</b>	<b>Metastasis Status</b>
<b>K1</b>	36~46,XY,-Y[7],-2[3],-4[3],-6[4],-8[3],-10[4],-11[4],-12[5],-15[6],-16[3],-17[3],-18[4],-20[6],-21[4],-22[3][cp23]/22~33,X,+Y[4],+1[3],+2[3],+3[3],+4[4],+5[3],+6[2],+6[2],+7[4],+8[2],+10[2],+11[2],+12[2],+13[2],+14[2],+16[3],+17[3],-18[3],+18[2],+19[2],+21[3],-22[5][cp6]/46,XY[61]	Liver Met+Muscle Met
<b>K2</b>	36~45,XY,-X[3],-1[3],-3[4],-5[3],-10[5],-11[3],-12[5],-13[4],-18[7],-20[3],-22[3][cp18]/28~34,X,+Y[2],+2[4],+3[2],+4[3],+5[2],+6[2],+7[2],+8[3],+10[4],+12[2],+15[2],+16[4],+17[4],+18[2],+19[4],+20[3],+21[2],+22[3][cp5]/46,XY[61]	-
<b>K3</b>	36~45,XY,-1[5],-2[3],-4[5],-5[7],-6[4],-7[4],-8[9],-9[3],-10[6],-11[3],-12[4],-13[4],-15[3],-17[7],-19[10],-20[3],-21[3],-22[7][cp27]/28~33,X,+Y[3],+1[3],+3[2],+5[3],+7[3],+9[2],+10[2],+11[2],+13[2],+14[3],+15[4],+16[2],+17[3],+19[4],+20[2],+21[2],+22[3][cp5]/46,XY[64]	-
<b>K4</b>	42~45,XY,-Y[4],-3[3],-10[5],-12[3],-20[3],-22[5][cp19]/46,XY[59]	Brain Met
<b>K5</b>	41~46,XX,-X[3],-8[3],der(18)del(18)(p11)del(18)(q12q22)[7][cp11]/40~45,XX,-19[cp4]/46~47,XX,+8[cp2]/46,XX[69]	-
<b>K6</b>	NMFE	-
<b>K7</b>	NMFE	-
<b>K8</b>	NMFE	Brain Met
<b>K9</b>	35~52,XY,-1[4],-3[5],-6[4],-6[3],-7[4],-8[3],-9[4],-10[5],-11[4],-13[3],-14[4],del(18)(p11)[9],-19[3],-20[6],-21[10],-22[5],+22[2][cp32]/19~30,X,+Y[2],+4[2],+6[2],+8[2],+9[2],+11[3],+14[2],+15[2],+20[2],-22[4][cp4]/46,XY[51]	Brain Met
<b>K10</b>	NMFE	-
<b>K11</b>	NMFE	-
<b>K12</b>	35~46,XY,-X[5],-Y[7],-1[6],-2[7],-3[4],-4[6],-5[9],-6[6],-7[7],-8[16],-9[9],-10[11],-11[4],-12[18],-13[7],-14[7],-15[5],-16[11],-17[5],-18[8],-19[19],-19[4],-20[15],-20[3],-21[8],-22[9][cp47]/24~33,X,+Y[5],+1[4],+2[10],+3[5],+4[6],+5[6],+6[7],+7[4],-8[3],+8[2],+9[3],+10[5],+11[8],+12[7],+13[8],+14[4],+15[8],+16[5],-17[4],+17[4],+18[5],+19[4],-20[3],+20[6],+21[7],-22[5][cp14]/46,XY[21]	Head and Neck Met
<b>K13</b>	36~46,XY,-X[6],-1[4],-2[6],-7[4],-8[4],-9[6],-10[6],-11[7],-12[8],-13[4],-15[6],-16[5],-17[10],-18[13],-19[8],-20[6],-22[10][cp39]/33,X,+Y[4],+1[4],+2[4],+3[3],+4[4],+5[2],+7[3],+9[2],+11[4],+12[3],+14[2],+15[3],+16[4],+17[3],+20[3],+21[2][cp5]/46,XY[42]	Brain Met+Bone Met

<b>K14</b>	35~46,XY,-X[6],-Y[10],-1[14],-2[12],-3[10],-4[10],-5[14],-6[6],-7[6],-8[13],-9[6],-10[10],-11[4],-12[10],-13[12],-14[12],-15[12],-16[15],-17[10],-18[10],-19[20],-20[12],-20[6],-22[8][cp53]/20~23,X,+Y[4],+1[12],-2[4],+2[6],+3[13],+4[8],+5[5],-6[7],+6[4],-7[3],+7[7],+8[10],-9[7],+9[5],-10[4],+10[5],-11[3],+11[13],+12[9],-13[5],+13[6],-14[5],+14[7],-15[3],+15[4],-16[3],+16[10],-17[4],+17[8],+18[7],+19[7],-20[3],+20[5],-21[6],+21[3],-22[4],+22[5][cp18]/46,XY[28]	-
<b>K15</b>	36~45,XY,-1[3],-3[7],-4[9],-5[7],-6[8],-7[5],-8[12],-9[7],-10[9],-12[5],-13[6],-14[14],-15[11],-16[14],-17[9],-18[9],-19[13],-19[4],-20[13],-21[14],-22[6][cp45]/28~32,X,+Y[11],+1[7],+2[5],+3[9],+4[6],+6[3],-7[3],+7[3],+8[8],+9[11],-10[4],+10[3],-11[3],+11[3],+13[8],+14[6],+15[6],+16[6],+17[5],+18[2],-19[5],-20[4],+21[5],+22[10][cp12]/46,XY[37]	-
<b>K16</b>	40~45,XY,-3[4],-5[6],-11[4],-14[4],-17[6],-19[7],-21[13],-22[6][cp36]/32~34,X,+Y[3],+1[2],+2[3],+8[2],+9[2],+11[3],+12[2],+13[3],+16[2],+20[3],+21[3][cp3]/46,XY[51]	-
<b>K17</b>	38~47,XY,-2[4],-7[7],-8[4],-9[3],-10[4],-11[4],-12[4],-14[6],-15[3],-19[4],-20[10],del(20)(q13)[4],-21[12],+21[4],-22[6][cp41]/30~34,X,+Y[6],-1[3],+1[3],+3[6],+4[3],+5[3],+6[2],+7[2],-8[3],+8[3],+9[3],+10[4],+11[2],+12[2],+13[3],+14[2],+15[2],+16[4],+18[3],+19[5],+21[3],+22[2][cp6]/46,XY[42]	Brain Met
<b>K18</b>	NMFE	-
<b>K19</b>	35~46,XY,-3[7],-5[8],-6[3],-8[8],-9[8],-10[8],-11[11],-11[4],-12[4],-13[3],-14[8],-15[6],-16[11],-17[8],-18[7],-19[8],-20[6],-21[4],-22[8][cp38]/21~34,X,-X[5],+Y[3],+1[3],+2[3],-3[3],+4[4],-6[3],+6[3],+7[5],+8[2],+9[2],+10[2],+12[3],+13[3],+14[3],+15[3],+17[6],+20[3],-22[3],+22[2][cp6]/46,XY[47]	-
<b>K20</b>	33~46,XX,-X[8],-2[3],-4[3],del(6)(q15q21)[5],-13[3],-13[3],-16[4],-17[5],-19[6],-20[3],-21[4],-22[5][cp32]/46,XX[51]	-
<b>K21</b>	37~47,XY,-Y[8],-6[6],-9[7],-10[3],-12[11],-13[8],-14[5],-16[3],-17[3],-18[6],-19[10],-20[6],-21[8],-22[5][cp36]/46,XY[55]	Bone Met
<b>K22</b>	38~50,XX,-X[5],+X[3],-6[4],-7[4],-12[6],-14[4],-17[8],-17[3],-18[6],-19[4],-22[4],del(22)(q12)[5],+mar2[3],+mar2x3 [2][cp29]/22~32,X,+X[4],+1[2],+3[2]+4[2],+5[2],+6[3],+8[3],+9[2],+11[2],+12[3],+13[4],+15[3],+16[3],+19[2],+21[2][cp5]/46,XX[48]	-
<b>K23</b>	36~46,XY,-1[3],-2[4],t(3;5)(p25;q31)[2],-4[7],-5[4],-6[4],-7[7],-8[13],-9[8],inv(9)(p12q13)[71],-10[4],-11[6],-12[10],-14[4],-15[3],-16[8],-17[8],-18[7],-18[3],-19[9],-20[6],-21[8],-22[5][cp84]/30~33,X,+Y[4],+1[4],+2[4],+3[4],del(3)(p22)[2],+4[2],+5[6],+6[4],+7[4],inv(9)(p12q13)[4],+10[4],+11[6],+12[2],+13[2],+14[4],+16[2],+17[6],+18[2],+20[2],+21[4],-22[4],+22[2][cp6]/46,XY[9]	-
<b>K24</b>	38~45,XY,-Y[4],-5[3],-7[3],-12[3],-16[3],-17[4],-19[5],-21[5][cp10]/46,XY[70]	-
<b>*SCLC-small-cell lung cancer; Met-Metastasis; NMFE- No Metaphase Found to Evaluate</b>		

# Effects of GDF-15 Level in Patients with Membranous Nephropathy\*

Aida Adikozalova<sup>1</sup> , Sebahat Usta Akgul<sup>2</sup> , Erol Demir<sup>3</sup> , Hayriye Senturk Ciftci<sup>2</sup> , Fatma Savran Oguz<sup>2</sup> , Halil Yazici<sup>3</sup> , Cigdem Kekik Cinar<sup>2</sup> 

<sup>1</sup>Institute of Graduate Studies in Health Sciences, Istanbul University, Istanbul, Turkiye

<sup>2</sup>Department of Medical Biology, Istanbul Faculty of Medicine, Istanbul University, Istanbul, Turkiye

<sup>3</sup>Division of Nephrology, Department of Internal Diseases, Istanbul Faculty of Medicine, Istanbul University, Istanbul, Turkiye

ORCID ID: A.A. 0000-0003-2897-3624; S.U.A. 0000-0003-0176-3344; E.D. 0000-0003-0128-5645; H.S.C. 0000-0003-3507-482X; F.S.O. 0000-0002-6018-8936; H.Y. 0000-0003-2526-3483; C.K.C. 0000-0003-2098-381X

**Cite this article as:** Adikozalova A, Usta Akgul S, Demir E, Senturk Ciftci H, Savran Oguz F, Yazici H, Kekik Cinar, C. Effects of GDF-15 level in patients with membranous nephropathy. *Experimed* 2024; 14(1): 40-45.

## ABSTRACT

**Objective:** Nephrotic syndrome is the most frequent cause of membranous nephropathy (MN) in adults. Growth differentiation factor (GDF)-15 is a cytokine released under stress and associated with increased incidence of chronic kidney disease and/or decreased renal function in conditions such as diabetic nephropathy, IgA nephropathy, lupus nephritis, and primary MN. The diagnosis of MN is made by biopsy, which is an invasive procedure. A non-invasive biomarker is needed for timely and risk-free diagnosis. This study aimed to estimate the GDF-15 level in patients with MN to determine if it can be used as a noninvasive biomarker for the diagnosis of MN.

**Materials and Methods:** The study included 88 patients with MN. Sera were obtained from peripheral blood collected from the patients. GDF-15 levels were analyzed using enzyme-linked immunosorbent assay (ELISA).

**Results:** GDF-15 level was high in older patients than in younger patients. The glomerular filtration rate was low in patients with increased GDF-15 levels. Furthermore, a decrease in GDF-15 levels was observed in patients in remission.

**Conclusion:** GDF-15 level may be used as a biomarker to predict the progression of MN rather than a diagnostic biomarker.

**Keywords:** Membranous nephropathy, GDF-15, ELISA

## INTRODUCTION

Membranous nephropathy (MN), a glomerulopathy, is one of the most important causes of idiopathic nephrotic syndrome in the adult age group (1). A definitive diagnosis can be made with a kidney biopsy. Considering that biopsy protocols differ among countries, there is a regional variance in the incidence of the disease. The disease is seen twice as often in men than in women. MN is a long-term disease that undergoes spontaneous remission in approximately 30% of the patients. Nonetheless, progression to end stage

kidney disease (ESKD) may develop within 5 to 15 years in 30–40% of the patients with MN (2). Approximately 75% of the MN cases are primary MN (idiopathic-IMN) and 25% are secondary MN (due to autoimmune diseases, infections, or malignancies).

Growth differentiation factor (GDF)-15 is a cytokine produced in several tissues in response to stress and whose levels increase in response to stimuli in some diseases. However, the underlying mechanisms remain unknown. GDF-15 levels are significantly increased in patients with

\*This article is derived from Aida Adikozalova's PhD dissertation in Medical Biology, conducted under the supervision of Prof. Dr. Cigdem Kekik Cinar, 10537977 of the Council of Higher Education Thesis Centre.

**Corresponding Author:** Aida Adikozalova **E-mail:** aslanaida8593@gmail.com

**Submitted:** 13.12.2023 **Revision Requested:** 25.03.2024 **Last Revision Received:** 01.04.2024 **Accepted:** 05.04.2024



Content of this journal is licensed under a Creative Commons Attribution-NonCommercial 4.0 International License.

IMN and negatively correlated with the glomerular filtration rate (eGFR) (3, 4).

Increased level of circulating GDF-15 has been linked to a decrease in estimated glomerular filtration rate (eGFR), kidney damage, and progression to ESKD, and it may be a marker of chronic kidney damage (5, 6). Based on the studies conducted to date, we hypothesized that high circulating GDF-15 levels may be used as a diagnostic biomarker of MN in patients.

## MATERIALS AND METHODS

### Study Population

Eighty-eight adult patients, who presented to the Department of Nephrology, Istanbul Faculty of Medicine, Istanbul University (Istanbul, Turkiye) between 2010 and 2017 and were diagnosed with MN based on biopsy examination, were included in the study. The study was approved by the clinical experiments local ethical committee of Istanbul University Istanbul Faculty of Medicine (No: 2018/1260; date: 03/10/2018), and informed written consent was obtained from the study participants. The study was conducted in accordance with the principles of the 1975's Helsinki Declaration. Blood samples were obtained at the time of diagnosis, and 51% of patients had stage II of MN. No control group was included in the study. The reference range of GDF-15 was 399–1335 pg/mL based on the comparison of sex, lifestyle, and biological factors between healthy individuals (7, 8).

**Table 1:** Demographic data of the patients

Characteristics	
Age, year	53.59 ± 13.82
Age at the time of diagnosis	46.3 ± 13.5
Sex, Male / Female, n	51/37
BMI, kg/m <sup>2</sup>	78.90 ± 14.7
Systolic blood pressure, mmHg	131.42 ± 19.2
Diastolic blood pressure, mmHg	81.13 ± 12.5
Serum albumin, g/dL	2.80 ± 0.8
Serum creatinine, mg/dL	0.9 ± 0.4
Serum creatinine on follow-up, mg/dL	1.2 ± 1.1
Hemoglobin, g/dL	12.93 ± 2.3
eGFR, mL/minute/1.73m <sup>2</sup>	102.21 ± 52.1
Proteinuria, mg	5677.79 ± 3545.6
Proteinuria on follow-up, mg	2869.82 ± 3003.5

Data are presented as mean ± SD unless stated otherwise  
BMI, body mass index; eGFR, estimated glomerular filtration rate

### Clinical Parameters

Proteinuria, proteinuria at follow-up, serum albumin, serum creatinine, serum creatinine at follow-up, eGFR hemoglobin, serum albumin, systolic blood pressure, diastolic blood pressure, BMI (kg/m<sup>2</sup>), remission and ESKD were compared with GDF-15 level. Immunosuppressive agents such as mycophenolate mofetil, cyclophosphamide, cyclosporine, and steroids and antihypertensive drugs such as angiotensin receptor blockers (ARBs) and/or angiotensin-converting enzyme inhibitors (ACEIs) were administered to the patients during the treatment process.

### Measurement of Serum GDF-15 Levels

Blood was obtained once from the patients at the diagnosis. The serums obtained from the blood samples were stored at -20°C until they were analyzed. The GDF-15 levels were measured using enzyme-linked immunosorbent assay (ELISA) (Human GDF-15; Thermo Fisher Scientific, Waltham, MA, USA) according to the manufacture's instructions, and the results were read at 450 nm.

### Statistical Analyses

The sample size was calculated using an online-based software (<http://clincalc.com/stats/SampleSize.aspx>). Based on the mean GDF-15 levels in literature, at least 81 participants were required for a 20% difference (significant difference), an alpha error of 0.05, and 80% power. However, we included 90 patients to compensate for patients who may be lost to

**Table 2:** Relationship between serum GDF-15 levels and the demographic and clinical parameters of the patient

Clinical parameters	N	r	p-value
Age, year	88	0.229	<b>0.032</b>
Proteinuria, mg	80	0.076	0.501
Proteinuria on follow-up, mg	74	0.333	<b>0.004</b>
Serum creatinine, mg/dL	88	0.268	<b>0.012</b>
Serum creatinine on follow-up, mg/dL	82	0.209	0.059
eGFR, mL/minute/1.73m <sup>2</sup>	88	-0.249	<b>0.019</b>
Hemoglobin, g/dL	86	-0.06	0.580
Serum albumin, g/dL	88	-0.11	0.308
Systolic blood pressure, mmHg	53	0.79	0.575
Diastolic blood pressure, mmHg	53	-0.27	0.850
BMI, kg/m <sup>2</sup>	52	0.052	0.713

eGFR, estimated glomerular filtration rate; BMI, body mass index; N, number; r, correlation coefficient, p<0.05 is significant.

follow-up. Statistical analyses of the data were performed using SPSS (version 29.0.0.0; IBM, Armonk, New York, USA). The Kolmogorov Smirnov test was used to assess normality of distribution of the continuous data. The normally distributed data are presented as mean ± standard deviation, and the non-normally distributed data are presented as median (minimum–maximum). To determine the relationship between a dependent variable and one or more explanatory variables, linear regression analysis was performed. The Pearson correlation test was used to assess the relationship between age and GDF-15 levels. The Chi-square and Fisher’s exact tests were used to evaluate categorical data, which are presented as numbers and percentages values, between the patient groups. A p-value of <0.05 was considered statistically significant. A receiver operating characteristic (ROC) curve demonstrating the prognostic sensitivity and specificity of GDF-15 levels was constructed using the eGFR value, which is an indicator of kidney disease progression (>90 mL/min and <90 mL/min). A GDF-15 value of >6500 pg/mL demonstrated 81% specificity and 77.8% sensitivity in predicting disease progression. The

patients were segmented into two groups depending on these cut-off values. Group 1 included patients with a GDF level of <6500 pg/mL, and Group 2 included patients with a GDF level of >6500 pg/mL. A GDF-15 cut-off value of 6500 pg/mL was specified to predict disease progression. The AUC value (0.684) for the GDF-15 level was within the confidence interval (95% CI) of 0.529 to 0.838 (p=0.003) (Figure 1).

## RESULTS

The mean age of the patients was 53.59 ± 13.82 years (range: 25–77), and the mean age of the patients at time of diagnosis was 46.30 ± 13.53 years (range: 19–70). The patient group included of 51 males (58%) and 37 females (42%) (Table 1).

### Demographic and Clinical Parameters and the GDF-15 Levels

The mean follow-up period in the patient group was 87.75 ± 29.30 months (range: 48–180; Inter Quartil Range: 48). There was no significance between the serum GDF-15 level and

**Table 3:** Comparison of patient characteristics in Groups 1 and 2

		<b>Group 1 (n = 53)</b>	<b>Group 2 (n = 35)</b>	<b>p-value</b>
Age, year		50.83 ± 13.6	57.77 ± 13.3	<b>0.002*</b>
Sex, Male / Female, n		30/23	21/14	0.752
Age at the time of diagnosis		43.26 ± 13.4	50.89 ± 12.6	<b>0.009*</b>
Weight, kg		79.2 ± 15.3	78.4 ± 14	0.847
Systolic blood pressure, mmHg		131.4 ± 21	131.5 ± 16.3	0.519
Diastolic blood pressure, mmHg		82.7 ± 12.8	79.7 ± 12.2	0.426
Serum albumin, g/dL		2.78 ± 0.9	2.84 ± 0.8	0.745
Serum creatinine, mg/dL		0.75 ± 0.3	1.1 ± 0.5	<b>&lt;0.0001</b>
Serum creatinine on follow-up, mg/dL		0.85 ± 0.31	1.7 ± 1.67	<b>0.001*</b>
Hemoglobin, g/dL		13.3 ± 2.6	12.4 ± 1.6	0.066
eGFR, mL/minute/1.73 m <sup>2</sup>		116.1 ± 51.01	81.2 ± 46.5	<b>0.002*</b>
Proteinuria, mg		5474.8 ± 3423.5	5998.7 ± 3765.4	0.523
Proteinuria on follow-up, mg		2014.9 ± 2104.2	4196.4 ± 3683	<b>0.002*</b>
Remission	%	39/11 73.58/20.75	16/17 37.14/48.57	<b>0.005*</b>
ESKD	%	50/1 94.33/1.88	30/3 85.71/8.57	0.134
ACEI or ARB	%	2/48 3.7/90.56	4/29 11.42/82.85	0.162

All data are presented as mean ± SD unless otherwise stated

eGFR, estimated glomerular filtration rate; ESKD, end stage kidney disease; ACEI, angiotensin-converting enzyme inhibitor; ARB, angiotensin II receptor blocker; SD, standard deviation.

The Student’s t-test, Chi-square and Fisher’s exact test were used. \*: p<0.05.

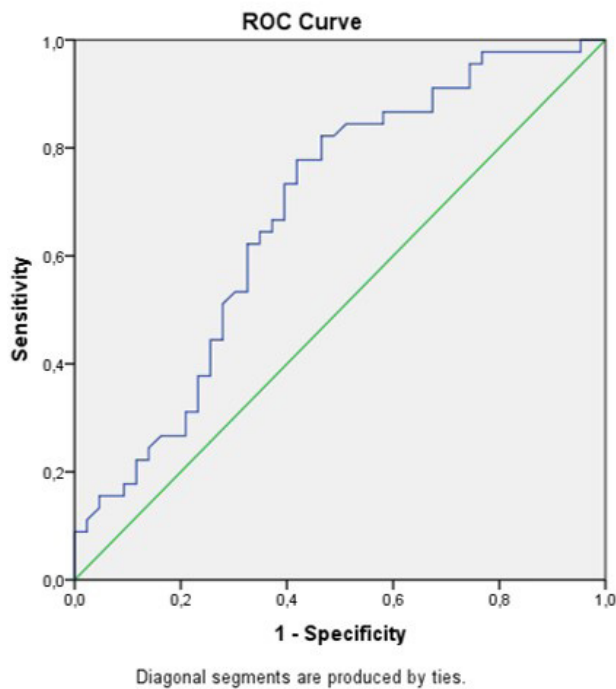


**Figure 1.** The ROC for GDF-15 level in patients with MN. The AUC value: 0.684; 95CI: 0.529-0.838; p-value: 0.003

proteinuria, follow-up creatinine level, albumin level during biopsy, hemoglobin level, and systolic and diastolic blood pressures ( $p > 0.05$ ). There was a positive correlation between increasing serum GDF-15 levels and increasing age ( $p = 0.032$ ), serum creatinine level ( $p = 0.012$ ) and follow-up proteinuria ( $p = 0.004$ ). However, there was a negative correlation between increasing serum GDF-15 levels and eGFR ( $p = 0.019$ ) (Table 2).

### Association Between GDF-15 Levels and Progression of Renal Disease

The patients in Group 2 were older ( $p = 0.009$ ), had higher serum creatinine levels ( $p < 0.0001$ ), higher follow-up proteinuria ( $p = 0.006$ ), and lower eGFR ( $p = 0.002$ ) than the patients in Group 1 (Table 3).

Logistic regression analysis of the GDF-15 level and age revealed a significant positive relation ( $p = 0.024$ ; OR, 1.040; 95% CI, 1.005–1.076). The Pearson correlation test demonstrated a low correlation between GDF-15 levels and age ( $r = 0.247$ ,  $p = 0.020$ ).

### Association Between GDF-15 Level and Prognosis

The GDF-15 level was statistically significantly low in patients in remission ( $p = 0.002$ ). However, it was higher in patients with an eGFR of  $< 90$  mL/min ( $p = 0.003$ ). There was no significant correlation between the GDF-15 level and development of ESKD ( $p = 0.392$ ) and treatment (ACEI/ARB,  $p = 0.36$ ) (Table 4). Approximately 62.5% ( $n = 55$ ) of the patients were administered immunosuppressive therapy.

## DISCUSSION

MN is the most common primary glomerular disease worldwide. Although spontaneous remission may occur, ESKD may develop in 30–40% of patients with MN within 5–15 years (2). Although MN is typically a disease of adults, rarely, it can be seen in children. The incidence is two fold more in adult men than in women. The progression of MN is faster in male and older adults than in women and younger adult patients (9). In our study, there was no significant difference in gender in the included patients. Furthermore, we did not detect a

**Table 4:** Relationship of GDF-15 level with poor prognosis.

			GDF-15 levels (Min–Max)	Median	p-value
eGFR	90* ≤	n = 43	1287.58–26760.73	7285.76	<b>0.003*</b>
	90* >	n = 45	744.36–19332.63	4500.22	
Remission	(+)	n = 55	936.74–26760.73	4357.37	<b>0.002*</b>
	(–)	n = 28	2300.22–25998.88	7369.09	
ESKD	(–)	n = 80	936.74–26760.73	5631.10	0.392
	(+)	n = 8	744.36–10118.92	7785.73	
ACEI or ARB	(–)	n = 6	1096.21–12118.79	7266.01	0.360
	(+)	n = 77	936.74–26760.73	6313.29	

GDF, growth differentiation factor; eGFR, estimated glomerular filtration rate; ESKD, end stage kidney disease; ACEI, angiotensin-converting enzyme inhibitor; ARB, angiotensin II receptor blocker

Mann–Whitney U Test was used to perform statistical analysis. \*:  $p < 0.05$ .

relationship between disease progression and sex or age. This may be attributed to the difference in disease progression among patients and the limited number of patients with advanced disease stage.

Under normal circumstances, GDF-15 is expressed in low concentrations in most organs. However, GDF-15 is expressed in high concentrations following injury to organs such as the heart, liver, and kidney. Recently, GDF-15 expression has been found to be increased in damaged organ tissues such as the heart and kidney in addition to other inflammatory markers (3, 10, 11). In a study which included patients with type 1 diabetes mellitus, there was no significant difference in the plasma concentrations of GDF-15 between the male and female patients (12). However, GDF-15 is positively correlated with age (5, 13-15). Tuegel et al. demonstrated that female gender, advanced age, and smoking were associated with elevated GDF-15 levels as independent factors (16). In this study, the GDF-15 level was positively correlated with age, which is consistent with the findings in literature. However, there was no significant difference between the serum GDF-15 level and the gender of the patients.

Ham et al. demonstrated that serum hemoglobin and eGFR values were low, and age and serum creatinine values were high in patients with a serum GDF-15 level of >2.15 ng/mL. Furthermore, they demonstrated that GDF-15 levels are negatively correlated with kidney function and positively correlated with disease progression in patients with IMN (3). Other studies have also demonstrated elevated GDF-15 levels in patients with chronic kidney injury and/or disease progression to ESKD (5, 6, 17). Wu et al. demonstrated that GDF-15 levels are significantly higher in patients with IMN than in healthy individuals and that the GDF-15 level is associated with kidney functions. Although GDF-15 level alone is not a prognostic biomarker, its concentrations may be utilized as a biomarker of the degree of renal failure in patients with IMN patients (4).

In our study, ESKD developed in eight of the 88 patients. Furthermore, we found that the serum GDF-15 value was >6500 pg/mL in 75% of the patients who developed ESKD. However, this difference was not statistically significant, and this may be attributed to the low number of patients with ESKD included in the study. Follow-up creatinine levels and proteinuria were high in patients with GDF-15 levels >6500 pg/mL than in patients with GDF-15 levels <6500 pg/mL. This indicated that there is a relationship between GDF-15 concentration and disease progression. Determining serum levels of GDF-15 is useful for risk stratification, especially in patients with normal creatinine levels (12, 18). Studies have indicated that plasma GDF-15 levels is positively correlated with serum creatinine level as well as proteinuria (9, 19). Similarly, in our study, we found a positive correlation between GDF-15 levels and follow-up levels of proteinuria and serum creatinine and an inverse correlation between GDF-15 level and eGFR. Further, there was a significant relationship between serum GDF-15 concentration at the time of diagnosis and remission; patients with low GDF-

15 concentrations had higher chances of remission.

The GDF-15 levels are reportedly significantly higher in patients with anemia (World Health Organization definition, male hemoglobin level <13 mg/dL and female hemoglobin level <12 mg/dL) than in patients without anemic (18-20). In our study, hemoglobin levels were low and GDF-15 concentrations were high in patients with an eGFR >90, which is consistent with the findings in literature.

In conclusion, herein, we aimed to determine whether GDF-15 level can be used as a biomarker to diagnose MN in patients without the need for biopsy. Our study findings revealed a positive correlation between GDF-15 level and follow-up proteinuria and a negative correlation between GDF-15 and eGFR and remission. These findings indicate that GDF-15 concentration can be used as an indicator of the course of the disease rather than as a diagnostic biomarker.

---

**Ethical Committee Approval:** This study was approved by the clinical experiments local ethical committee of Istanbul University Istanbul Faculty of Medicine (No: 2018/1260; date: 03/10/2018).

**Informed Consent:** Informed written consent was obtained from the study participants.

**Peer-review:** Externally peer-reviewed.

**Author Contributions:** Conception/Design of Study- A.A., H.Y., C.K.C.; Data Acquisition- A.A., E.D., Data Analysis/Interpretation- A.A., S.U.A., H.S.C., C.K.C., Drafting Manuscript-AA, HY, CKC, Critical Revision of Manuscript- F.S.O., HY, C.K.C., Final Approval and Accountability- H.Y., C.K.C., Technical or Material Support- E.D., H.Y., C.K.C., Supervision- H.Y., H.S.C., C.K.C.

**Conflict of Interest:** The authors declare that they have no conflict of interest.

**Financial Disclosure:** The study was supported by a grant from the Istanbul University Scientific Research and Project commission (No: TYL-2018-32358).

## REFERENCES

1. Stanescu HC, Arcos-Burgos M, Medlar A, Bockenbauer D, Kottgen A, Dragomirescu L, et al. Risk HLA-DQA1 and PLA2R1 alleles in idiopathic membranous nephropathy. *N Engl J Med* 2011; 364: 616-26.
2. Lai WL, Yeh TH, Chen PM, Chan CK, Chiang WC, Chen YM, et al. Membranous nephropathy: a review on the pathogenesis, diagnosis, and treatment. *J Formos Med Assoc* 2015; 114: 102-11.
3. Ham YR, Song CH, Bae HJ, Jeong JY, Yeo MK, Choi DE, et al. Growth differentiation factor-15 as a predictor of idiopathic membranous nephropathy progression: a retrospective study. *Dis Markers* 2018: 1463940.
4. Wu L, Luo L, Zhou L, Li N, Qin, X. GDF-15 and sST-2 act as biomarkers of disease severity but not independent predictors in idiopathic membranous nephropathy. *Int Immunopharmacol* 2022; 111: 109150.

5. Lajer M, Jorsal A, Tarnow L, Parving HH, Rossing P. Plasma growth differentiation factor-15 independently predicts all-cause and cardiovascular mortality as well as deterioration of kidney function in type 1 diabetic patients with nephropathy. *Diabetes Care* 2010; 33: 1567-72.
6. Ho JE, Hwang SJ, Wollert KC, Larson MG, Cheng S, Kempf T, et al. Biomarkers of cardiovascular stress and incident chronic kidney disease. *Clin Chem* 2013; 59: 1613-20.
7. Krintus M, Braga F, Kozinski M, Borille S, Kubica J, Sypniewska G, et al. A study of biological and lifestyle factors, including within-subject variation, affecting concentrations of growth differentiation factor 15 in serum. *Clin Chem Lab Med* 2019; 57(7): 1035-43.
8. Hamon S M, Griffin T P, Islam M N, Wall D, Griffin MD, O'Shea PM. Defining reference intervals for a serum growth differentiation factor-15 (GDF-15) assay in a Caucasian population and its potential utility in diabetic kidney disease (DKD). *Clin Chem Lab Med* 2019; 57(4): 510-20.
9. Zhu H, Han Q, Zhang D, Wang Y, Gao J, Yang X, et al. The clinicopathological features of patients with membranous nephropathy. *Int J Nephrol Renovasc Dis* 2018; 11: 33.
10. Breit SN, Johnen H, Cook AD, Mohammad MG, Kuffner T, Zhanget HP, et al. The TGF- $\beta$  superfamily cytokine, MIC-1/GDF15: a pleotrophic cytokine with roles in inflammation, cancer and metabolism. *Growth Factors* 2011; 29: 187-95.
11. Lankeit M, Kempf T, Dellas C, Cuny M, Tapken H, Peter T, et al. Growth differentiation factor-15 for prognostic assessment of patients with acute pulmonary embolism. *Am J Respir Crit Care Med* 2018; 177: 1018-25.
12. Ferrari N, Pfeffer U, Dell'Eva R, Ambrosini C, Noonan DM, Albini A. The transforming growth factor- $\beta$  family members bone morphogenetic protein-2 and macrophage inhibitory cytokine-1 as mediators of the antiangiogenic activity of N-(4-hydroxyphenyl) retinamide. *Clin Cancer Res* 2005; 11: 4610-19.
13. Kahli A, Guenancia C, Zeller M, Grosjean S, Stamboul K, Rochette L, et al. Growth differentiation factor-15 (GDF-15) levels are associated with cardiac and renal injury in patients undergoing coronary artery bypass grafting with cardiopulmonary bypass. *PLoS One* 2014; 9(8): e105759.
14. Frimodt-Møller M, von Scholten BJ, Reinhard H, Jacobsen PK, Hansen TW, Persson FI, et al. Growth differentiation factor-15 and fibroblast growth factor-23 are associated with mortality in type 2 diabetes—an observational follow-up study. *PLoS One* 2018; 13(4): e0196634.
15. Kim JS, Kim S, Won CW, Jeong KH. Association between plasma levels of growth differentiation factor-15 and renal function in the elderly: Korean frailty and aging cohort study. *Kidney Blood Press Res* 2019; 44: 405-14.
16. Tuegel C, Katz R, Alam M, Bhat Z, Bellovich K, Boer L, et al. GDF-15, galectin 3, soluble ST2, and risk of mortality and cardiovascular events in CKD. *Am J Kidney Dis* 2018; 72: 519-28.
17. Breit SN, Carrero JJ, Tsai VWW, Yagoutifam N, Luo W, Kuffner T, et al. Macrophage inhibitory cytokine-1 (MIC-1/GDF15) and mortality in end-stage renal disease. *Nephrol Dial Transplant* 2012; 27: 70-5.
18. Zhang W, Chu HC, Xue F. Assessing preoperative plasma growth-differentiation factor-15 for prediction of acute kidney injury in patients undergoing cardiac surgery. *Critical Care* 2017; 21: 53.
19. Short CD, Feehally J, Gokal R, Mallick NP. Familial membranous nephropathy. *Br Med J* 1984; 289: 1500.
20. World Health Organization: Nutritional anemias: Report of a WHO Scientific Group. *World Health Organ Tech Rep Ser* 1968; 405: 5-37.

# Effect of Ellagic Acid and Cryptotanshinone on Cell Viability/Cytotoxicity, Metastasis, and Oxidative Stress in Triple-Negative Breast Cancer Cells

Umit Yilmaz<sup>1</sup> , Mehmet Fatih Seyhan<sup>2</sup> 

<sup>1</sup>Department of Physiology, Faculty of Medicine, Karabuk University, Karabuk, Türkiye

<sup>2</sup>Department of Molecular Biology and Genetics, Faculty of Arts and Sciences, Istanbul Yeni Yuzuil University, Istanbul, Türkiye

ORCID ID: U.Y. 0000-0003-0248-3483, F.S. 0000-0002-6218-0049

**Cite this article as:** Yilmaz U, Seyhan MF. Effect of ellagic acid and cryptotanshinone on cell viability/cytotoxicity, metastasis, and oxidative stress in triple-negative breast cancer cells? *Experimed* 2024; 14(1): 46-53.

## ABSTRACT

**Objective:** Triple-negative breast cancer (TNBC) has the highest rate of metastases and relapses as well as the worst overall survival of all breast cancers. Here, we aimed to investigate the effects of ellagic acid and cryptotanshinone, which are known to have antioxidant, antimutagenic, anticancer, and apoptotic effects, on cell viability/cytotoxicity, metastasis, and oxidative stress in MDA-MB-231 cells.

**Materials and Methods:** The effects of various concentrations of ellagic acid and cryptotanshinone on cell viability or cytotoxicity in TNBC cells were determined by WST-1. A scratch assay was performed to determine the effects of ellagic acid and cryptotanshinone on cell migration and metastasis, and a DCF-DA test was performed to determine the reactive oxygen species (ROS) levels.

**Results:** MDA-MB-231 cells exposed to cryptotanshinone exhibited reduced cell proliferation by approximately 50%, particularly at 20 µg/mL after 48 h. The cell viability decreased by 75% at 20 µg/mL after 72 h of cryptotanshinone exposure. After 48 h of exposure to ellagic acid at 40 µg/mL, the scratch in the MDA-MB-231 cells closed. In addition, treatment with cryptotanshinone at 25 µg/mL covered the scratch after 72 h. Ellagic acid (40 µg/mL) induced oxidative stress at 24 h, and cryptotanshinone (25 µg/mL) at 48 and 72 h. Furthermore, the fluorescence intensity of MDA-MB-231 cells was increased by exposure to ellagic acid (40 µg/mL) and cryptotanshinone (25 µg/mL) after 24 h compared to the negative control.

**Conclusion:** Ellagic acid and cryptotanshinone may inhibit cell proliferation, suppress cell migration, and induce the accumulation of intracellular ROS in MDA-MB-231 cells.

**Keywords:** Triple-negative breast cancer, MDA-MB-231, cell culture, ellagic acid, cryptotanshinone

## INTRODUCTION

Breast cancer (BC) tumors can become resistant to treatment, and with the formation of resistance, the BC tumors are not limited to the primary area and can metastasize to other regions (1). Triple-negative breast cancer (TNBC) is a type of BC with high rates of metastasis and recurrence and has the worst overall survival rates of all BC subtypes. Estrogen, progesterone, and human epidermal growth factor receptor 2 (HER-2) receptors are absent in TNBC (2). Considering that TNBC does not respond to chemotherapy and radiotherapy, its high

incidence and mortality rates, and the limitations in treatment effectiveness, have resulted in the need to find alternative treatments for TNBC (3).

In recent years, natural plant phenolic and flavonoid compounds have attracted attention because of their anticarcinogenic, antioxidant, and antiinflammatory activities and their potential to be used as an adjunct to cancer treatment (3). Furthermore, phytochemicals have been among the alternative cancer treatments in recent years because of their anticarcinogenic, antiinflammatory, and antitumor effects. Phytochemicals play an active

**Corresponding Author:** Umit Yilmaz **E-mail:** umit.yilmaz@karabuk.edu.tr

**Submitted:** 02.02.2024 **Revision Requested:** 04.03.2024 **Last Revision Received:** 28.03.2024 **Accepted:** 01.04.2024



Content of this journal is licensed under a Creative Commons Attribution-NonCommercial 4.0 International License.

role in many steps of cancer suppression. They protect DNA from oxidative damage, activate carcinogen metabolism and detoxification, prevent cell proliferation, and induce cellular cytotoxicity (4).

Ellagic acid is a phytochemical polyphenol compound with antioxidant properties that is found in fresh berries, such as raspberries, strawberries, and pomegranates, and shelled fruits, such as walnuts, chestnuts, and hazelnuts (5). Ellagic acid has antioxidant, antimutagenic, anticancer, and apoptotic effects. Ellagic acid can clear cancer-causing chemicals from the serum; thereby, it prevents carcinogens from binding to DNA, acts as an antioxidant, limits carbon tetrachloride toxicity and lung fibrosis, stimulates the immune system, and induces the death of cancer cells (6). It has previously been shown to suppress the development of some tumors caused by carcinogens in cell culture and animal experiments (7).

In addition, ellagic acid plays a protective role against cancer because of its antiproliferative, antiangiogenic, and antimetastatic effects and by inhibiting the cell cycle, regulating several intracellular signaling pathways, and inducing apoptosis (8, 9). Ellagic acid has exhibited antitumor activity in BC cell lines by affecting signaling pathways such as PI3K/Akt, NFκ-B, CDK6, TGF-β/Smad3, and Akt/mTOR. Moreover, ellagic acid blocks vascular endothelial growth factor (VEGF), a protein involved in angiogenesis (10).

Cryptotanshinone is a lipophilic compound that is extracted from the roots of the plant species *Salvia miltiorrhiza Bunge* (Danshen), which is used in China for the treatment of cardiovascular diseases, hepatitis, diabetes, and chronic liver failure (11). This compound has the potential to prevent ischemia and atherosclerosis and also has antiinflammatory, anticancer, antioxidative, and antiaggregant effects (12). Cryptotanshinone plays a role in the treatment of angiogenesis-related diseases by inhibiting the proliferation of endothelial cells (13). In addition to its antipermeability and antiangiogenic effects, cryptotanshinone has antiinflammatory properties, as demonstrated by its interaction with other cytokines and chemokines (14). Cryptotanshinone has been shown to induce apoptosis (15) and function as an antimetastatic agent (16) in some cancer cell culture studies. Cryptotanshinone suppresses estrogen receptor (ER)-α-mediated transcriptional activity, glycolysis, cell proliferation, migration, and invasion in BC cell lines. In addition, cryptotanshinone treatment causes cell cycle arrest, induces apoptosis, and increases sensitivity to chemotherapeutic drugs in BC cell lines (17). Cryptotanshinone exerts these effects by downregulating the PKM2/β-catenin and ERα-dependent IGF-1/Akt/mTOR signaling pathways, reducing CCNA2 and CDK1 expression, downregulating the GPER-mediated PI3K/Akt signaling pathway, or inducing the mitochondria-derived ROS/FOXO1 pathway.

The efficacy of ellagic acid is demonstrated by arresting the cell cycle of BC cells in the G0/G1 phase, stimulating apoptosis through TGF-β/Smad3 signaling, inhibiting the CDK6 or PI3K/

Akt pathway, and suppressing angiogenesis-related activities, including proliferation (10). Similarly, cryptotanshinone arrests the cell cycle of BC cells in the G2/M phase, reduces the expression of cyclin D, or suppresses the PI3K/Akt signaling pathway (18). Ellagic acid and cryptotanshinone have been reported to induce apoptosis via similar pathways in BC cells. However, the effects of these two antioxidants on oxidative stress-mediated cell death in TNBC have not been comprehensively examined. Here, the effects of ellagic acid and cryptotanshinone were investigated on cell viability/cytotoxicity, metastasis, and oxidative stress levels in TNBC (MDA-MB-231) cells, which are BC cells that are resistant to chemotherapy and radiotherapy.

## MATERIALS AND METHODS

### Cell Culture

In this study, the MDA-MB-231 (ER/PR-Her2/neu-) BC cell line (ATCC, Rockville, MD, USA) was used to determine the effectiveness of ellagic acid and cryptotanshinone. MDA-MB-231 cells were grown in a medium containing Dulbecco's Modified Eagle Medium/Nutrient Mixture F-12 (DMEM-F12), 10% fetal bovine serum (FBS) (v/v), and 1% penicillin/streptomycin (v/v) at 37°C under 5% CO<sub>2</sub> conditions. The experiments began when MDA-MB-231 cells reached confluency.

### Determination of the Effectiveness of Ellagic Acid and Cryptotanshinone on Cell Viability

A WST-1 assay was used to determine the effect of ellagic acid and cryptotanshinone on cell proliferation in MDA-MB-231 cell lines. For the WST-1 assay, MDA-MB-231 cells were seeded into 96-well plates at a density of  $1 \times 10^4$  cells/well in 100 μL. The MDA-MB-231 cells were then incubated for 24 h to observe cell proliferation and differentiation. The ellagic acid and cryptotanshinone compounds were dissolved in dimethyl sulfoxide (DMSO) to prepare intermediate dilutions of 0.1 mg ellagic acid and 0.05 mg cryptotanshinone. The cytotoxic effect of the agents on the cells was determined by applying them to the cells over a range of doses. The most effective doses were determined, and the cells were exposed to these final concentrations. Following the concentration that induced the appropriate conditions in the cells were observed under the microscope and were 5, 10, 15, 20, 25, 40, 50, 75, 90, and 100 μg/mL of ellagic acid, and 2.5, 5, 7.5, 10, 20, 25, 37.5, 45, and 50 μg/mL of cryptotanshinone, which were then applied to MDA-MB-231 cells at the various doses. The proliferation of MDA-MB-231 cells was analyzed using a Cell Proliferation Reagent WST-1 kit (Roche, USA). The WST-1 compound (10 μL) was added to each well, and after 3 h of incubation at 37°C, measurements at a wavelength of 450 nm (reference wavelength 620 nm) were taken at 24, 48, and 72 h using a multiscan spectrophotometer device (MultiSkkan Go, Thermo Scientific, USA). The absorbance of control cells that were not exposed to ellagic acid or cryptotanshinone was determined to be 100%, and the percentages of the applied doses were

calculated by comparing them with the control. The experiment was performed in four replicates.

### Determination of Cell Migration Rates Using the *in Vitro* Scratch Test Assay

To measure the migration speed, the medium was adjusted to contain 3% FBS (v/v). MDA-MB-231 cells were seeded into 6-well plates at a density of  $5 \times 10^5$  cells/well and incubated for 24 h. After the cells covered the plate in a single layer, a straight line was drawn in the middle of the plate using a 10  $\mu$ L pipette tip. Thereafter, the medium was removed, and the plate was rinsed with 1–2 mL of fresh medium to remove any residue. The selected doses of ellagic acid and cryptotanshinone were applied before the medium was added to the cells, and then 5 mL of the scratch assay medium (containing 3% FBS) was added to the cells. Images were obtained by scanning under a fluorescence microscope with a 10 $\times$  magnification objective at 0, 24, and 48 h, and the rate of scratch closure was calculated using Image J software. The scratch closure rate was compared quantitatively to the control and expressed as a percentage (19).

### Detection of the ROS Levels in Cells

2',7'-Dichlorofluorescein diacetate (DCF-DA) (Merck, Germany) is a widely used ROS indicator that is used to detect intracellular peroxides. DCF-DA enters the cell via passive diffusion and undergoes oxidation in the presence of intracellular ROS to form DCF, which is a strong fluorescent substance and can be easily detected under a fluorescence microscope. To determine the intracellular ROS levels, the ellagic acid and cryptotanshinone doses were applied to the MDA-MB-231 and control cells in 12-well plates containing round coverslips and washed once with phosphate-buffered saline (PBS). Then 0.5 mL of DCF-DA solution was prepared in serum-free medium and added to the cells, with a final concentration of 10  $\mu$ M. This was kept in the dark at 37°C for 30 min. After quickly and gently washing three times with PBS, it was fixed with paraformaldehyde and viewed under a fluorescent microscope (Carl-Zeiss, Axio Observer, Germany). For the positive control, cells were exposed to the same conditions as the tested cells but were incubated with 250  $\mu$ M of H<sub>2</sub>O<sub>2</sub> (20).

### Statistical Analyses

A two-way analysis of variance test with the Tukey post-hoc test was used for the comparison of cell viability in the MDA-MB-231 cell lines with the control. The statistical analysis of all experiments was performed using the GraphPad Prism 6 program. At least three independent replicates were performed for all experiments. A value of  $p < 0.05$  was considered statistically significant.

### RESULT

#### Ellagic Acid and Cryptotanshinone may Inhibit Cell Proliferation in MDA-MB-231 Cells

The cytotoxic effect of ellagic acid at doses of 5, 10, 15, 20, 25, 40, 50, 75, 90, and 100  $\mu$ g/mL for 24, 48, and 72 h was investigated in the MDA-MB-231 cell line (Figure 1a). After the MDA-MB-231 cells were exposed for 24 h to ellagic acid, cell proliferation was observed to increase compared to the control at concentrations of 5, 10, 15, 20, and 25  $\mu$ g/mL ( $p < 0.05$ ). However, under the same conditions, a decrease in cell proliferation was observed at the doses  $\geq 40$   $\mu$ g/mL, but with no statistical significance ( $p > 0.05$ ). There was no observed effect on cell viability or cytotoxicity in the MDA-MB-231 cell line after 48 and 72 h of exposure to ellagic acid ( $p > 0.05$ ). This may be because ellagic acid is sensitive to light and has a short half-life.

The cytotoxic effect of cryptotanshinone at concentrations of 2.5, 5, 7.5, 10, 20, 25, 37.5, 45, and 50  $\mu$ g/mL for 24, 48, and 72 h was investigated on the MDA-MB-231 cell line (Figure 1b). It was revealed that exposure of MDA-MB-231 cells to cryptotanshinone for 24 h did not affect cell viability at all doses. However, exposure of MDA-MB-231 cells to cryptotanshinone at doses of 20, 25, 37.5, and 45  $\mu$ g/mL for 48 h reduced cell viability by approximately 50% ( $p < 0.05$ ).

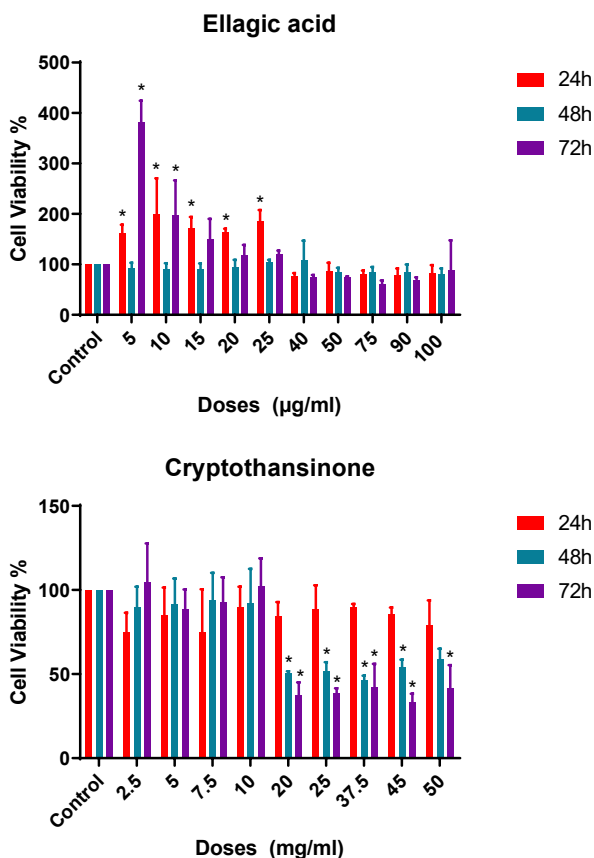


**Figure 1a.** Effects of ellagic acid and b. Cryptotanshinone on cell proliferation in MDA-MB-231 cells.

Moreover, cell viability was decreased by 75% after 72 h of exposure to cryptotanshinone at doses of 20, 25, 37.5, 45, and 50  $\mu\text{g/mL}$  ( $p < 0.05$ ). Low concentrations of cryptotanshinone had no cytotoxic effect on the MDA-MB-231 cells.

The half-maximal inhibitory concentration ( $IC_{50}$ ) values of ellagic acid and cryptotanshinone are shown in Table 1. According to the results of the WST-1 cell proliferation assay, ellagic acid at 40  $\mu\text{g/mL}$  and cryptotanshinone at 25  $\mu\text{g/mL}$  were selected as the most effective concentrations, and these concentrations were used to determine cell migration and detect ROS levels.

### Ellagic Acid and Cryptotanshinone may Suppress the Migration of MDA-MB-231 Cells

In the scratch test assay, MDA-MB-231 cells were examined at 0, 24, and 48 h after being treated with ellagic acid and cryptotanshinone, and their images were recorded. The *in vitro* scratch test assay was performed on MDA-MB-231 cells, and it was observed that the scratch healed within 24 h. Exposure of the MDA-MB-231 cell line to ellagic acid at a concentration of 40  $\mu\text{g/mL}$ , resulted in the scratch being covered after 48 h. Interestingly, after exposure to 25  $\mu\text{g/mL}$  of cryptotanshinone, it was found that scratch was covered after

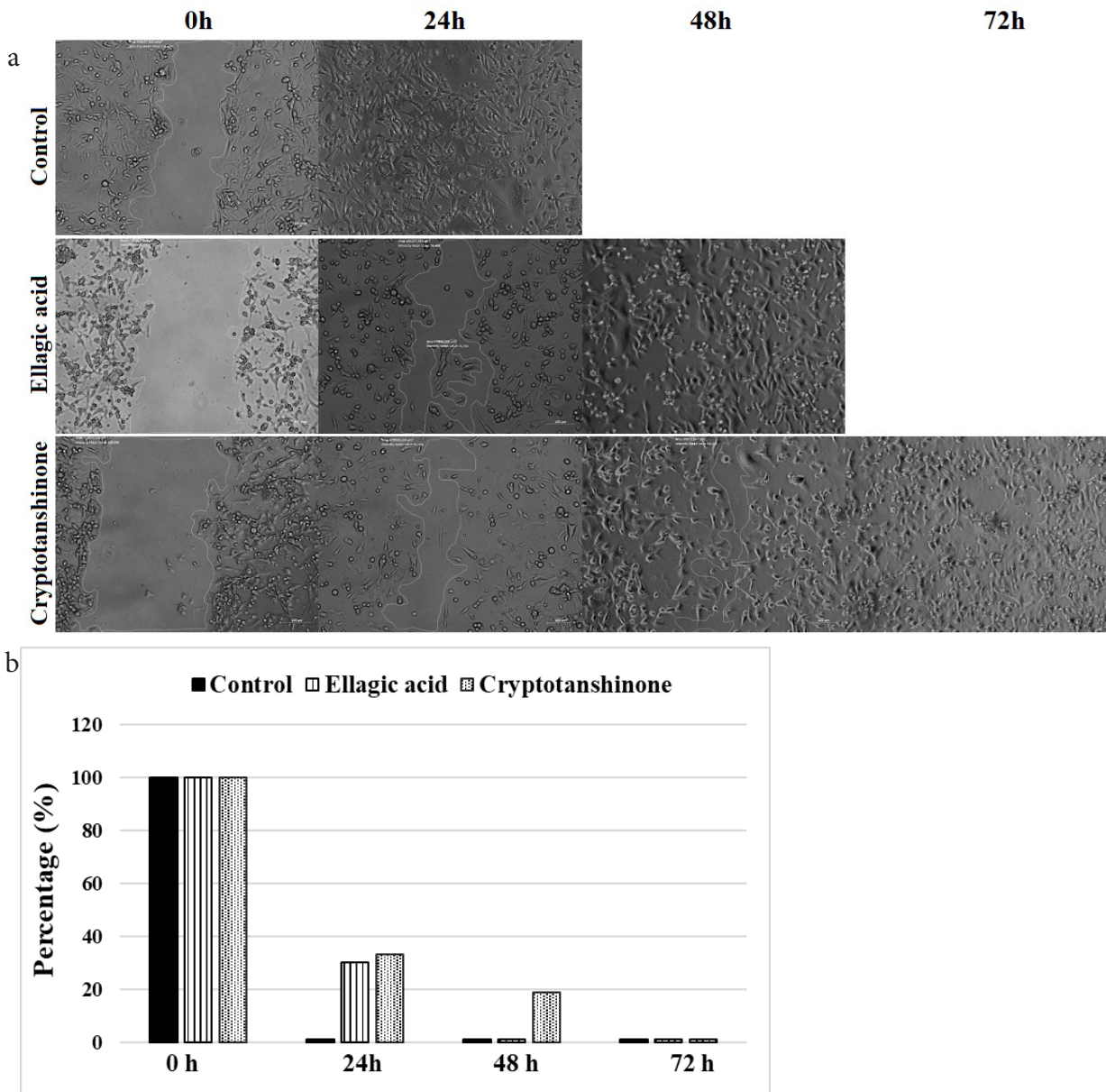


**Figure 2.** Ellagic acid and cryptotanshinone may suppress the migration of MDA-MB-231 cells.

a. Images were obtained by scanning with a fluorescence microscope at a 10 $\times$  magnification objective. b. The closure areas of the cells in the scratch test assay are given as a percentage compared to the control.

**Table 1.** Half-maximal inhibitory concentration (IC<sub>50</sub>) values of ellagic acid and cryptotanshinone

	24 h	48 h	72 h
Cryptotanshinone (µg/mL)	Unstable	41.98	25.90
Ellagic acid (µg/mL)	141.2	372.4	103.8

72 h; therefore, according to these results, it can be inferred that cryptotanshinone is the most effective material in terms of inhibiting cell migration. The closure areas of the cells in the scratch test assay are given as percentages compared to the control (Figure 2).

### Ellagic Acid and Cryptotanshinone may Induce the Generation of ROS in MDA-MB-231 Cells

ROS is a key regulator of many cellular activities, including cellular metabolism, the cell cycle, and programmed cell death. Fluorescent DCF-DA was used to determine the effect of ellagic acid and cryptotanshinone on the accumulation of intracellular ROS in the MDA-MB-231 cell line. After treatment with ellagic acid and cryptotanshinone for 24, 48, and 72 h, the cells were imaged using an inverted microscope with a fluorescent attachment. According to the DCF-DA cellular ROS assay experiment, minimum fluorescence was observed in the control group at 24 and 48 h. However, there was a statistically significant increase in fluorescence intensity in MDA-MB-231 cells after 24 h of treatment with ellagic acid (40 µg/mL) compared to the negative control ( $p < 0.0001$ ), but no statistically significant difference in fluorescence intensity was observed after 48 and 72 h of exposure to ellagic acid. After exposure to cryptotanshinone at a concentration of 25 µg/mL, a higher fluorescence intensity was measured in the MDA-MB-231 cells compared to the control at 24 h, and this difference is statistically significant ( $p < 0.0001$ ). However, cryptotanshinone exposure for 48 and 72 h revealed no statistically significant difference. As a result, it was determined that ellagic acid and cryptotanshinone induced oxidative stress, and the 24 h fluorescence intensity was higher than that of the 48 and 72 h of exposure (Figure 3a, b).

### DISCUSSION

TNBC is a subtype of BC in which the estrogen, progesterone, and HER-2 receptors are not involved. TNBC is associated with a higher grade and more aggressive biological characteristics, and it accounts for approximately 20% of all BC cases. These features make TNBC one of the most challenging diseases to treat in clinical practice (2, 3).

Ellagic acid, a small molecular polyphenol, is a powerful antioxidant that acts either directly as an antioxidant or by inducing antioxidant cellular enzyme systems (21). In addition, ellagic acid has anticarcinogenic properties, as it inhibits tumor cell proliferation, induces apoptosis, and disrupts angiogenesis (22). Ellagic acid suppressed BC cell growth,

migration, and invasion and blocked tumor initiation and metastasis by increasing the activity of the PI3K signaling pathway inhibitor (23). In addition, ellagic acid inhibited the proliferation and migration of BC cells *in vivo* and *in vitro* (MDA-MB-231) and exhibited antiangiogenesis effects through the VEGFR-2 signaling pathway by inhibiting the expression of P-VEGFR2 (24). In MCF-7 cells, ellagic acid significantly enhanced radiation-induced cytotoxicity, inhibited cell growth by blocking the cell cycle, and enhanced apoptosis (25). Ellagic acid inhibited cell proliferation by inducing the TGF-β/Smad3 pathway in MCF-7 cells (26), arrested the cell cycle in the G0/G1 phase, inhibited proliferation, and induced apoptosis (27). Yousuf et al. reported that ellagic acid reduced the proliferation and colonization of MCF-7 and MDA-MB-231 cells and induced apoptosis through the inhibition of CDK6 (28). The results of this study are consistent with previous studies, and our results showed that ellagic acid inhibited cell proliferation, suppressed cell migration, and induced the accumulation of intracellular ROS in MDA-MB-231 cells. Ellagic acid may reduce cell proliferation by increasing the accumulation of intracellular ROS and inducing apoptosis.

Cryptotanshinone is a lipid-soluble diterpenoid derivative found in plants of the genus *Salvia*, of which *S. miltiorrhiza* Bunge, known as Danshen, is rich in diterpenes. Cryptotanshinone may inhibit the growth of tumor cells in various cancer types through its antitumor activity and enhanced antitumor immunity (29). Cryptotanshinone exhibits anticancer activity in different cancer cells because of its strong STAT3 inhibitor attribute. Cryptotanshinone showed immunomodulatory and antitumor effects by inhibiting the JAK2/STAT3 pathway and regulating the secretion of related cytokines in an experimental BC model (30). In addition, cryptotanshinone inhibited tumor growth in both the animal model of BC and the MCF-7 cell line (31). Cryptotanshinone has been shown to be chemically homogeneous with estrogen, and the combination of arsenic and cryptotanshinone induced endoplasmic reticulum stress and apoptosis in MCF-7 cells (32). In addition, ROS generated by cryptotanshinone induced apoptosis in the MCF-7 cell line by causing endoplasmic reticulum stress (33). The ability of cryptotanshinone to inhibit BC cells is dependent on ER-α (34). Cryptotanshinone effectively inhibited the gene expression of ER-α as well as transactivation and suppressed the growth of ZR-75-1 and MCF-7 cells (35). MCF-7 cells are more sensitive to cryptotanshinone than MDA-MB-231 cells, and cryptotanshinone inhibits the proliferation and metastasis of ER-positive cancer cells (36). There are a few studies that have investigated the effects of cryptotanshinone on MDA-MB-231 cells. Cryptotanshinone reduced glycolysis-related proteins and PKM2/β-catenin signaling in MCF-7 and MDA-MB-231 cells. In addition, cryptotanshinone demonstrated anticancer activity in MCF-7 and MDA-MB-231 cells by inhibiting cell proliferation, migration, and invasion (37). Cryptotanshinone inhibits the proliferation of the SKBR-3 BC cells through G-protein-coupled ER-mediated PI3K/Akt pathway inhibition (38). In addition, Shi et al. showed that cryptotanshinone exerts its antiproliferative

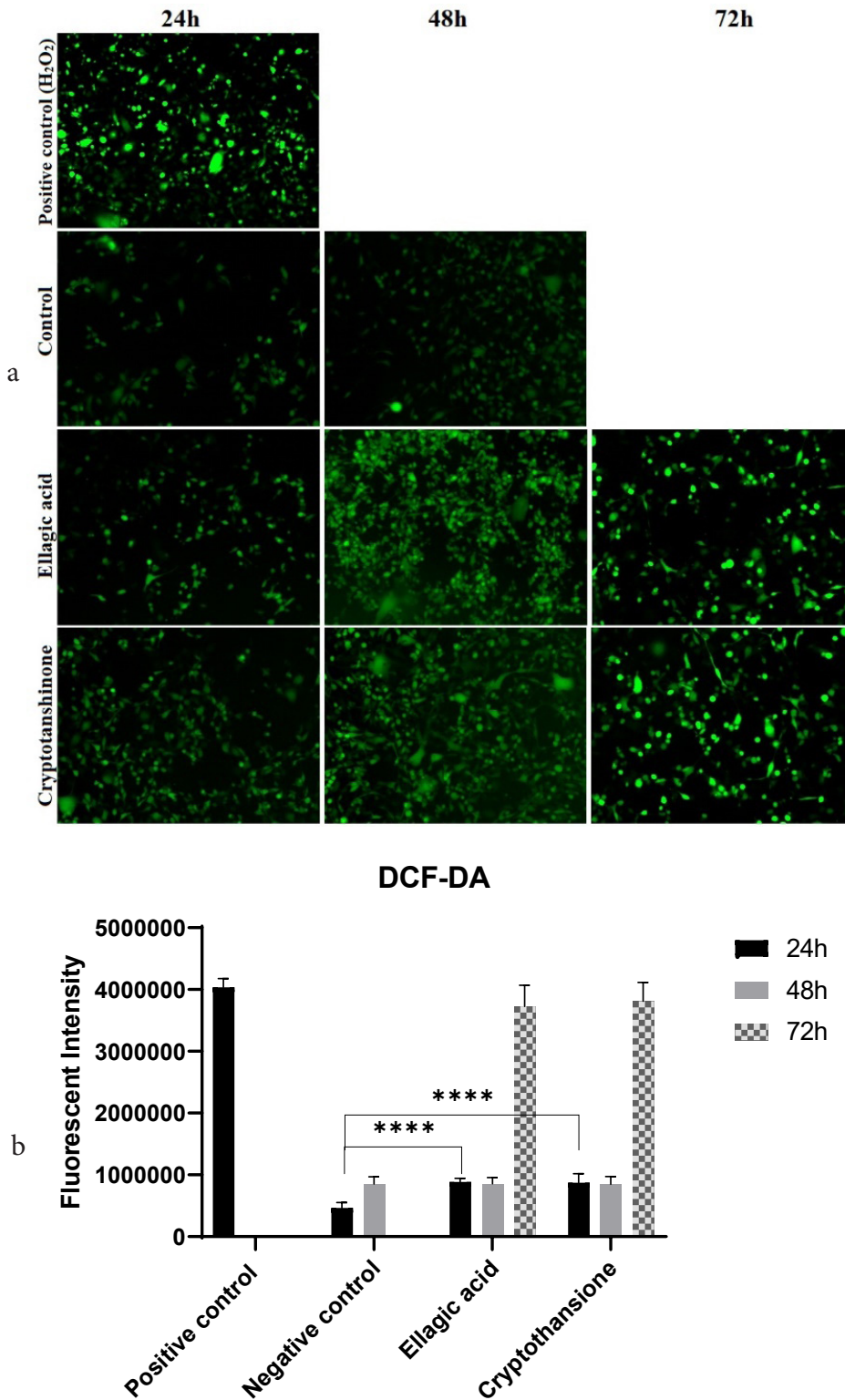


**Figure 3.** Ellagic acid and cryptotanshinone may induce the generation of reactive oxygen species in MDA-MB-231 cells. a. Fluorescence microscopic image of cells. b. Fluorescence intensity measurement which indicates the enhancement of ROS in cells treated ellagic acid and cryptotanshinone. Groups with the asterisk symbol (\*\*\*\*) on the graph indicate that they are statistically different from the control group ( $p < 0.0001$ ).

effect on MCF-7 cells by inhibiting the G-protein-coupled ER-mediated PI3K/Akt pathway (18). In addition, tanshinone-I suppressed the proliferation and angiogenesis of MCF-7 and MDA-MB231 cells (39). In the results of this study, we found that cryptotanshinone inhibited cell proliferation and migration and increased the accumulation of intracellular ROS in MDA-MB-231 cells. Cryptotanshinone may reduce cell proliferation through an increase in the accumulation of intracellular ROS and the induction of apoptosis. There are a few studies that have investigated the effects of cryptotanshinone on TNBC cells. In this regard, our study provides preliminary data for future studies.

Phytochemicals are potential candidates because of their diverse pharmacological activities. Mitochondria are the main source of intracellular ROS generation, and intracellular ROS levels play an important role in cancer processes. It has been reported that high levels of intracellular ROS activate oxidative stress and apoptosis, which leads to cell death, and low levels of intracellular ROS activate angiogenesis, which initiates the spread and metastasis of tumor cells (40). In the results of this study, we found that ellagic acid and cryptotanshinone inhibited cell proliferation, suppressed cell migration, and induced the accumulation of intracellular ROS in MDA-MB-231 cells. These results demonstrate that ellagic acid and cryptotanshinone may be effective for the treatment of TNBC, and suggest that further *in vitro* studies of ellagic acid and cryptotanshinone should target molecular pathways to develop treatment options for TNBC.

**Ethics Committee Approval:** Since a commercial cell line was used in the study, there is no need for an ethics committee.

**Peer-review:** Externally peer-reviewed.

**Author Contributions:** Conception/Design of Study- U.Y., M.F.S.; Data Acquisition- U.Y., M.F.S.; Data Analysis/ Interpretation- U.Y., M.F.S.; Drafting Manuscript- U.Y.; Critical Revision of Manuscript- U.Y.; Final Approval and Accountability- U.Y., M.F.S.

**Conflict of interest:** The authors declare that they have no conflict of interest.

**Financial Disclosure:** This work was supported by the Research Fund of Karabuk University [Project No. 22-DS-118].

## REFERENCES

- Sung H, Ferlay J, Siegel RL, Laversanne M, Soerjomataram I, Jemal A, et al. Global cancer statistics 2020: GLOBOCAN estimates of incidence and mortality worldwide for 36 cancers in 185 countries. *CA Cancer J Clin* 2021; 71(3): 209-49.
- Lee A, Djamgoz MBA. Triple negative breast cancer: Emerging therapeutic modalities and novel combination therapies. *Cancer Treat Rev* 2018; 62: 110-22.
- Diaz P, Jeong SC, Lee S, Khoo C, Koyyalamudi SR. Antioxidant and anti-inflammatory activities of selected medicinal plants and fungi containing phenolic and flavonoid compounds. *Chin Med* 2012; 7(1): 26.
- Chikara S, Nagaprashantha LD, Singhal J, Horne D, Awasthi S, Singhal SS. Oxidative stress and dietary phytochemicals: Role in cancer chemoprevention and treatment. *Cancer Lett* 2018; 413: 122-34.
- Vekiari SA, Gordon MH, Garcia-Macias P, Labrinea H. Extraction and determination of ellagic acid content in chestnut bark and fruit. *Food Chem* 2008; 110(4): 1007-11.
- Ramadan DT, Ali MAM, Yahya SM, El-Sayed WM. Correlation between antioxidant/antimutagenic and antiproliferative activity of some phytochemicals. *Anticancer Agents Med Chem* 2019; 19(12): 1481-90.
- Kaur H, Ghosh S, Kumar P, Basu B, Nagpal K. Ellagic acid-loaded, tween 80-coated, chitosan nanoparticles as a promising therapeutic approach against breast cancer: In-vitro and in-vivo study. *Life Sci* 2021; 284: 119927.
- Ceci C, Lacal PM, Tentori L, De Martino MG, Miano R, Graziani G. Experimental evidence of the antitumor, antimetastatic and antiangiogenic activity of ellagic acid. *Nutrients* 2018; 10(11) : 1756.
- Cheshomi H, Bahrami AR, Matin MM. Ellagic acid and human cancers: a systems pharmacology and docking study to identify principal hub genes and main mechanisms of action. *Mol Divers* 2021; 25(1): 333-49.
- Golmohammadi M, Zamanian MY, Jalal SM, Noraldeen SAM, Ramirez-Coronel AA, Oudaha KH, et al. A comprehensive review on ellagic acid in breast cancer treatment: from cellular effects to molecular mechanisms of action. *Food Sci Nutr* 2023; 11(12): 7458-68.
- Yu XY, Lin SG, Chen X, Zhou ZW, Liang J, Duan W, et al. Transport of cryptotanshinone, a major active triterpenoid in *Salvia miltiorrhiza* Bunge widely used in the treatment of stroke and Alzheimer's disease, across the blood-brain barrier. *Curr Drug Metab* 2007; 8(4): 365-78.
- Chen W, Lu Y, Chen G, Huang S. Molecular evidence of cryptotanshinone for treatment and prevention of human cancer. *Anticancer Agents Med Chem* 2013; 13(7): 979-87.
- Chen Q, Zhuang Q, Mao W, Xu XM, Wang LH, Wang HB. Inhibitory effect of cryptotanshinone on angiogenesis and Wnt/beta-catenin signaling pathway in human umbilical vein endothelial cells. *Chin J Integr Med* 2014; 20(10): 743-50.
- Tang S, Shen XY, Huang HQ, Xu SW, Yu Y, Zhou CH, et al. Cryptotanshinone suppressed inflammatory cytokines secretion in RAW264.7 macrophages through inhibition of the NF-kappaB and MAPK signaling pathways. *Inflammation* 2011; 34(2): 111-8.
- Kim SA, Kang OH, Kwon DY. Cryptotanshinone induces cell cycle arrest and apoptosis of NSCLC cells through the PI3K/Akt/GSK-3beta pathway. *Int J Mol Sci* 2018; 19(9): 2739.
- Chen Z, Zhu R, Zheng J, Chen C, Huang C, Ma J, et al. Cryptotanshinone inhibits proliferation yet induces apoptosis by suppressing STAT3 signals in renal cell carcinoma. *Oncotarget* 2017; 8(30): 50023-33.
- Dalil D, Iranzadeh S, Kohansal S. Anticancer potential of cryptotanshinone on breast cancer treatment; a narrative review. *Front Pharmacol* 2022; 13: 979634.
- Shi D, Li H, Zhang Z, He Y, Chen M, Sun L, et al. Cryptotanshinone inhibits proliferation and induces apoptosis of breast cancer MCF-7 cells via GPER mediated PI3K/AKT signaling pathway. *PLoS One* 2022; 17(1): e0262389.

19. Jiang L, Wang Y, Liu G, Liu H, Zhu F, Ji H, et al. C-Phycocyanin exerts anti-cancer effects via the MAPK signaling pathway in MDA-MB-231 cells. *Cancer Cell Int* 2018; 18: 12.
20. Xia M, Yu H, Gu S, Xu Y, Su J, Li H, et al. p62/SQSTM1 is involved in cisplatin resistance in human ovarian cancer cells via the Keap1-Nrf2-ARE system. *Int J Oncol* 2014; 45(6): 2341-8.
21. Han DH, Lee MJ, Kim JH. Antioxidant and apoptosis-inducing activities of ellagic acid. *Anticancer Res* 2006; 26(5A): 3601-6.
22. Labrecque L, Lamy S, Chapus A, Mihoubi S, Durocher Y, Cass B, et al. Combined inhibition of PDGF and VEGF receptors by ellagic acid, a dietary-derived phenolic compound. *Carcinogenesis* 2005; 26(4): 821-6.
23. Shi L, Gao X, Li X, Jiang N, Luo F, Gu C, et al. Ellagic acid enhances the efficacy of PI3K inhibitor GDC-0941 in breast cancer cells. *Curr Mol Med* 2015; 15(5): 478-86.
24. Wang N, Wang ZY, Mo SL, Loo TY, Wang DM, Luo HB, et al. Ellagic acid, a phenolic compound, exerts anti-angiogenesis effects via VEGFR-2 signaling pathway in breast cancer. *Breast Cancer Res Treat* 2012; 134(3): 943-55.
25. Ahire V, Kumar A, Mishra KP, Kulkarni G. Ellagic acid enhances apoptotic sensitivity of breast cancer cells to gamma-radiation. *Nutr Cancer* 2017; 69(6): 904-10.
26. Zhang T, Chen HS, Wang LF, Bai MH, Wang YC, Jiang XF, et al. Ellagic acid exerts anti-proliferation effects via modulation of Tgf-beta/Smad3 signaling in MCF-7 breast cancer cells. *Asian Pac J Cancer Prev* 2014; 15(1): 273-6.
27. Chen HS, Bai MH, Zhang T, Li GD, Liu M. Ellagic acid induces cell cycle arrest and apoptosis through TGF-beta/Smad3 signaling pathway in human breast cancer MCF-7 cells. *Int J Oncol* 2015; 46(4): 1730-8.
28. Yousuf M, Shamsi A, Khan P, Shahbaaz M, AlAjmi MF, Hussain A, et al. Ellagic acid controls cell proliferation and induces apoptosis in breast cancer cells via inhibition of cyclin-dependent kinase 6. *Int J Mol Sci* 2020; 21(10): 3526.
29. Wu YH, Wu YR, Li B, Yan ZY. Cryptotanshinone: a review of its pharmacology activities and molecular mechanisms. *Fitoterapia* 2020; 145: 104633.
30. Noori S, Nourbakhsh M, Imani H, Deravi N, Salehi N, Abdolvahabi Z. Naringenin and cryptotanshinone shift the immune response towards Th1 and modulate T regulatory cells via JAK2/STAT3 pathway in breast cancer. *BMC Complement Med Ther* 2022; 22(1): 145.
31. Zhou J, Xu XZ, Hu YR, Hu AR, Zhu CL, Gao GS. Cryptotanshinone induces inhibition of breast tumor growth by cytotoxic CD4+ T cells through the JAK2/STAT4/ perforin pathway. *Asian Pac J Cancer Prev* 2014; 15(6): 2439-45.
32. Zhang YF, Zhang M, Huang XL, Fu YJ, Jiang YH, Bao LL, et al. The combination of arsenic and cryptotanshinone induces apoptosis through induction of endoplasmic reticulum stress-reactive oxygen species in breast cancer cells. *Metallomics* 2015; 7(1): 165-73.
33. Park IJ, Kim MJ, Park OJ, Choe W, Kang I, Kim SS, et al. Cryptotanshinone induces ER stress-mediated apoptosis in HepG2 and MCF7 cells. *Apoptosis* 2012; 17(3): 248-57.
34. Pan Y, Shi J, Ni W, Liu Y, Wang S, Wang X, et al. Cryptotanshinone inhibition of mammalian target of rapamycin pathway is dependent on oestrogen receptor alpha in breast cancer. *J Cell Mol Med* 2017; 21(9): 2129-39.
35. Li S, Wang H, Hong L, Liu W, Huang F, Wang J, et al. Cryptotanshinone inhibits breast cancer cell growth by suppressing estrogen receptor signaling. *Cancer Biol Ther* 2015; 16(1): 176-84.
36. Li H, Gao C, Liang Q, Liu C, Liu L, Zhuang J, et al. Cryptotanshinone is a intervention for ER-positive breast cancer: an integrated approach to the study of natural product intervention mechanisms. *Front Pharmacol* 2020; 11: 592109.
37. Zhou J, Su CM, Chen HA, Du S, Li CW, Wu H, et al. Cryptanshinone inhibits the glycolysis and inhibits cell migration through PKM2/beta-catenin axis in breast cancer. *Onco Targets Ther* 2020; 13: 8629-39.
38. Shi D, Zhao P, Cui L, Li H, Sun L, Niu J, et al. Inhibition of PI3K/AKT molecular pathway mediated by membrane estrogen receptor GPER accounts for cryptotanshinone induced antiproliferative effect on breast cancer SKBR-3 cells. *BMC Pharmacol Toxicol* 2020; 21(1): 32.
39. Gong Y, Li Y, Abdolmaleky HM, Li L, Zhou JR. Tanshinones inhibit the growth of breast cancer cells through epigenetic modification of Aurora A expression and function. *PLoS One* 2012; 7(4): e33656.
40. Aggarwal V, Tuli HS, Varol A, Thakral F, Yerer MB, Sak K, et al. Role of reactive oxygen species in cancer progression: molecular mechanisms and recent advancements. *Biomolecules*. 2019; 9(11):735.

# Assessing the Impact of Hypercapnic Stimulation on Brain Connectivity Metrics During Functional Magnetic Resonance Imaging

Idiz Iset<sup>1</sup> , Ali Bayram<sup>1</sup> 

<sup>1</sup>Department of Neuroscience, Aziz Sancar Institute of Experimental Medicine, Istanbul University, Istanbul, Turkiye

ORCID ID: I.I. 0000-0002-9764-7956; A.B. 0000-0002-6588-3479

**Cite this article as:** Iset I, Bayram A. Assessing the impact of hypercapnic stimulation on brain connectivity metrics during functional magnetic resonance imaging. *Experimed* 2024; 14(1): 54-60.

## ABSTRACT

**Objective:** Functional connectivity serves as a widely employed metric in neuroscience research focusing on the dynamics of the brain. Additionally, non-neuronal physiological oscillations are acknowledged as being able to impact functional connectivity. This study aimed to explore the effects of non-neuronal hypercapnic stimulation on the activity of intrinsic connectivity networks (ICNs), as well as the dynamic changes in connectivity between them.

**Materials and Methods:** The study involved 10 healthy participants, encompassed their functional magnetic resonance imaging (fMRI) scans with carbon dioxide-enriched air stimuli in a block paradigm, with group independent component analysis (GICA) being used for defining ICNs. Similarity analysis has been conducted between the connectivity changes in the network components and the end-tidal partial pressure of carbon dioxide (PETCO<sub>2</sub>).

**Results:** The study has identified 40 components representing 10 ICNs. Of these, 11 components representing seven ICNs were found to have significantly correlated time courses with PETCO<sub>2</sub>. Among the networks without correlated components, the dynamic functional connectivity metrics of the language network and the subcortical network have been found to be significantly modulated by PETCO<sub>2</sub>.

**Conclusion:** The cerebrovascular reactivity to a hypercapnic stimulus is a factor that influences changes in the blood oxygenation level-dependent fMRI signal. This non-neuronal effect is detectable for ICN components derived by the GICA technique and must be considered when making inferences about network connectivity metrics.

**Keywords:** Cerebrovascular reactivity, hypercapnic stimulation, functional magnetic resonance imaging, functional network connectivity, intrinsic connectivity networks

## INTRODUCTION

Functional connectivity, commonly characterized as the coordination of activity among different brain regions, represents the communication and transfer of information within the brain. In order to investigate connectivity, one study conducted an examination of the similarity in blood oxygen level dependent (BOLD) signals from different brain regions through the use of functional magnetic resonance imaging (fMRI) during both task activations and resting state (1). Studies on resting state functional connectivity offer insights into the spontaneous low-frequency

BOLD oscillations within the brain (2, 3). This approach is particularly preferred as it requires minimal active participation from subjects, thus allowing the detection of connectivity networks.

Intrinsic connectivity networks (ICNs, also known as resting state networks) refer to a collection of brain regions that exhibit similarities in their BOLD time series acquired during resting state. Investigating the dynamics of the brain using functional connectivity allows researchers to identify ICNs and evaluate cognitive tasks, conditions, and diseases from a network perspective. Functional connectivity analysis

**Corresponding Author:** Ali Bayram **E-mail:** ali.bayram@istanbul.edu.tr

**Submitted:** 26.01.2024 **Revision Requested:** 17.03.2024 **Last Revision Received:** 22.03.2024 **Accepted:** 14.04.2024 **Published Online:** 18.04.2024



Content of this journal is licensed under a Creative Commons Attribution-NonCommercial 4.0 International License.

of fMRI data and the detection of connectivity networks can be conducted through two fundamental methods. The first involves the detection of brain voxels correlated with the average BOLD response of a predetermined brain region or seed region based on a hypothesis (4). The second method employs a data-driven, exploratory approach known as independent component analysis (ICA) (5). ICA has the ability to extract meaningful information from complex data without the need for a priori anatomical assumptions or subjective selection of seed areas. Another aspect of ICA is its capability to isolate sources of noise to some extent. In functional neuroimaging, the presence of noise such as physiological artifacts or scanner-related distortions can significantly impact the quality and interpretability of the data. By decomposing mixed signals into independent components, ICA can help identify and separate out noise sources (6), thereby enhancing the signal-to-noise ratio and improving the overall robustness of the analysis.

While ICA can aid in isolating sources of noise, importance is had in recognizing that BOLD signal changes may indeed arise from non-neuronal sources. However, BOLD fMRI alterations may result from neuronal activation via neurovascular coupling, or they can originate from various other physiological processes influencing cerebral blood flow (CBF), oxygenation, or volume. In this sense, BOLD fMRI can be utilized not only for studying neuronal activity but also for assessing vascular health (7). This process is linked to cerebrovascular reactivity (CVR), which refers to the ability of blood vessels in the brain to dilate or constrict in response to a hypercapnic stimulus. Hypercapnic stimulation can be achieved by breathing carbon dioxide-enriched air or breath-holding, which in turn triggers an increase in CBF and results in an increase in the BOLD signal. Thus, CVR can be assessed by analyzing the variations of the BOLD signal during breathing paradigms (8). Importantly, given that both CVR and functional connectivity rely on the analysis of BOLD echo planar imaging (EPI), estimating connectivity parameters becomes plausible using CVR data.

This study aimed to explore how the BOLD response, which varies in response to a hypercapnic stimulus, impacts ICNs. This exploration is important for understanding the extent to which these networks, traditionally seen as neuronal, are influenced by physiological signals.

## MATERIALS AND METHODS

### MRI Dataset and Physiological Recordings

This study used the MRI data shared by Blockley et al. at the Oxford University Research Archive (9). The published research article that utilized this data focused on the feasibility of reliably calculating CVR maps within clinically acceptable scan durations. It explored the use of CO<sub>2</sub>-enriched air with a sinusoidally modulated stimulus paradigm as an alternative to the Toronto block paradigm, in which the hypercapnic stimuli are administered in block form (9). Despite the sinusoidal breathing paradigm being considered a promising alternative, this study has chosen to use only the MRI data acquired during

the Toronto breathing paradigm. Additionally, it utilized the partial pressure of end-tidal CO<sub>2</sub> (PETCO<sub>2</sub>) data obtained during the MRI scans.

The MRI dataset comprises functional and structural images from 10 healthy participants (5 females; age range 19–21) and were acquired using a 3T scanner. The fMRI scans were consisted of 210 EPI volumes lasting 7 minutes, with time of repetition (TR) equal to 2000 ms and time of echo (TE) equal to 30 ms, covering the whole brain at a voxel size of 3.4 x 3.4 x 5 mm<sup>3</sup>. Additionally, T1-weighted structural scans were obtained with 1.5 mm isotropic voxels. For the hypercapnic stimulation during functional imaging, a gas mixture (CO<sub>2</sub>-enriched air) was breathed by the participants and administered using a gas blender (RespirAct™ Gen 3, Thornhill Research Inc., Toronto, Canada). The Toronto protocol had two hypercapnia blocks with an increase of 10 mmHg from the subject's specific baseline level of PETCO<sub>2</sub> and lasted 45 s and 120 s. The protocol has three baseline level periods: 1) lasting 60 seconds at the beginning, 2) lasting 90 seconds between two blocks, and 3) lasting 105 seconds at the end (10). Further details about the scanning parameters and experimental setup were described in the reference paper (9).

### Data Analysis

#### Preprocessing

All preprocessing steps were performed using the program FMRIB's Software Library (FSL v6.0; [www.fmrib.ox.ac.uk/fsl](http://www.fmrib.ox.ac.uk/fsl)). Field maps and functional images were used during the preprocessing stages to cover motion and distortion correction and slice timing correction (11, 12). Structural and functional images were co-registered using a boundary-based registration method (13) and normalized to the Montreal Neurological Institute (MNI) space. Segmentation procedures were employed to derive grey matter masks for individual subjects. These masks were then utilized to compute the subject-specific global signal (GS) representing the average brain signal encompassed within this defined mask. Spatial smoothing with a 5 mm full width at half maximum (FWHM) kernel was applied as the final stage of preprocessing (14).

#### Group Independent Component Analysis

Preprocessed functional data were decomposed into functional networks using the Group ICA of fMRI Toolbox (GIFT; <http://mialab.mrn.org/software/gift/>), and 100 common spatially independent components (ICs) were detected (15). Variance normalization was applied prior to the GICA analysis. In the first stage of dimension reduction, 200 subject-specific principal components were obtained. Subsequently, a second-dimension reduction was implemented on the aggregated group data that was composed of sequentially added principal components from all participants, resulting in 100 principal components. The Infomax algorithm was utilized to maximize the spatial independence of the data (15). To increase the reliability of the ICA algorithm, the procedure was repeated 20

times with the ICASSO method, in which the most central run was chosen as the resulting IC. A group information-guided ICA (GIG-ICA) approach within the GIFT was used to derive subject-specific ICs that match the obtained group components while preserving their spatial independence (16).

The commonly used method in the component labeling process is the visual inspection of three complementary pieces of information from the components: the spatial map, time series, and spectral power (17). As a result of the evaluation, 40 of the 100 components were defined as the network components of the ICNs. The cortical network atlas of the program Functional Connectivity Toolbox (CONN v20b) (18) and the network parcellation atlas of Yeo et al. (19) were used to label the network components. Additionally, the subcortical network was labeled, as it had not been defined in either atlas.

### The Similarity of Time Courses Between the Network Components and PETCO<sub>2</sub>

To investigate the level of temporal similarity, the study employs a comprehensive analysis pipeline as illustrated in Figure 1. The focus centers on assessing the correlation between the time course of the PETCO<sub>2</sub> and the defined network components. To ensure accurate temporal alignment before the correlation analysis, the study employs GS as the reference signal. Calculating the GS involves transforming the gray matter probabilistic map produced in the segmentation stage into a mask consisting of voxels above a threshold value of 0.5 and then extracting the average BOLD time series of the gray matter mask.

The reference GS was initially utilized to correct the temporal delay of the PETCO<sub>2</sub> time course for each subject by employing cross-correlation, thereby ensuring synchronization (time-locked) with the GS. The open-source Rapidtide v2.2.7 software package (20) was used for the cross-correlation calculation. Further refinement was performed by adjusting the temporal position of the PETCO<sub>2</sub> time course using component delay times relative to the GS. However, the conventional cross-correlation method, which identifies time delays based on maximum correlation, was deemed unsuitable due to potential uncorrelatedness between the ICA-derived component time courses and the PETCO<sub>2</sub> time course. Consequently, component delay times were determined using the average time courses within the component maps. A threshold ( $t > 2.0$ ) was applied to the spatial map of the relevant component, and the gray matter mask was multiplied while creating the component ROIs. The average signal within the component ROI was calculated, and the time delay of this signal as detected through cross-correlation with GS was considered to be equal to the time delay of the corresponding component time course. Delay times for the 40 components were used separately to correct the time lag between the component time courses and PETCO<sub>2</sub> time course, and then the correlation coefficients were calculated (Figure 1).

### Statistical Analyses for Time Series Correlation

Random PETCO<sub>2</sub> signals were selected from each participant's own post-calibration period for use in the non-parametric statistical analysis in order to make a noise estimate. This process was repeated for each participant, with the PETCO<sub>2</sub> signal taken from 10 random time periods obtained by shifting 10 s. A total of 100 random correlation values (10 for each participant) were found in the resulting random correlation pool. Fisher's z-transformation was applied to the correlation values before making the statistical inference. Statistical analysis was performed using SPSS (IBM SPSS Statistics, v22; <https://www.ibm.com/tr-tr/products/spss-statistics>) to test whether the coupled correlation value differed from this random correlation pool with an independent samples t-test, with a multiple-comparison correction (Bonferroni correction) being applied to the results.

### PETCO<sub>2</sub>-Modulated Dynamic Functional Network Connectivity Analysis

The study assesses the PETCO<sub>2</sub> signal's modulation of the dynamic functional connectivity change between ICN component pairs. This involves computing sliding-window correlation coefficients between the time-courses of ICN components, referred to as dynamic functional network connectivities (dFNCs) and subsequently assessing PETCO<sub>2</sub>'s modulatory effect on the resulting dFNCs through regression analysis. The GIFT toolbox (21) was utilized for the sliding-window analysis, and additional modifications were made to the dFNC codes to enable regression analysis.

Detrending, despiking, and low-pass filtering ( $<0.15$  Hz) were applied to the time series of the ICN components. The correlation value was used as the connectivity metric in consecutive time windows. The size of the selected time windows was chosen as 30 TR (60 s), and the shifting amount for consecutive time windows was chosen as 1 TR (2 s). The selection of the time window width was carefully balanced to avoid being excessively wide, which could lead to a loss of dynamism; this also prevents it from being too short, which would increase sensitivity to noise (22). In addition, each window was convolved with a Gaussian kernel with a 3TRFWHM to eliminate possible discontinuities due to sudden drops at the beginning and end of the time windows. Connectivity calculations were made for a total of 180 windows, resulting in dFNCs comprising 180 values. The PETCO<sub>2</sub> signal for which the regression analysis will be performed was averaged within the same time window and subsequently reduced to 180 values.

### Statistical Analysis for Regression

The randomize command in FSL was employed for the statistical inference of the regression coefficients using non-parametric permutation (500 permutations) (23). Multiple-comparison (family-wise error) correction was applied for each ICN component pair, with the significance threshold set at  $pFWE < 0.05$ .

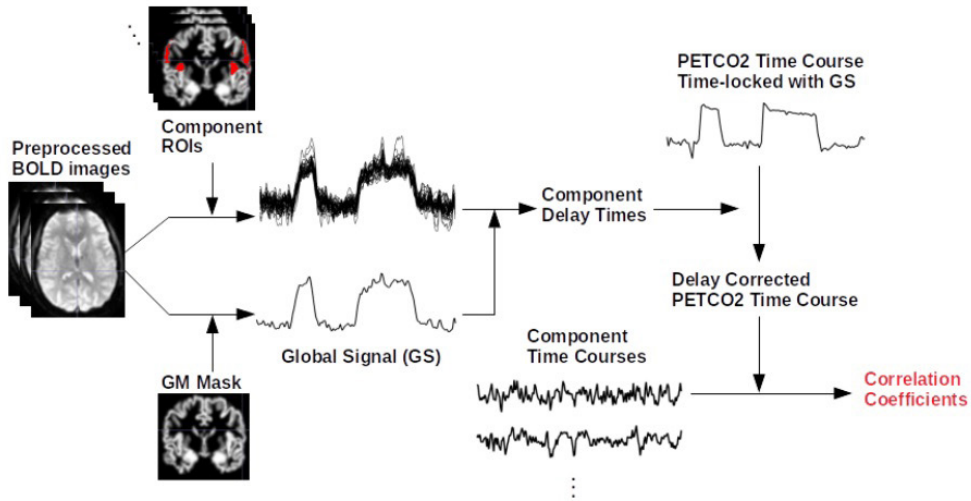


**Figure 1.** Correlation analysis pipeline with time delay correction for each component time course.

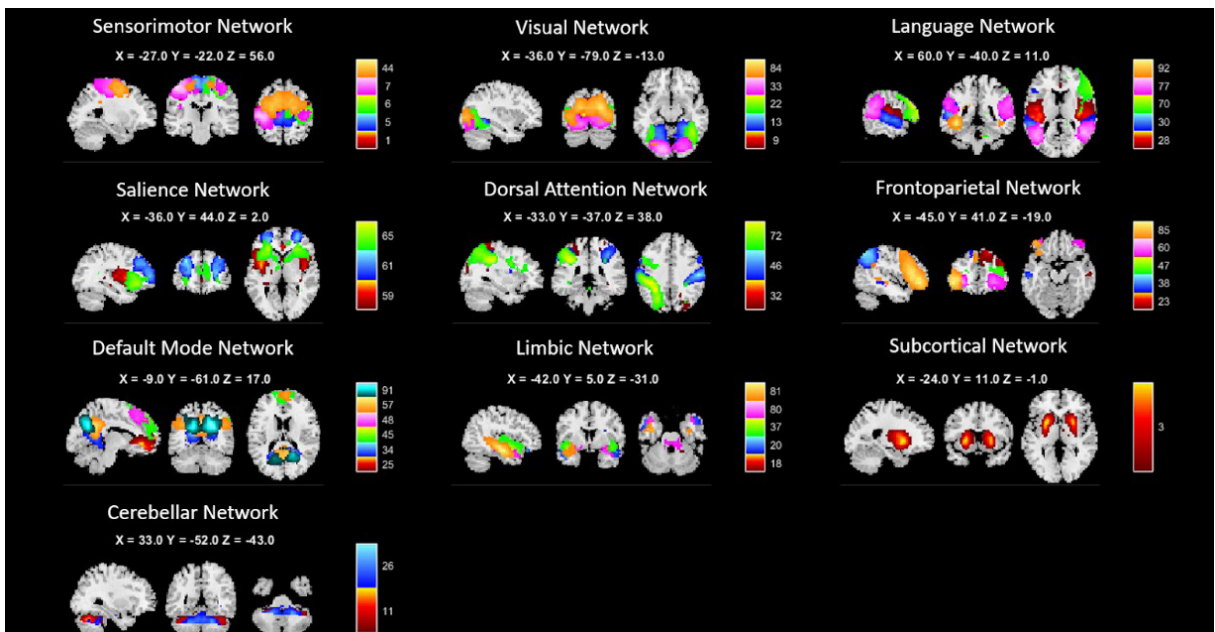


**Figure 2.** Grouped spatial maps of the ICN components determined to be included in a connectivity network as a result of the GICA analysis.

## RESULTS

### Group Independent Component Analysis Results

Following the GICA analysis, a total of 100 independent components were acquired. Upon evaluation, 40 of these 100 components were identified as network components within

the ICNs (Figure 2).

The default mode network includes six different ICs covering the posterior cingulate cortex, medial prefrontal cortex, and left lateral parietal regions. The frontoparietal network contains five ICs that comprise the left lateral prefrontal cortex and left and right posterior parietal cortices. The dorsal attention network consists of the left inferior parietal sulcus and right

**Table 1.** ICN components and their significance levels showing significant correlation with the PETCO<sub>2</sub> signal change

Comp. Number	Corresponding ICN	mean r-value	p-value
44	Sensorimotor, Superior	0.42	0.001
9	Visual, Medial	0.38	<0.001
32	Dorsal Attention, IPS(L)	0.46	<0.001
46	Dorsal Attention, IPS(R)	0.35	<0.001
23	FrontoParietal, PPC (R)	0.36	<0.001
47	Frontoparietal	0.32	<0.001
25	Default Mode, MPFC	0.34	<0.001
45	Default	0.32	0.001
57	Default Mode, PCC	0.41	<0.001
37	Limbic	0.27	0.001
26	Cerebellar, Anterior	0.29	<0.001

inferior parietal sulcus. The visual network is represented by five ICs that correspond to the right lateral, medial, and occipital ICs. The sensorimotor network consists of five ICs that cover the superior, left, and right lateral sensorimotor regions. The cerebellar network encompasses the anterior cerebellar ICs. The salience network comprises the left insula and the right prefrontal cortex region. The language network is represented by the left and right posterior superior temporal gyri and the right inferior parietal gyrus. Additionally, the limbic network includes five ICs, and the subcortical network consists of one IC.

### Correlation Analysis Results Between ICN Components and PETCO<sub>2</sub> Signal Change

The subject-wise average temporal shifts applied to the time series of the network components prior to the correlation analysis were in the range of -1.30 to +1.36 seconds with respect to the GS. Significant ICN components exceeding the Bonferroni-corrected significance threshold ( $p < 0.05/40$ ) as a result of the two-sample t-test are shown in Table 1. According to the two-sample t-test, the ICN components that show a significant correlation with the PETCO<sub>2</sub> signal include: the superior component of the sensorimotor network; the medial component of the visual network; the left and right intraparietal sulcus components of the dorsal attention network; the posterior parietal cortex component of the frontoparietal network; the medial prefrontal cortex and posterior parietal cortex components of the default mode network; the limbic network; and the anterior component of the cerebellar network.

### Regression Analysis Results Between dFNC and the PETCO<sub>2</sub> Change

The matrix of t-values (Figure 3) resulting from the regression analysis revealed relationships between the dFNC values and PETCO<sub>2</sub> time course. Notably, significant cells were observed within the three components of the visual network (visual, lateral (R), visual, occipital, visual, medial), despite the absence of significant correlations between their time courses and the PETCO<sub>2</sub> signal. Additionally, other significant findings include dynamic connectivity between the sensorimotor, lateral (R) component and the subcortical network, as well as between the sensorimotor, lateral (R) component and language, posterior part of the superior temporal gyrus (pSTG)(L) component. These results highlight specific interactions influenced by the PETCO<sub>2</sub> signal within the examined ICNs.

### DISCUSSION

This study has used fMRI data, which captures cognitive brain activity, while measuring cerebrovascular reactivity through hypercapnic stimulation. During fMRI, hypercapnic stimulation increases the blood flow rate due to vasodilation, thus increasing the measured functional response. GICA was performed to detect intrinsic connectivity networks in this dataset. Thus, the study has investigated how non-neuronal hypercapnic stimulation affects ICNs that have been obtained using fMRI data. The components obtained as a result of the GICA were examined, and the components representing ICNs were successfully identified. In this respect, the ICNs defined in the literature have been shown to be detectable under conditions definable as the stress testing of brain vessels. Recent studies are found in the literature that support this finding. Hou et al. (24) measured resting state and CVR in two separate fMRI scans and reported static functional connectivity metrics to be calculable despite the presence of hypercapnic stimulation. However, dynamic connectivity analyses were not performed on the time series of the network components obtained with GICA, and they did not investigate their correlation with the PETCO<sub>2</sub> signal.

Lewis et al. (25) investigated static and dynamic connectivity in CVR data and interpreted the correlation between the detected ICNs and the PETCO<sub>2</sub> signal in the study as the CVR of these networks. They reported the sensorimotor and visual networks to exhibit high CVR. These findings are consistent with the current study's finding that the dynamic connectivity of the sensorimotor and visual networks is modulated by the PETCO<sub>2</sub> signal.

In addition, the high correlation between ICN and PETCO<sub>2</sub> time series has been suggested as being attributable to the spare capacity the cerebral circulation has for increasing CBF (i.e., the vascular reserve of the relevant network) (25). Meanwhile, Tong et al. (26) reported GICA to be able to produce networks that do not actually exist by applying synthetic time delays to the BOLD signal. They interpreted this as the ICA being highly sensitive

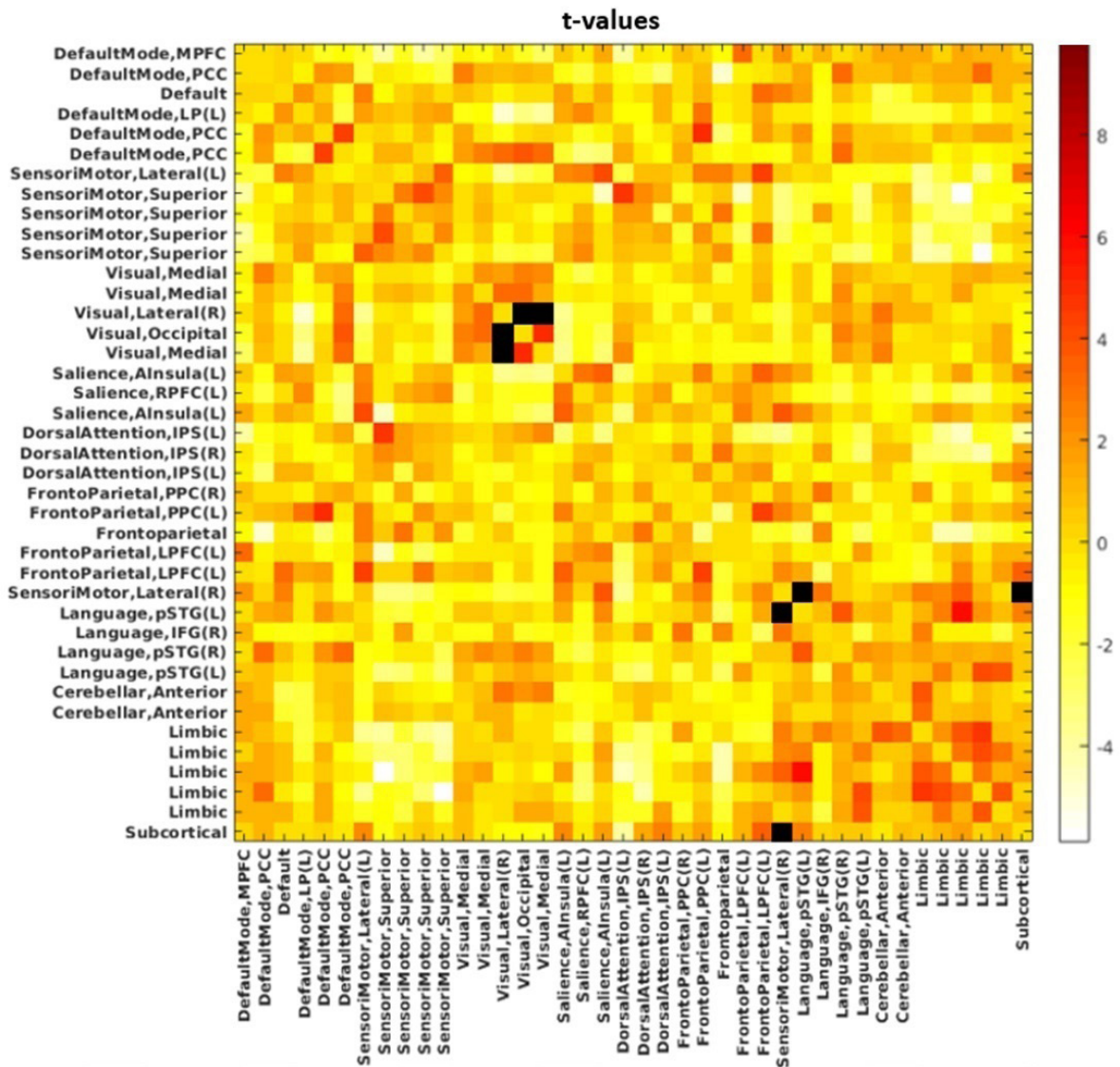


**Figure 3.** Matrix of t-values resulting from the regression analysis between the dFNC values and PETCO<sub>2</sub> time course. Each cell represents the statistical significance of the relationship between the corresponding pair of dFNC values and PETCO<sub>2</sub>, providing insights into the modulatory effect of PETCO<sub>2</sub> on dynamic functional connectivity within ICNs. The color bar represents t-values, with statistically significant pairs being shown in black. (MPFC = Medial Prefrontal Cortex; PCC = Posterior Cingulate Cortex; LP = Lateral Parietal; RPFC = Rostral Prefrontal Cortex; AInsula = Anterior Insula; IPS = Inferior Parietal Sulcus; LPFC = Lateral Prefrontal Cortex, IFG = Inferior Frontal Gyrus, pSTG = Posterior Superior Temporal Gyrus)

to time delays in the BOLD signal. When evaluated from this perspective, the correlation between the PETCO<sub>2</sub> time series and ICN time series may be due to network-specific delays in the systemic signal. In this case, the observed correlation may be an indicator of the systemic oscillations reflected onto the network.

The current study's findings show the network components to be similar to the PETCO<sub>2</sub> time series, whereas network components that do not show a direct correlation may have significant modulation with PETCO<sub>2</sub> in a dynamic connectivity analysis.

The facts that hypercapnic stimulation affected the connectivity metrics in nine of the 10 networks and that this finding indicates a more widespread effect than shown in the literature can be interpreted in two ways. The first reason may be that, when determining ICNs, they are separated into many components, resulting in components with a high contamination. The second reason may be that, through this study's unique approach, a second time delay correction made for each network component has allowed the effect to be revealed more precisely.

Despite the use of non-parametric statistics, the study is limited by a small sample size. Because the dataset originated from a different study, a larger sample could not be obtained, nor could a power analysis be conducted. As a result, care should be used when generalizing the findings, as the small sample size may limit statistical power and increase the possibility of bias.

## CONCLUSION

The CVR to a hypercapnic stimulus exerts a significant influence on the alterations observed in the BOLD fMRI signal. This non-neuronal effect manifests notably in ICN components derived through the GICA technique. The intricate relationship between CVR and the BOLD fMRI signal underscores the importance of acknowledging non-neuronal factors in the study of neural networks. As scientists investigate the functional connectivity of the brain, especially by employing methodologies such as GICA, incorporating non-neuronal influences becomes critical for precise interpretations and robust network connectivity metrics.

**Ethic Committee Approval:** The data used in the study was downloaded from Oxford University Research Archive. Ethics committee approval is not required.

**Peer-review:** Externally peer-reviewed.

**Author Contributions:** Conception/Design of Study- A.B., I.I.; Data Analysis/Interpretation- I.I.; Drafting Manuscript- A.B.; Critical Revision of Manuscript- A.B.; Final Approval and Accountability- A.B.

**Conflict of Interest:** The authors declare that they have no competing interests.

**Financial Disclosure:** This study was funded by the Scientific and Technological Research Council of Turkey (TUBITAK) ARDEB 3501 Grant No: 1225188.

## REFERENCES

1. Friston KJ. Functional and effective connectivity in neuroimaging: A synthesis. *Hum Brain Mapp* 1994; 2(1-2): 56-78.
2. Biswal BB, Yetkin F, Haughton VM, Hyde JS. Functional connectivity in the motor cortex of resting human brain using echo-planar MRI. *Magn Reson Med* 1995; 34(4): 537-41.
3. Fox MD, Raichle ME. Spontaneous fluctuations in brain activity observed with functional magnetic resonance imaging. *Nat Rev Neurosci* 2007; 8(9): 700-11.
4. Raichle ME, MacLeod AM, Snyder AZ, Powers WJ, Gusnard DA, Shulman GL. A default mode of brain function. *Proc Natl Acad Sci U S A*. 2001; 98(2): 676-82.
5. Calhoun VD, Adali T, Stevens MC, Kiehl KA, Pekar JJ. Semi-blind ICA of fMRI: A method for utilizing hypothesis-derived time courses in a spatial ICA analysis. *Neuroimage* 2005; 25(2): 527-38.
6. Beckmann CF, Smith SM. Probabilistic independent component analysis for functional magnetic resonance imaging. *IEEE Trans Med Imaging* 2004; 23(2): 137-52.
7. Sleight E, Stringer MS, Marshall I, Wardlaw JM, Thrippleton MJ. Cerebrovascular Reactivity Measurement Using Magnetic Resonance Imaging: A Systematic Review. *Front Physiol* 2021; 12: 643468.
8. Liu TT. Reprint of "Noise contributions to the fMRI signal: An Overview". *Neuroimage* 2017; 154: 4-14.
9. Blockley NP, Harkin JW, Bulte DP. Rapid cerebrovascular reactivity mapping: Enabling vascular reactivity information to be routinely acquired. *Neuroimage* 2017; 159: 214-23.
10. Sobczyk O, Battisti-Charbonney A, Poublanc J, Crawley AP, Sam K, Fierstra J, et al. Assessing cerebrovascular reactivity abnormality by comparison to a reference atlas. *J Cereb Blood Flow Metab* 2015; 35(2): 213-20.
11. Jenkinson M, Bannister P, Brady M, Smith S. Improved optimization for the robust and accurate linear registration and motion correction of brain images. *Neuroimage* 2002; 17(2): 825-41.
12. Jenkinson M, Beckmann CF, Behrens TE, Woolrich MW, Smith SM. FSL. *Neuroimage* 2012; 62(2): 782-90.
13. Greve DN, Fischl B. Accurate and robust brain image alignment using boundary-based registration. *Neuroimage* 2009; 48(1): 63-72.
14. Smith SM, Brady JM. SUSAN-A new approach to low level image processing. *Int J Comput Vis* 1997; 23(1): 45-78.
15. Calhoun VD, Adali T. Multisubject independent component analysis of fMRI: a decade of intrinsic networks, default mode, and neurodiagnostic discovery. *IEEE Rev Biomed Eng* 2012; 5: 60-73.
16. Du Y, Fan Y. Group information guided ICA for fMRI data analysis. *Neuroimage* 2013; 69: 157-97.
17. Griffanti L, Douaud G, Bijsterbosch J, Evangelisti S, Alfaro-Almagro F, Glasser MF, et al. Hand classification of fMRI ICA noise components. *Neuroimage* 2017; 154: 188-205.
18. Nieto-Castanon A. Handbook of functional connectivity magnetic resonance imaging methods in CONN. Boston, MA: Hilbert Press; 2020.
19. Yeo BT, Krienen FM, Sepulcre J, Sabuncu MR, Lashkari D, Hollinshead M, et al. The organization of the human cerebral cortex estimated by intrinsic functional connectivity. *J Neurophysiol* 2011; 106(3): 1125-65.
20. Frederick B. Rapidity, ver. 2.2.7 [computer program]. Belmont (MA): GitHub; 2022. [cited 20 January 2024]. Available from: <https://github.com/bbfrederick/rapidity>.
21. Allen EA, Erhardt EB, Wei Y, Eichele T, Calhoun VD. Capturing inter-subject variability with group independent component analysis of fMRI data: A simulation study. *Neuroimage* 2012; 59(4): 4141-59.
22. Vergara VM, Mayer AR, Kiehl KA, Calhoun VD. Dynamic functional network connectivity discriminates mild traumatic brain injury through machine learning. *Neuroimage Clin* 2018; 19: 30-7.
23. Winkler AM, Ridgway GR, Webster MA, Smith SM, Nichols TE. Permutation inference for the general linear model. *Neuroimage* 2014; 92: 381-97.
24. Hou X, Liu P, Gu H, Chan MY, Li Y, Peng S, et al. Estimation of brain functional connectivity from hypercapnia BOLD MRI data: Validation in a lifespan cohort of 170 subjects. *Neuroimage* 2019; 186: 455-63.
25. Lewis N, Lu H, Liu P, Hou X, Damaraju E, Iraj A, et al. Static and dynamic functional connectivity analysis of cerebrovascular reactivity: An fMRI study. *Brain Behav* 2020; 10(6): e01516.
26. Tong Y, Hocke LM, Fan X, Janes AC, Frederick Bd. Can apparent resting state connectivity arise from systemic fluctuations? *Front Hum Neurosci* 2015; 9: 285.

# Artificial Intelligence-Enhanced Application of CRISPR-Cas13a for Cancer Gene Therapy: A Breakthrough Concept

Tungki Pratama Umar<sup>1</sup> 

<sup>1</sup>Division of Surgery and Interventional Science, University College London, London, United Kingdom

ORCID ID: T.P.U. 0000-0001-6975-8096

**Cite this article as:** Umar TP. Artificial intelligence-enhanced application of CRISPR-Cas13a for cancer gene therapy: a breakthrough concept. *Experimed* 2024; 14(1): 61-62.

## INTRODUCTION

The invention of the clustered regularly interspaced short palindromic repeat (CRISPR) and CRISPR-associated protein (CRISPR-Cas) technologies have been a revolutionary molecular instrument that allows for exquisite gene manipulation and radically transformed the field of molecular biology. Additionally, these technologies have provided prospective precise therapeutic implications for various clinical demands, including non-infectious diseases such as cancer as well as infectious diseases such as COVID-19. Another intriguing research area involves how this technology has integrated with other forms of technological innovation, such as artificial intelligence (AI). Therefore, this letter seeks to address the application of CRISPR, more specifically CRISPR-Cas13a (a ribonucleic acid/RNA editing technology), and its combination with AI for cancer gene therapy.

### The possible role of CRISPR in cancer gene therapy

Gene therapy is a significant medical advancement, particularly with regard to cancer treatment. Nevertheless, being able to effectively deliver an intended therapy to the targeted cell has proven difficult, despite the abundance of gene modification techniques available such as gene silencing, antisense treatment, ribonucleic acid interference (RNAi), and gene editing (1).

With its ability to target RNA, CRISPR-Cas13a has excellent potential for cancer gene therapy. CRISPR-Cas13a disrupts gene expression in cancer cells while causing minor damage to healthy tissue by targeting the specific RNA sequences associated with the malignancy. CRISPR-Cas13a is a remarkable substitute for Cas9, which directly targets DNA. This process creates new opportunities for precise and controlled genetic expression. With its RNA-centric applications, CRISPR-Cas13a reduces off-target effects and improves specificity compared to RNAi systems, with a knockdown efficiency of over 90% (3). Meanwhile, the well-known CRISPR-Cas9 may also be responsible for off-target DNA editing and irreversible genomic changes; therefore, CRISPR-Cas13a provides a safer way to modify genes (2).

According to one study, the novel Cas13a expression vector that uses the decoy minimal promoter-Cas13a-U6-guide RNA (DMP-Cas13a-U6-gRNA [DCUg]) was able to reduce the expression of endogenous oncogenes efficiently and specifically at both the mRNA and protein levels while also suppressing the expression of reporter genes in the human hepatoma cells; 293T and HepG2. This additionally resulted in a reduced growth and increased apoptosis of hepatoma cells with no impact on the normal hepatocytes (4).

### CRISPR-Cas13a and AI for Cancer Gene Therapy

Genome editing has been revolutionized by combining AI with CRISPR-Cas13a. AI is essential for maximizing the

**Corresponding Author:** Tungki Pratama Umar **E-mail:** [tungkipratama@gmail.com](mailto:tungkipratama@gmail.com)

**Submitted:** 12.12.2023 **Revision Requested:** 09.01.2024 **Last Revision Received:** 11.01.2024 **Accepted:** 05.02.2024 **Published Online:** 25.03.2024



Content of this journal is licensed under a Creative Commons Attribution-NonCommercial 4.0 International License.

precision and efficiency of genome editing due to its capacity for analyzing enormous datasets and spotting intricate patterns, primarily in cancer gene therapy. AI algorithms collaborate to discover the best sites for CRISPR-Cas13a by examining genomic data and locating specific RNA sequences linked to the targeted genetic abnormalities, thus enabling researchers to anticipate and evaluate the effects of CRISPR-Cas13a treatments beforehand. Researchers can make well-informed decisions regarding the specificity of genetic modifications as a result of these predictive capabilities.

### Promising Results and Challenges

Researchers have shown disrupting cancer-related RNA sequences with CRISPR-Cas13a in conjunction with AI to effectively prevent the growth of tumors in preclinical models. Using this molecular scalpel, researchers are able to examine genetic abnormalities linked to cancer. Delivering the RNA to the intended cells, reducing off-target effects, and handling ethical issues in human trials are among the hurdles that still need to be overcome. Off-target effects are reduced by Cas13a's accuracy and AI's predictive power but are still a cause for concern. Furthermore, incorporating AI requires a large amount of data to function (such as the whole transcriptome), and this is also a challenge that must be resolved before being fully incorporated with CRISPR-Cas13a.

### Conclusion

The promise of AI and CRISPR-Cas13a in cancer gene therapy is a harmony of development and hope. With the use of AI and CRISPR-Cas13a's molecular precision alongside AI's

computational power, cancer treatments may be administered with unprecedented precision and adaptability in the future.

---

**Peer-review:** Externally peer-reviewed.

**Conflict of Interest:** The author declare that they have no competing interests.

**Financial Disclosure:** The author declare that this study has received no financial support.

### REFERENCES

1. Roma-Rodrigues C, Rivas-García L, Baptista PV, Fernandes AR. Gene therapy in cancer treatment: why go nano? *Pharmaceutics* 2020; 12(3): 233.
2. Rao K. CRISPR-Cas13 and its applications in human therapeutics. *J High Sch Sci* 2021; 5(4): 1–21.
3. Granados-Riveron JT, Aquino-Jarquín G. CRISPR–Cas13 precision transcriptome engineering in cancer. *Cancer Res* 2018; 78(15): 4107–13.
4. Gao J, Luo T, Lin N, Zhang S, Wang J. A new tool for CRISPR-Cas13a-based cancer gene therapy. *Mol Ther Oncolytics* 2020; 19: 79–92.

# EXPERIMED

## AIMS AND SCOPE

Experimed is a scientific, open access periodical published in accordance with independent, unbiased, and double-blinded peer-review principles. It is the official online-only publication of İstanbul University Aziz Sancar Institute of Experimental Medicine and published three times a year in April, August, and December.

The journal targets national and international audiences, has both national and international members in the editorial board, and aims to enhance international author contributions.

As of 2022 the publication language of the journal is only English. The manuscripts submitted for publication in the journal must be scientific work in English.

Experimed aims to contribute to the literature by publishing manuscripts at the highest scientific level on all fields of basic and clinical medical sciences. The journal publishes original articles, case reports, reviews, and letters to the editor that are prepared in accordance with ethical guidelines.

The scope of the journal includes but not limited to; experimental studies in all fields of medical sciences.

The target audience of the journal includes specialists and professionals working and interested in all disciplines of basic and clinical medical sciences.

There are no article processing charges or submission fees for any submitted or accepted articles. All expenses of the journal are covered by the İstanbul University.

Statements or opinions expressed in the manuscripts published in the journal reflect the views of the author(s) and not the opinions of the İstanbul University Aziz Sancar Institute of Experimental Medicine, editors, editorial board, and/or publisher; the editors, editorial board, and publisher disclaim any responsibility or liability for such materials.

Editor in Chief: Prof. Dr. Bedia Cakmakoglu

Address: İstanbul University, Aziz Sancar Institute of Experimental Medicine, Vakıf Gureba Avenue, 34093, Çapa, Fatih, İstanbul, Türkiye

Phone: +90 212 414 2000-33305

Fax: +90 212 532 4171

E-mail: [bedia@istanbul.edu.tr](mailto:bedia@istanbul.edu.tr)

Editor in Chief: Prof. Dr. Hesenov Muşviq CƏLALOĞLU

Department of General Surgery, Chairman of the Azerbaijan Association of Endoscopic Laparoscopic Surgeons Public Union, Azerbaijan Medical University, Baku, Azerbaijan.

E-mail: [hesenov@amu.edu.az](mailto:hesenov@amu.edu.az)

Publisher: İstanbul University Press

Address: İstanbul University Central Campus, 34452 Beyazıt, Fatih / İstanbul - Türkiye

Phone: +90 212 440 0000

# EXPERIMED

## INSTRUCTIONS TO AUTHORS

### Context

Experimed is an international, scientific, open access periodical published in accordance with independent, unbiased, and double-blinded peer-review principles. The journal is the official on-line-only publication of Istanbul University Aziz Sancar Institute of Experimental Medicine and it is published triannually on April, August, and December. The publication language of the journal is English.

Experimed aims to contribute to the literature by publishing manuscripts at the highest scientific level on all fields of basic and clinical medical sciences. The journal publishes original articles, case reports, reviews, and letters to the editor that are prepared in accordance with ethical guidelines.

### Editorial Policy

The editorial and publication processes of the journal are shaped in accordance with the guidelines of the International Council of Medical Journal Editors (ICMJE), the World Association of Medical Editors (WAME), the Council of Science Editors (CSE), the Committee on Publication Ethics (COPE), the European Association of Science Editors (EASE), and National Information Standards Organization (NISO). The journal conforms to the Principles of Transparency and Best Practice in Scholarly Publishing ([doaj.org/bestpractice](http://doaj.org/bestpractice)).

Originality, high scientific quality, and citation potential are the most important criteria for a manuscript to be accepted for publication. Manuscripts submitted for evaluation should not have been previously presented or already published in an electronic or printed medium. The journal should be informed of manuscripts that have been submitted to another journal for evaluation and rejected for publication. The submission of previous reviewer reports will expedite the evaluation process. Manuscripts that have been presented in a meeting should be submitted with detailed information on the organization, including the name, date, and location of the organization.

### Peer-Review Policy

Only those manuscripts approved by its every individual author and that were not published before in or sent to another journal, are accepted for evaluation. Submitted manuscripts that pass preliminary control are scanned for plagiarism using iThenticate software. After plagiarism check, the eligible ones are evaluated by editor-in-chief for their originality, methodology, the importance of the subject covered and compliance with the journal scope. The selected manuscripts are sent to at least three national/international external referees for evaluation and publication decision is given by editor-in-chief upon modification by the authors in accordance with the referees' claims. Editor-in-chief evaluates manuscripts for their scientific content without regard to ethnic origin, gender, sexual orientation, citizenship, religious belief or political philosophy of the authors and ensures a fair double-blind peer review of the selected manuscripts.

Editor in chief does not allow any conflicts of interest between the authors, editors and reviewers and is responsible for final decision for publication of the manuscripts in the Journal.

Reviewers' judgments must be objective. Reviewers' comments on the following aspects are expected while conducting the review.

- Does the manuscript contain new and significant information?
- Does the abstract clearly and accurately describe the content of the manuscript?
- Is the problem significant and concisely stated?
- Are the methods described comprehensively?
- Are the interpretations and conclusions justified by the results?
- Is adequate references made to other Works in the field?
- Is the language acceptable?

Reviewers must ensure that all the information related to submitted manuscripts is kept as confidential and must report to the editor if they are aware of copyright infringement and plagiarism on the author's side.

A reviewer who feels unqualified to review the topic of a manuscript or knows that its prompt review will be impossible should notify the editor and excuse himself from the review process.

The editor informs the reviewers that the manuscripts are confidential information and that this is a privileged interaction. The reviewers and editorial board cannot discuss the manuscripts with other persons. The anonymity of the referees is important.

### Ethical Principles

The Journal takes as principle to comply with the ethical standards of World Medical Association (WMA) Declaration of Helsinki – Ethical Principles for Medical Research Involving Human Subjects and WMA Statement on Animal Use in Biomedical Research.

An approval of research protocols by the Ethics Committee in accordance with international standards mentioned above is required for experimental, clinical, and drug studies and for some case reports. If required, ethics committee reports or an equivalent official document will be requested from the authors. For manuscripts concerning experimental research on humans, a statement should be included that shows that written informed consent of patients and volunteers was obtained following a detailed explanation of the procedures that they may undergo. For studies carried out on animals, the measures taken to prevent pain and suffering of the animals should be stated clearly. Information on patient consent, the name of the ethics committee, and the ethics committee approval number should also be stated in the Materials and Methods section of the manuscript. It is the authors' responsibility to carefully protect the patients' anonymity. For photographs that may reveal the identity of the patients, signed releases of the patient or of their legal representative should be enclosed.

For studies involving animals, it is required to obtain approval of research protocols from an ethics committee. The committee reviews protocols to ensure compliance with applicable regulations and guidelines, including the Guide for the Care and Use of Laboratory Animals (8th Edition, 2011) and the International Guiding Principles for Biomedical Research Involving Animals (2012). These guidelines offer comprehensive instructions on how to carry out animal research ethically and humanely and are widely acknowledged as the benchmark for such research.

# EXPERIMED

Authors should provide detailed explanation of the ethical treatment of animals in their manuscripts, including measures taken to avoid pain and distress. This is crucial to ensure the humane conduct of the study and enable verification that it conforms to the relevant ethical criteria. The ARRIVE checklist is a useful tool authors can use to present this information clearly and thoroughly.

## Plagiarism

Experimed is extremely sensitive about plagiarism. All submissions are screened by a similarity detection software (iThenticate by CrossCheck) at any point during the peer-review or production process. Even if you are the author of the phrases or sentences, the text should not have unacceptable similarity with the previously published data.

When you are discussing others' (or your own) previous work, please make sure that you cite the material correctly in every instance.

In the event of alleged or suspected research misconduct, e.g., plagiarism, citation manipulation, and data falsification/fabrication, the Editorial Board will follow and act in accordance with COPE guidelines.

## Authorship

Each individual listed as an author should fulfill the authorship criteria recommended by the International Committee of Medical Journal Editors

(ICMJE - [www.icmje.org](http://www.icmje.org)). The ICMJE recommends that authorship be based on the following 4 criteria:

1. Substantial contributions to the conception or design of the work; or the acquisition, analysis, or interpretation of data for the work; AND
2. Drafting the work or revising it critically for important intellectual content; AND
3. Final approval of the version to be published; AND
4. Agreement to be accountable for all aspects of the work in ensuring that questions related to the accuracy or integrity of any part of the work are appropriately investigated and resolved.

In addition to being accountable for the parts of the work he/she has done, an author should be able to identify which co-authors are responsible for specific other parts of the work. In addition, authors should have confidence in the integrity of the contributions of their co-authors.

All those designated as authors should meet all four criteria for authorship, and all who meet the four criteria should be identified as authors. Those who do not meet all four criteria should be acknowledged in the title page of the manuscript.

Experimed requires corresponding authors to submit a signed and scanned version of the authorship contribution form (available for download through <http://experimed.istanbul.edu.tr/en/>) during the initial submission process in order to act appropriately on authorship rights and to prevent ghost or honorary authorship. If the editorial board suspects a case of "gift authorship," the submission will be rejected without further review. As part of the submission of the manuscript, the corresponding author should also send a

short statement declaring that he/she accepts to undertake all the responsibility for authorship during the submission and review stages of the manuscript.

## Conflict of Interest

The journal requires the authors and all individuals taking part in the evaluation process to disclose any existing or potential conflict of interest (such as financial ties, academic commitments, personal relationships, institutional affiliations) that could unduly influence one's responsibilities. To disclose potential conflicts of interest, the ICMJE Potential Conflict of Interest Disclosure Form should be filled in and submitted by authors as explained in the Author Form of the journal. Cases of a potential conflict of interest are resolved within the scope of COPE Conflict of Interest Flowcharts and ICMJE Conflict of Interest guidelines.

Besides conflict of interest, all financial support received to carry out research must be declared while submitting the paper.

The Editorial Board of the journal handles all appeal and complaint cases within the scope of COPE guidelines. In such cases, authors should get in direct contact with the editorial office regarding their appeals and complaints. When needed, an ombudsperson may be assigned to resolve cases that cannot be resolved internally. The Editor in Chief is the final authority in the decision-making process for all appeals and complaints.

## Copyright and Licensing

Authors publishing with the journal retain the copyright to their work licensed under the Creative Commons Attribution-NonCommercial 4.0 International license ("<https://creativecommons.org/licenses/by-nc/4.0/>" CC BY-NC 4.0) which permits unrestricted, non-commercial use, distribution, and reproduction in any medium, provided the original work is properly cited.

## Open Access Statement

The journal is an open access journal and all content is freely available without charge to the user or his/her institution. Except for commercial purposes, users are allowed to read, download, copy, print, search, or link to the full texts of the articles in this journal without asking prior permission from the publisher or the author. This is in accordance with the HYPERLINK "<https://www.budapestopenaccessinitiative.org/read>" BOAI definition of open access.

The open access articles in the journal are licensed under the terms of the Creative Commons Attribution-NonCommercial 4.0 International ("<https://creativecommons.org/licenses/by-nc/4.0/deed.en>" CC BY-NC 4.0) license.

## Disclaimer

Statements or opinions expressed in the manuscripts published in Experimed reflect the views of the author(s) and not the opinions of the editors, the editorial board, or the publisher; the editors, the editorial board, and the publisher disclaim any responsibility or liability for such materials. The final responsibility in regard to the published content rests with the authors.

# EXPERIMED

## MANUSCRIPT PREPARATION

The manuscripts should be prepared in accordance with ICMJE-Recommendations for the Conduct, Reporting, Editing, and Publication of Scholarly Work in Medical Journals (updated in December 2015 - <http://www.icmje.org/icmje-recommendations.pdf>). Authors are required to prepare manuscripts in accordance with the CONSORT guidelines for randomized research studies, STROBE guidelines for observational original research studies, STARD guidelines for studies on diagnostic accuracy, PRISMA guidelines for systematic reviews and meta-analysis, ARRIVE guidelines for experimental animal studies, and TREND guidelines for non-randomized public behavior.

Manuscripts can only be submitted through the journal's online manuscript submission and evaluation system, available at <http://experimed.istanbul.edu.tr/en/>. Manuscripts submitted via any other medium will not be evaluated.

Manuscripts submitted to the journal will first go through a technical evaluation process where the editorial office staff will ensure that the manuscript has been prepared and submitted in accordance with the journal's guidelines. Submissions that do not conform to the journal's guidelines will be returned to the submitting author with technical correction requests.

Authors are required to submit the following:

- Copyright Agreement Form,
- ICMJE Potential Conflict of Interest Disclosure Form (should be filled in by all contributing authors)

during the initial submission. These forms are available for download at <http://experimed.istanbul.edu.tr/en/>.

### Preparation of the Manuscript

**Title page:** A separate title page should be submitted with all submissions and this page should include:

- The full title of the manuscript as well as a short title (running head) of no more than 50 characters,
- Name(s), affiliations, ORCID IDs and highest academic degree(s) of the author(s),
- Grant information and detailed information on the other sources of support,
- Name, address, telephone (including the mobile phone number) and fax numbers, and email address of the corresponding author,
- Acknowledgment of the individuals who contributed to the preparation of the manuscript but who do not fulfill the authorship criteria.

**Abstract:** A English abstract should be submitted with all submissions except for Letters to the Editor. The abstract of Original Articles should be structured with subheadings (Objective, Material and Method, Results, and Conclusion). Please check Table 1 below for word count specifications.

**Keywords:** Each submission must be accompanied by a minimum of three to a maximum of six keywords for subject indexing at the end of the abstract. The keywords should be listed in full without abbreviations. The keywords should be selected from the National Library of Medicine, Medical Subject Headings database (<https://www.nlm.nih.gov/mesh/MBrowser.html>).

### Manuscript Types

**Original Articles:** This is the most important type of article since it provides new information based on original research. The main text of original articles should be structured with Introduction, Material and Method, Results, and Discussion subheadings. Please check Table 1 for the limitations for Original Articles.

Statistical analysis to support conclusions is usually necessary. Statistical analyses must be conducted in accordance with international statistical reporting standards (Altman DG, Gore SM, Gardner MJ, Pocock SJ. Statistical guidelines for contributors to medical journals. *Br Med J* 1983; 7; 1489-93). Information on statistical analyses should be provided with a separate subheading under the Materials and Methods section and the statistical software that was used during the process must be specified.

Units should be prepared in accordance with the International System of Units (SI).

**Editorial Comments:** Editorial comments aim to provide a brief critical commentary by reviewers with expertise or with high reputation in the topic of the research article published in the journal. Authors are selected and invited by the journal to provide such comments. Abstract, Keywords, and Tables, Figures, Images, and other media are not included.

**Review Articles:** Reviews prepared by authors who have extensive knowledge on a particular field and whose scientific background has been translated into a high volume of publications with a high citation potential are welcomed. These authors may even be invited by the journal. Reviews should describe, discuss, and evaluate the current level of knowledge of a topic in clinical practice and should guide future studies. The main text should contain Introduction, Clinical and Research Consequences, and Conclusion sections. Please check Table 1 for the limitations for Review Articles.

**Case Reports:** There is limited space for case reports in the journal and reports on rare cases or conditions that constitute challenges in diagnosis and treatment, those offering new therapies or revealing knowledge not included in the literature, and interesting and educative case reports are accepted for publication. The text should include Introduction, Case Presentation, Discussion, and Conclusion subheadings. Please check Table 1 for the limitations for Case Reports.

**Letters to the Editor:** This type of manuscript discusses important parts, overlooked aspects, or lacking parts of a previously published article. Articles on subjects within the scope of the journal that might attract the readers' attention, particularly educative cases, may also be submitted in the form of a "Letter to the Editor." Readers can also present their comments on the published manuscripts in the form of a "Letter to the Editor." Abstract, Keywords, and Tables, Figures, Images, and other media should not be included. The text should be unstructured. The manuscript that is being commented on must be properly cited within this manuscript.

# EXPERIMED

**Table 1.** Limitations for each manuscript type

Type of manuscript	Word limit	Abstract word limit	Reference limit	Table limit	Figure limit
Original Article	3500	200 (Structured)	30	6	7 or total of 15 images
Review Article	5000	200	50	6	10 or total of 20 images
Case Report	1000	200	15	No tables	10 or total of 20 images
Letter to the Editor	500	No abstract	5	No tables	No media

## Tables

Tables should be included in the main document, presented after the reference list, and they should be numbered consecutively in the order they are referred to within the main text. A descriptive title must be placed above the tables. Abbreviations used in the tables should be defined below the tables by footnotes (even if they are defined within the main text). Tables should be created using the "insert table" command of the word processing software and they should be arranged clearly to provide easy reading. Data presented in the tables should not be a repetition of the data presented within the main text but should be supporting the main text.

## Figures and Figure Legends

Figures, graphics, and photographs should be submitted as separate files (in TIFF or JPEG format) through the submission system. The files should not be embedded in a Word document or the main document. When there are figure subunits, the subunits should not be merged to form a single image. Each subunit should be submitted separately through the submission system. Images should not be labeled (a, b, c, etc.) to indicate figure subunits. Thick and thin arrows, arrowheads, stars, asterisks, and similar marks can be used on the images to support figure legends. Like the rest of the submission, the figures too should be blind. Any information within the images that may indicate an individual or institution should be blinded. The minimum resolution of each submitted figure should be 300 DPI. To prevent delays in the evaluation process, all submitted figures should be clear in resolution and large in size (minimum dimensions: 100 × 100 mm). Figure legends should be listed at the end of the main document.

All acronyms and abbreviations used in the manuscript should be defined at first use, both in the abstract and in the main text. The abbreviation should be provided in parentheses following the definition.

When a drug, product, hardware, or software program is mentioned within the main text, product information, including the name of the product, the producer of the product, and city and the country of the company (including the state if in USA), should be provided in parentheses in the following format: "Discovery St PET/CT scanner (General Electric, Milwaukee, WI, USA)"

All references, tables, and figures should be referred to within the main text, and they should be numbered consecutively in the order they are referred to within the main text.

Limitations, drawbacks, and the shortcomings of original articles should be mentioned in the Discussion section before the conclusion paragraph.

## References

While citing publications, preference should be given to the latest, most up-to-date publications. Authors are responsible for the accuracy of references. References should be prepared according to Vancouver reference style. If an ahead-of-print publication is cited, the DOI number should be provided. Journal titles should be abbreviated in accordance with the journal abbreviations in Index Medicus/ MEDLINE/PubMed. When there are six or fewer authors, all authors should be listed. If there are seven or more authors, the first six authors should be listed followed by "et al." In the main text of the manuscript, references should be cited using Arabic numbers in parentheses. The reference styles for different types of publications are presented in the following examples.

**Journal Article:** Rankovic A, Rancic N, Jovanovic M, Ivanović M, Gajović O, Lazić Z, et al. Impact of imaging diagnostics on the budget – Are we spending too much? *Vojnosanit Pregl* 2013; 70: 709-11.

**Book Section:** Suh KN, Keystone JS. Malaria and babesiosis. Gorbach SL, Barlett JG, Blacklow NR, editors. *Infectious Diseases*. Philadelphia: Lippincott Williams; 2004.p.2290-308.

**Books with a Single Author:** Sweetman SC. *Martindale the Complete Drug Reference*. 34th ed. London: Pharmaceutical Press; 2005.

**Editor(s) as Author:** Huizing EH, de Groot JAM, editors. *Functional reconstructive nasal surgery*. Stuttgart-New York: Thieme; 2003.

**Conference Proceedings:** Bengissson S, Sothemin BG. Enforcement of data protection, privacy and security in medical informatics. In: Lun KC, Degoulet P, Piemme TE, Rienhoff O, editors. *MEDINFO 92. Proceedings of the 7th World Congress on Medical Informatics*; 1992 Sept 6-10; Geneva, Switzerland. Amsterdam: North-Holland; 1992. pp.1561-5.

**Scientific or Technical Report:** Cusick M, Chew EY, Hoogwerf B, Agrón E, Wu L, Lindley A, et al. Early Treatment Diabetic Retinopathy Study Research Group. Risk factors for renal replacement therapy in the Early Treatment Diabetic Retinopathy Study (ETDRS), Early Treatment Diabetic Retinopathy Study Kidney Int: 2004. Report No: 26.

# EXPERIMED

**Thesis:** Yılmaz B. Ankara Üniversitesindeki Öğrencilerin Beslenme Durumları, Fiziksel Aktiviteleri ve Beden Kitle İndeksleri Kan Lipidleri Arasındaki İlişkiler. H.Ü. Sağlık Bilimleri Enstitüsü, Doktora Tezi. 2007.

**Manuscripts Accepted for Publication, Not Published Yet:** Slots J. The microflora of black stain on human primary teeth. Scand J Dent Res. 1974.

**Epub Ahead of Print Articles:** Cai L, Yeh BM, Westphalen AC, Roberts JP, Wang ZJ. Adult living donor liver imaging. Diagn Interv Radiol. 2016 Feb 24. doi: 10.5152/dir.2016.15323. [Epub ahead of print].

**Manuscripts Published in Electronic Format:** Morse SS. Factors in the emergence of infectious diseases. Emerg Infect Dis (serial online) 1995 Jan-Mar (cited 1996 June 5): 1(1): (24 screens). Available from: URL: [http:// www.cdc.gov/ncidod/EID/cid.htm](http://www.cdc.gov/ncidod/EID/cid.htm).

## REVISIONS

When submitting a revised version of a paper, the author must submit a detailed "Response to the reviewers" that states point by point how each issue raised by the reviewers has been covered and where it can be found (each reviewer's comment, followed by the author's reply and line numbers where the changes have been made) as well as an annotated copy of the main document. Revised manuscripts must be submitted within 30 days from the date of the decision letter. If the revised version of the manuscript is not submitted within the allocated time, the revision option may be canceled. If the submitting author(s) believe that additional time is required, they should request this extension before the initial 30-day period is over.

Accepted manuscripts are copy-edited for grammar, punctuation, and format. Once the publication process of a manuscript is completed, it is published online on the journal's webpage as an ahead-of-print publication before it is included in its scheduled issue. A PDF proof of the accepted manuscript is sent to the corresponding author and their publication approval is requested within 2 days of their receipt of the proof.

Editor in Chief: Prof. Dr. Bedia Cakmakoglu  
Address: Istanbul University, Aziz Sancar Institute of Experimental Medicine, Vakıf Gureba Avenue, 34093, Capa, Fatih, Istanbul, Türkiye  
Phone: +90 212 414 2000-33305  
Fax: +90 212 532 4171  
E-mail: [bedia@istanbul.edu.tr](mailto:bedia@istanbul.edu.tr)

Editor in Chief: Prof. Dr. Hesenov Muşviq CƏLALOĞLU  
Department of General Surgery, Chairman of the Azerbaijan Association of Endoscopic Laparoscopic Surgeons Public Union, Azerbaijan Medical University, Baku, Azerbaijan.  
E-mail: [hesenov@amu.edu.az](mailto:hesenov@amu.edu.az)

Publisher: Istanbul University Press  
Address: Istanbul University Central Campus, 34452 Beyazit, Fatih / Istanbul - Türkiye  
Phone: +90 212 440 0000